Experimental investigation of atomic fluorine and oxygen densities in plasma etch processes

A thesis for the degree of

DOCTOR OF PHILOSOPHY

Presented to

DUBLIN CITY UNIVERSITY

By

Sharathkumar Babu Janarthanaram M.Tech.

School of Physical Sciences

Dublin City University

Research Supervisor:

Prof. Miles Turner

January 2018

Declaration

I hereby certify that this material, which I now submit for assessment on the programme of study leading to the award of PhD is entirely my own work, that I have exercised reasonable care to ensure that the work is original, and does not to the best of my knowledge breach any law of copyright, and has not been taken from the work of others save and to the extent that such work has been cited and acknowledged within the text of my work.

Signed: ______________________ ID No. : 13210396 Date: _____________

This thesis is dedicated to my mom and dad for their eternal love, support and motivation

Acknowledgements

I feel immense pleasure to express my deep sense of gratitude to my supervisor Prof. Miles Turner for giving me the opportunity to pursue PhD at DCU. I would like to thank him for his exceptional guidance, support, motivation throughout my research. I would also like to thank Dr. Stephen Daniels for his encouragement, valuable inputs to my research and access to laboratory facilities. I'm much grateful to Dr. Paul Swift for sharing his knowledge in plasma physics and unconditional support provided in my research. Special thanks to technical staff Conor Murphy, Pat Wogan, Des Lavelle for their exceptional assistance throughout my PhD. I would also like to extend my thanks to my colleagues such as Samir, Jim, Sean, Gurusharan, Shailesh, Stephen, Cleo, Nishanth and Cezar. Many thanks to Sheila, Sarah and Fionna for their administrative support all through my PhD at DCU.

Apart from my research, next thing I got more involved was Volleyball in DCU. I would like to thank my Volleyball friends- Alix, Piyush, Paula, Gabi, Philip, Ionut, Carla, Saki, Benny, Katie, and Shraddha for all the fun and cheerful memories. I would also like to thank my friends Saikumar, Venkatesh (Gurunatha), Rajesh, Venkat, Lakshmi, Mithun, Aravind, Neel, Utsav, Koel who always made me to feel at home with their food, care and support. I would like to extend my thanks to Rajesh & family, Jessen & family, Prasanna for all the joyful time.

Special thanks to my close friends Vino, Vivek, Kishore, Viki, Rahul, Puli, Senthil, BM, Karthi, CP, Bharath, Suresh, Jagan, Divya, Deepika, Swapna, Kirthiga, Janu, Tanya, Hema and Akshaya for their love and care all through my life. I would also like to thank Vichu, Vijay, Karthick and Harish for their motivation and support during my research.

I'm very much grateful to my parents Renuka and Janarthanaram for their eternal love and emotional support throughout my PhD. I would also like to

thank my sisters, brothers and family members for their support all through my research. I thank the Almighty for taking care of me with good health throughout my research.

Last but not least, I would like to thank Irish Research Council and Intel Ireland for providing funding to my research work.

Contents

Declaration i

Acknowledgements iii

List of Figures x

List of Tables xvi

List of Symbols xvii

List of Publications xix

Conferences xx

Abstract xxi

Chapter 1- Introduction and Thesis Motivation 1

1 Introduction 2

1.1 Capacitively-coupled radio frequency discharge 4

1.2 Plasma Sheath 7

1.3 Radical species in plasma etch process 8

1.4 Motivation of this work 9

1.5 Thesis outline 13

1.6 References 14

Chapter 2- Experimental tools and diagnostic techniques 23

2.1 Reactive ion etcher- Plasmalab system 100 25

2.2 Mass spectrometry 27

2.2.1 Appearance potential mass spectrometry and calibration procedure 29

2.3 Optical emission spectroscopy 34

2.3.1 Actinometry 35

2.3.2 Optical sensor for actinometry 40

2.4 Probe diagnostics 42

2.4.1 Langmuir probe 42

2.4.2 Principle of Langmuir probe 43

2.4.3 Procedure to determine plasma parameters 44

2.4.4 Commercial Langmuir probe- The Smart-Probe 50

2.4.5 Hairpin probe 51

2.4.6 Octiv VI probe 53

2.5 References 53

Chapter 3- Investigation of fluorine radical concentration in a capacitively coupled SF_6/O_2/Ar discharge as a function of O_2 concentration 62

3.1 Motivation 63

3.2 Role of oxygen radicals in SF_6 discharge 64

3.3 Absolute fluorine atom density in SF_6/O_2/Ar plasma- Effects of O_2 concentration 67

3.4 Validation of fluorine actinometry 69

3.5 Dissociation fraction and fluorine production efficiency 72

3.6 Conclusion 75

3.7 References 76

Chapter 4- Investigation of atomic fluorine density by varying gas pressure in a capacitively coupled SF_6/O_2/Ar discharge 79

4.1 Motivation 80

4.2 Pressure variation of absolute fluorine atom density in SF_6/O_2/Ar plasma 81

4.3 Relative variation of [F] using actinometry and its validation 84

4.3.1 Electrical characteristics in SF_6/O_2/ Ar plasma as function of gas pressure 86

4.3.2 Dissociative excitation- Improvement to fluorine actinometry 89

4.4 Conclusion 94

4.5 References 95

Chapter 5- Investigation of absolute fluorine atom density as a function of applied rf power in a capacitively coupled $SF_6/O_2/Ar$ discharge 100

5.1 Motivation 101

5.2 Variation of absolute atomic fluorine density measurements in $SF_6/O_2/Ar$ plasma discharge as a function of rf power 103

5.3 Validation of fluorine actinometry- Effect of rf power 107

5.3.1 Proportionality constant for fluorine actinometry and its dependence 111

5.4 Conclusion 122

5.5 References 123

Chapter 6- Re-investigation of electron kinetics as a function of gas pressure in O_2 plasma; Measurement of absolute atomic oxygen density using actinometry and Langmuir probe 129

6.1 Motivation 130

6.2 Investigation of kinetic behavior of electrons in O_2 plasma as a function of discharge pressure 131

6.2.1 Investigation of structure observed on measured EEPF 133

6.3 Investigation of heating mode transition in O_2 discharge using Langmuir probe with L2 setup at 200 W rf power 135

6.3.1 Comparison of O_2 electron kinetics measured between two Langmuir probe arrangements- Effects of Inadequate probe compensation 137

6.4 Measurement of absolute atomic oxygen density using optical emission spectroscopy and Langmuir probe 144

6.5 Conclusion 151

6.6 References 152

Chapter 7- Conclusions 155

7.1 APMS- Variation of absolute fluorine atom density 156

7.1.1 Effect of O_2 content 156

7.1.2 Effect of gas pressure and rf power 157

7.2 Fluorine actinometry- For industrial applications 158

7.3 Electron kinetics in oxygen discharge 160

7.4 Highlights of this work 161

7.5 Scope for future work 163

Appendix A- Report on Mass spectrometer 164

A.1 Introduction 165

A.2 Experiment 165

A.3 Precautions & Observations 166

A.3.1 Filaments 166

A.3.2 SEM detector 167

A.3.2.1 Operating Voltage 168

A.3.3 Tuning EQP Analyser 170

A.3.3.1 RGA Tune 170

A.3.3.2 MAP Scans 172

A.3.4 Penning Gauge 172

A.3.5 Bake-Out 177

A.3.6 Electron Energy Calibration 178

A.4 Acquisition technique 180

A.5 Conclusion 183

A.6 References 184

List of Figures

1.1 Schematic of asymmetric capacitively coupled RF discharge 4

2.1 Schematic of Oxford instruments Plasmalab system 100 26

2.2 Schematic of Hiden Analytical mass spectrometer EQP 300 28

2.3 Electron energy scan of fluorine ions: signal shown were residual signal (●), background signal (■) and plasma on signal (▲) 31

2.4 Instrument response function for Hiden EQP 300 mass spectrometer [17] 33

2.5 Schematic diagrams of the excited states involved in fluorine (left) and argon (right) used to monitor the density of ground state atoms by actinometry 38

2.6 Schematic of an Ocean optics HR 4000 spectrometer with plasma discharge for actinometry 41

2.7 Typical I-V characteristics measure using Langmuir probe in Ar discharge at 20 mTorr and 200 W. 'A' denotes ion saturation region, 'B' denotes electron retardation region and 'C' denotes electron saturation region 42

2.8 Probe I-V characteristics (solid lines) obtained using Smart probe and calculated ion current, , i_i^c (○) in 20 mTorr Ar plasma discharge with applied rf power of 200 W. V_P =27.3 V 48

2.9 Probe I-V characteristics (solid lines) obtained using Smart probe and calculated ion current, , i_i^c (○) in 300 mTorr Ar plasma discharge with applied rf power of 200 W. V_P =34.7 V 49

2.10 Schematic of the Smart-Probe- commercial Langmuir probe system used in this work 51

3.1 Time variation of fluorine signal, F^+ measured using mass spectrometry for fixed electron energy of 21 eV; pressure and RF power were kept constant at 60 mTorr and 500 W respectively. The F^+ signals measured in pure SF_6 plasma for 190 s > time > 380 s and between time 190 – 380 s in SF_6/O_2 (90/10%) discharge 65

3.2 Absolute fluorine atom density measured using APMS in $SF_6/O_2/Ar$ plasma by varying O_2 content in feedstock mixture at 70 mTorr (●) and 200 mTorr (♦) gas pressure for 100 W rf power 67

3.3 Relative fluoirne atom densities measured at 70 mTorr gas pressure using APMS (♦) and actinometry (■) was compared as function of O_2 concentration in a capacitively coupled discharge operated at 100 W rf power 69

3.4 Relative fluoirne atom densities measured at 200 mTorr gas pressure using APMS (♦) and actinometry (■) was compared as function of O_2 concentration in a capacitively coupled discharge 70

operated at 100 W rf power

3.5 Electron density measured using Hairpin probe in a capactively coupled discharge operated at 100 W rf power and 70 mTorr gas pressure in $SF_6/O_2/Ar$ plasma for varying O_2 concentration 71
3.6 Dissociation fractions as a function of O_2 concentration in 70 mTorr (■) and 200 mTorr (♦) gas discharges in $SF_6/O_2/Ar$ plasma operated at 100 W rf power 72
3.7 Production efficiency of fluorine calculated from APMS (■) measurements and predicted values from actinometry (♦) measurements were plotted as a function of SF_6 partial pressure in $SF_6/O_2/Ar$ plasma with total gas pressure of 70 mTorr operated at 100 W rf power 74
3.8 Production efficiency of fluorine calculated from APMS (■) measurements and predicted values from actinometry (♦) measurements were plotted as a function of SF_6 partial pressure in $SF_6/O_2/Ar$ plasma with total gas pressure of 200 mTorr operated at 100 W rf power 75
4.1 Pressure variation of absolute fluorine atom density measured using APMS in $SF_6/O_2/Ar$ (70/26/4%) capacitively coupled discharge operated at 100 W rf power 82
4.2 Pressure variation of electron density measured using hairpin probe in $SF_6/O_2/Ar$ (70/26/4%) capacitively coupled discharge operated at 100 W rf power 83
4.3 Dissociation fraction as a function of gas pressure in in $SF_6/O_2/Ar$ (70/26/4%) capacitively coupled discharge operated at 100 W rf power 84
4.4 Relative fluorine atom densities measured using APMS (●) and actinometry (□) were compared in $SF_6/O_2/Ar$ (70/26/4%) capacitively coupled discharge operated at 100 W rf power 85
4.5 Pressure dependence on phase shift angle measured using Octiv probe in $SF_6/O_2/Ar$ (70/26/4%) capacitively coupled discharge operated at 100 W rf power 86
4.6 Pressure dependence on rf current amplitude (○) and active rf current (□) measured using Octiv probe in $SF_6/O_2/Ar$ (70/26/4%) capacitively coupled discharge operated at 100 W rf power 87
4.7 Pressure dependence on rf voltage (□) measured using Octiv probe in $SF_6/O_2/Ar$ (70/26/4%) capacitively coupled discharge operated at 100 W rf power 89
4.8 Plot of fluorine density measured using APMS, $[F]_{APMS}$ vs actinometric signal, (I_F/I_{Ar}) [Ar] to investigate additional excitation mechanism contribution to actinometric signal in $SF_6/O_2/Ar$ (70/26/4%) capacitively coupled discharge operated at 100 W rf power 91
4.9 Production efficiency of fluorine atom calculated using APMS (□) and dissociative contribution (◊) as function of gas pressure in $SF_6/O_2/Ar$ (70/26/4%) capacitively coupled discharge operated at 100 W rf power 92

4.10 Relative number densities of [F] using APMS (●), [F] using actinometry (□) and SF_6 using ideal gas law (▲) in a capacitively coupled discharge 94
Figure 5.1 Variation of absolute [F] as a function of rf power. The feedstock mixtures were **a**. 85% SF_6, 10% O_2 and 5% Ar at 40 mTorr (◊); **b**. 76% SF_6, 20% O_2 and 4% Ar at 70 mTorr (○); **c**. 66% SF_6, 30% O_2 and 4% Ar at 200 mTorr (□). 104
5.2 Electron density variations as a function of rf power at 40 mTorr (○), 70 mTorr (□) and 200 mTorr (Δ) gas pressures with feedstock mixtures of 85% SF_6, 10% O_2 and 5% Ar, 76% SF_6, 20% O_2 and 4% Ar and 66% SF_6, 30% O_2 and 4% Ar respectively 105
5.3 Dissociation fraction as a function of rf power at 40 mTorr (◊), 70 mTorr (○) and 200 mTorr (□) gas pressures with feedstock mixtures of 85% SF_6, 15% O_2 and 5% Ar, 76% SF_6, 20% O_2 and 4% Ar and 66% SF_6, 30% O_2 and 4% Ar respectively 106
5.4 A comparison of relative atomic fluorine concentration measured using actinometry (□) and APMS (○) at 40 mTorr gas pressure in $SF_6/O_2/Ar$ (85/10/5%) discharge 108
5.5 A comparison of relative atomic fluorine concentration measured using actinometry (□) and APMS (○) at 70 mTorr gas pressure in $SF_6/O_2/Ar$ (76/20/4%) discharge 109
5.6 A comparison of relative atomic fluorine concentration measured using actinometry (□) and APMS (○) at 200 mTorr gas pressure in $SF_6/O_2/Ar$ (66/30/4%) discharge 110
5.7 Evaluation of proportionality constant for fluorine actinometry in $SF_6/O_2/Ar$ (66/30/4%) discharge operated at 200 mTorr gas pressure 113
5.8 Linear dependence of proportionality constant, *K* with gas temperature at fixed pressure of actinometer (argon) for power variation investigation in $SF_6/O_2/Ar$ (66/30/4%) discharge 113
5.9 Relative variations of [F] measured at LADC (□) and LAEE (◊) as a function of applied power in 200 mTorr $SF_6/O_2/Ar$ (66/30/4%) discharge 114
5.10 Radial variation of electron density measured using hairpin probe in 200 mTorr $SF_6/O_2/Ar$ (66/30/4%) discharge operated at 600 W applied rf power 114
5.11 F emission line intensity obtained using LADC (□) and LAEE (◊) measurements as a function of applied power in 200 mTorr $SF_6/O_2/Ar$ (66/30/4%) discharge 116
5.12 F emission line intensity obtained using LADC (□) and LAEE (◊) measurements as a function of gas pressure in $SF_6/O_2/Ar$ (70/26/4%) discharge operated at 100 W rf power 117
5.13 Comparison of [F] computed using fluorine actinometry and proportionality factor (□) with absolute [F] measured using APMS (○) in 70 mTorr $SF_6/O_2/Ar$ (76/20/4%) discharge 118

5.14 Comparison of [F] computed using fluorine actinometry and proportionality factor (□) with absolute [F] measured using APMS (○) for various gas pressure in $SF_6/O_2/Ar$ (70/26/4%) discharge operated at 100 W rf power	119
5.15 Comparison of [F] computed using fluorine actinometry and proportionality factor (□) with absolute [F] measured using APMS (○) for variation of O_2 content in 70 mTorr $SF_6/O_2/Ar$ discharge operated at 100 W rf power	120
5.16 Comparison of [F] computed using fluorine actinometry and proportionality factor (□) with absolute [F] measured using APMS (○) for variation of O_2 content in 200 mTorr $SF_6/O_2/Ar$ discharge operated at 100 W rf power	121
5.17 Comparison of [F] computed using fluorine actinometry signal measured with Horiba Yvon OES (Δ) and Ocean optics (□) spectrometers, with absolute [F] measured using APMS (○) in 40 mTorr $SF_6/O_2/Ar$ (85/15/5%) discharge for various applied rf power	122
6.1 Evolution of EEPFs with increase in O_2 pressure at 200 W rf power in capacitively-coupled plasma	131
6.2 Electron density, n_e (○) and effective electron temperature, T_{eff} (Δ) as a function of O_2 gas pressure in a capacitively-coupled plasma operated at 200 W rf power	133
6.3 Schematic of visually observed plasma confinement with increase in O_2 gas pressure at 200 W rf capacitive discharge	133
6.4 Schematics of Langmuir probe with standard setup L1 and (b) Langmuir probe with modified reference electrode position L2	134
6.5 EEPFs measured using two Langmuir probe setups, L1 and L2 in 20 mTorr and 300 mTorr argon discharges operated at 200 W rf power	135
6.6 Pressure evolutions of EEPFs measured using Langmuir probe with L2 arrangement in O_2 discharge operated at 200 W rf power	136
6.7 Variations of electron density n_e (○) and effective electron temperature T_{eff} (□) measured using Langmuir probe with L2 setup for different gas pressures in O_2 discharge operated at 200 W	137
6.8 Comparison of EEPFs measured using two different Langmuir probe arrangements L1 & L2 in O_2 discharge operated at 200 W rf power for different gas pressures	138
6.9 Comparison of electron density (left) and effective electron temperature (right) measured using Langmuir probe with L1 (□) and L2 (○) arrangements for different gas pressures in O_2 discharge at 200 W	139
6.10 Calculated ionization rate using L2 Langmuir probe arrangement (○) was compared to ionization rate in reference [9](□)	140
6.11 (a) Spatial arrangement of Langmuir probe with dimensions of probe assembly. (b) Schematic of different positions of Langmuir probe in spatial direction	141
6.12 Plots of EEPFs measured spatially in 300 mTorr Ar discharge operated at 100 W as function of distance from powered electrode (PE)	142

6.13 Measured EEPFs as a function of distance from discharge centre (DC) in radial direction for different (200, 400 & 600 mTorr) O_2 pressures operated at 200 W 143
6.14 Evolution of EEDF as a function of pressure in O_2-Ar discharge operated at 100 W 144
6.15 Measurements of electron density (◊) and effective electron temperature (○) as a function of gas pressure in O_2-Ar discharge operated at 100 W 145
6.16 Variations of temperatures of low (Δ) and high (□) energy electron groups as a function of gas pressure in O_2-Ar discharge operated at 100 W 145
6.17 Variations of calculated k_e^{Ar}/k_e^{O}(◊) and $k_e^{diss\ O}/k_e^{O}$(□) as a function of pressure in O_2-Ar discharge operated at 100 W 148
6.18 Atomic oxygen density determined using actinometric signal and excitation rate co-efficients calculated from EEDF measured using Langmuir probe (□) as a function of gas pressure in O_2-Ar discharge operated at 100 W 149
6.19 Pressure variation of relative atomic oxygen density measured using actinometry (■) was compared with TALIF measurements (Δ) from [24] in O_2-Ar discharge operated at 100 W rf power 150
6.20 Variations of atomic oxygen production rate through dissociative excitation mechanism as a function of pressure in O_2-Ar discharge operated at 100 W rf power 151
A.1 Experimental setup of Hiden EQP 300 mass spectrometer 165
A.2 Schematic of electron impact ionisation source in EQP 300 167
A.3 Detector operating curve [3] 169
A.4 Detector operating curves on different dates with shift in plateau region 169
A.5 Detector operating curves on different dates with poor signal-to-noise ratio 168
A.6 Typical RGA tune scan at 40 amu (argon) generated at 5.2×10^{-7} Torr EQP pressure 171
A.7 Typical RGA energy spectra from a probe with a. (on left) maximum signal intensity at a negative energy voltage indicates slight–contaminated source and b. (on right) maximum signal intensity at a positive voltage indicates clean source. Both the scans were performed at 40 amu with 5.2×10^{-7} Torr EQP pressure 172
A.8 Pictures of the contaminated gauge with the debris in the gauge (left) and debris made to fall on the paper (right) when gauge was tapped 173
A.9 MAP scans (of few parameters) comparison of clean and contaminated gauge at 40 amu generated at 5.2×10^{-7} Torr EQP pressure 174

A.10 Mass spectrum with argon gas. Mass offset (m/e = 40 to 42) was observed due to contamination in EQP 175
A.11 Electron energy scan of N in N_2 plasma with the contaminated gauge (left) in comparison to appearance potential scans for N (right) with the plasma on and off from Hiden [3] 175
A.12 Penning gauge was in direct line of sight to quadrupole. This set up will contaminate the EQP probe if debris were formed in the gauge 176
A.13 Mass spectrum before and after bake-out with no gas 177
A.14 Argon electron energy scans (a) E_{th} = 15 eV with argon pressure of 60 mTorr and emission current of 500 µA. (b) E_{th} = 18 eV with argon pressure of 5 mTorr and emission current of 100 µA 178
A.15 Variation of ionization threshold for Argon for different pressure at 100 µA and 300 µA emission current 179
A.16 Electron energy scans of F^+ in $SF_6/O_2/Ar$ plasma with 100 µA emission current and 40 mTorr gas pressure 180
A.17 Residual electron energy scan of F^+ before each plasma strike with no gas flow at 100 µA emission current 181
A.18 Background electron energy scan of F^+ before each plasma strike with 85% SF_6, 10% O_2 and 5% Ar at 100 µA emission current and 40 mTorr gas pressure 181
A.19 Residual electron energy scan of F^+ before each plasma strike with no gas flow at 100 µA emission current using new acquisition technique 183

List of Tables

3.1 Fluorine production through SF_6-O_2 gas-phase reaction and their respective reaction rates co-efficient 66

5.1 Value of *K* evaluated in fluorine based discharges 112

6.1: Electron parameters measured using two different Langmuir probe arrangements 135

6.2 Experimental values and constants [19] for determining [O] 147

List of Symbols

n_e	Electron density (m^{-3})
n_i	Ion density (m^{-3})
I_e	Electron emission current from the ionizer (A)
$\sigma(\varepsilon)$	Electron energy dependent ionization cross section (m^2)
β	Extraction efficiency of the ions (a.u)
$T(m_{X^+})$	Species mass dependent transmission efficiency of the quadrupole (a.u)
$\theta(m_{X^+})$	Species mass dependent sensitivity of the SEM detector (a.u)
l_{ion}	Length of the ionizer (m)
k_e^X	Direct excitation rate coefficient (cm^3s^{-1})
k_{de}^X	Dissociative excitation rate coefficient (cm^3s^{-1})
V_P	Plasma potential (V)
V_F	Floating potential (V)
V_B	Probe bias voltage (V)
T_{eff}	Effective electron temperature (eV)
$f(\varepsilon)$	Electron energy distribution function (eV^{-1} m^{-3})
ε	Electron energy (eV)
$f_e(\varepsilon)$	Electron energy probability function ($eV^{-3/2}$ m^{-3})
I_T	Total probe current (A)
I_e	Current from electrons (A)
I_i	Current from ions (A)
T_e	Electron temperature (eV)

λ_D	Debye length (m)
k_B	Boltzmann constant (JK^{-1})
m_i	Mass of ion (kg)
m_e	Mass of electron (kg)
r_p	Probe tip radius (m)
$\in$	Relative permittivity of the medium around the probe (a.u)
f_r	Resonance frequency (GHz)
c	Speed of light (ms^{-1})
L	Resonator length (m)
f_{ro}	Resonance frequency in vacuum (GHz)

List of Publications

Samir Kechkar, **Sharath Kumar Babu**, Paul Swift, Cezar Gaman, Stephen Daniels, and Miles Turner, "Investigation of absolute atomic fluorine density in a capacitively coupled $SF_6/O_2/Ar$ and SF_6/Ar discharge", ***Plasma Sources Science and Technology***, 23 (2014) 065029.

Samir Kechkar, Paul Swift, Sean Kelly, **Sharath Kumar Babu**, Stephen Daniels, and Miles Turner, "Investigation of the electron kinetics in O_2 capacitively coupled plasma with the use of a Langmuir probe", ***Plasma Sources Science and Technology***, 26 (2017) 065009.

Manuscripts in preparation

Sharath Kumar Babu, Sean Kelly, Samir Kechkar, Paul Swift, Miles Turner, and Stephen Daniels "Experimental investigation of improved actinometry in oxygen discharge".

Sharath Kumar Babu, Samir Kechkar, Paul Swift, Sean Kelly, Miles Turner, and Stephen Daniels "Investigation of fluorine actinometry in SF_6 based plasma discharge".

Sharath Kumar Babu, Paul Swift, Samir Kechkar, Miles Turner, and Stephen Daniels "Proportionality constant for fluorine actinometry calculated in SF_6 based plasma discharge".

Conferences

Sharath Kumar Babu, Samir Kechkar, Paul Swift, Stephen Daniels, and Miles Turner, "*Actinometry of Atomic Fluorine in a Capacitively Coupled Discharge with a mixture of SF_6 and O_2*", poster presentation at 69th Annual Gaseous Electronics Conference- October 10th-14th, 2016, Ruhr-University Bochum, Germany.

Sharath Kumar Babu, Samir Kechkar, Paul Swift, Miles Turner and Stephen Daniels, "*Investigation on structure observed in measured electron energy probability function in capacitively coupled oxygen discharge*", poster presentation at Intel Ireland Research Conference 2014, Dublin and Radio frequency workshop organized by National Centre for Plasma Science and Technology, 2015, Dublin (**received the best poster presentation award**).

Sharath Kumar Babu, Samir Kechkar, Cezar Gaman, Paul Swift, Miles Turner and Stephen Daniels, "*Insights into various challenges in measuring absolute fluorine radical density in SF_6 plasma and measured absolute fluorine radical density in capacitively-coupled $SF_6/O_2/Ar$ and SF_6/Ar discharge*", poster presentation at Intel Ireland Research Conference 2014, Dublin.

Sharath Kumar Babu, Samir Kechkar, Stephen Daniels, and Miles Turner, "*Investigation of actinometry signal and comparison to absolute [O] measurements obtained using TALIF (two-photon absorption laser-induced fluorescence)*", poster presentation at Intel Ireland Research Conference 2013, Dublin.

Abstract

B. Sharath Kumar

Experimental investigation of atomic fluorine and oxygen densities in plasma etch processes

It was well known that atomic fluorine and oxygen radicals play a vital role in plasma etching processes. This thesis investigates the density of fluorine and oxygen radical species using different diagnostic techniques in a parallel-plate capacitively coupled reactive ion etching plasma source. The behaviour of absolute atomic fluorine density in $SF_6/O_2/Ar$ plasma was investigated using appearance potential mass spectrometry as a function of feedstock mixture, gas pressure and applied rf power. Contrary to naive expectations, atomic fluorine density was found to increase with dilution of O_2 in SF_6 discharge operated at 100 W and reached a peak value at ≈ 20-30 % O_2 content. This increase in fluorine atom density can be due to decrease in fluorine atom loss rate at walls through surface recombination and production of fluorine atoms through gas-phase reactions involving SF_x (where x = 1-5) and atomic oxygen. However, atomic fluorine density was found to decrease with further addition of oxygen to discharge due to decrease in SF_6 partial pressure.

Absolute fluorine atom density investigated using APMS technique, was found to increase with increase in gas pressure in $SF_6/O_2/Ar$ discharge (70/26/4 %) operated at 100 W rf power. Increase in fluorine atom density can be mainly due to increase in SF_6 partial pressure as electron density was found to be in weak correlation with pressure.

A non-invasive, compact and low cost industrial sensor would always be essential to monitor any variations in the plasma. Optical emission spectroscopy was one of such diagnostic tool and using it relative variations in radical density in plasma discharge can be monitored by a popular technique known as

actinometry. In this thesis, fluorine actinometry technique was adopted to investigate relative fluorine density variations in capacitively coupled discharge and for validation of fluorine actinometry, relative [F] measurements were compared with APMS measurements. At low pressure conditions, actinometric limitation was violated as relative [F] measured using actinometry had poor correlation with APMS measurements. This could be largely due to additional excitation contribution to fluorine actinometric signal. With negligible changes to discharge characteristics, addition of significant amount of O_2 to SF_6 discharge could possible suppress additional excitation contribution to fluorine signal as relative [F] measured using actinometry and APMS established good agreement. At higher pressures, fluorine actinometric data was proportional to APMS measurements and thus, fluorine actinometric behaviour was validated. Proportionality constant (K) required for fluorine actinometry, was evaluated and its dependence at different discharge conditions were analysed.

Kinetics behaviour of electrons in O_2 discharge as a function of gas pressure was investigated using Langmuir probe. Discharge transition in oxygen plasma was investigated from pressure evolution of electron energy probability function (EEPF), electron density and temperature. However, structure was observed in measured EEPF for pressure > 400 mTorr at 200 W rf power and EEPF tail found to enhance which violated inverse proportionality between ionization rate and neutral gas density in accordance to particle balance equation. Such unusual EEPF characteristic was caused mainly due to inadequate rf compensation in the probe and unaccounted variations in plasma potential when probe tip was biased. In addition to this, the behaviour of absolute [O] was investigated as a function of gas pressure using actinometry and Langmuir probe. Good agreement was achieved when relative variations of [O] from actinometry were compared to TALIF measurements under similar experimental conditions.

Actinometric technique was successfully validated in monitoring the variations of ground state fluorine and oxygen for discharge pressures $\geq$ 200 mTorr and can be adopted in industry to monitor radical species in processing plasmas. It should be mentioned that optical emissions lines used in this work to monitor [F] and [O] could have significant dissociative contribution at low pressures.

Chapter 1- Introduction and Thesis Motivation

1 Introduction

In gaseous state, significant number of atoms tend to release some or all of their electrons when heated and transform into an ‘ionized’ state. This state is known as plasma, the fourth state of matter [1]. Plasma systems are usually complex as they contain radicals, ions, electrons and metastables. Several mechanisms generate plasmas. The most common techniques used in laboratories using applied electrical power are radio frequency, direct current and microwave. As mentioned earlier, plasmas are complex due to the presence of a range of reactive species. There are numerous reactions at gas-surface interfaces and in the gas phase. The most common applications of plasma include manufacture of micro or nano-sized integrated chips (ICs) in semiconductor industries using plasma processes such as etching, deposition and surface modification [1]. These processes are based on interaction between the gas-phase plasma species and the surfaces or substrates. In most cases, the plasma chemistry in these processes is not clearly interpreted as it involves complex chemical reactions on a molecular level.

Plasma chemistry can be influenced by the various systems variables like gas pressure, gas flow rate, substrate temperature, power applied, reactor - configuration and materials of construction, which were used for process optimization. The outcome of any plasma process would be sensitive to these parameters. Precise control of plasma assisted processes will be important as the industry moving towards nano-sized integrated circuits in accordance with Moore’s law. A major challenge in integrated circuits manufacturing is process drift, dependent on generated plasma species. Process drift can be monitored with the help of plasma diagnostics by measuring the radical densities in the plasma. The radical density in the plasma may be sensitive to small changes in any of the above system variables. The aim of the present research was to develop methodologies to monitor variation in radical density in the plasma across various system variables.

Non-invasive sensors are required for industrial purposes to monitor process drifts through variations in radical density. Validation of such sensors would be essential with more reliable diagnostic techniques. Some of the commonly used reliable diagnostics techniques to measure radical densities include appearance potential mass spectrometry, vacuum ultraviolet absorption spectroscopy and two-photon absorption laser induced fluorescence spectroscopy. However, it may not be practically possible to use these diagnostics with the plasma sources in an industrial environment because these diagnostics would be expensive, time consuming and not feasible to set up. The primary requirements for a sensor to operate in an industrial environment are that it should be economical, easy to use and provide real time information about variations in the process. A sensor used in this work was actinometry which complies with industrial requirements to monitor process drifts in any plasma processes. Actinometry is an optical diagnostic tool that can monitor atomic or molecular density in the plasma using optical emission spectroscopy. The basic principle is to compare the optical intensities of specie of unknown density to species of known density, called actinometer.

In this work, the main focus was to measure fluorine radical density in fluorine-based plasmas as are commonly used to etch SiO_2 and Si layers in modern semiconductor industries. Fluorine atom density can also be measured using the actinometric technique. But it would be relative fluorine density since for absolute measurements, excitation rate constant and electron distribution function must be known. An important motive was to test the validity of actinometry for measurement of fluorine radical density by comparing the results with reliable diagnostic techniques. A reasonable agreement in relative radical density between actinometry and other reliable diagnostic techniques can help to evaluate the proportionality constant required for actinometry to calculate the absolute radical density.

1.1 Capacitively-coupled radio frequency discharge

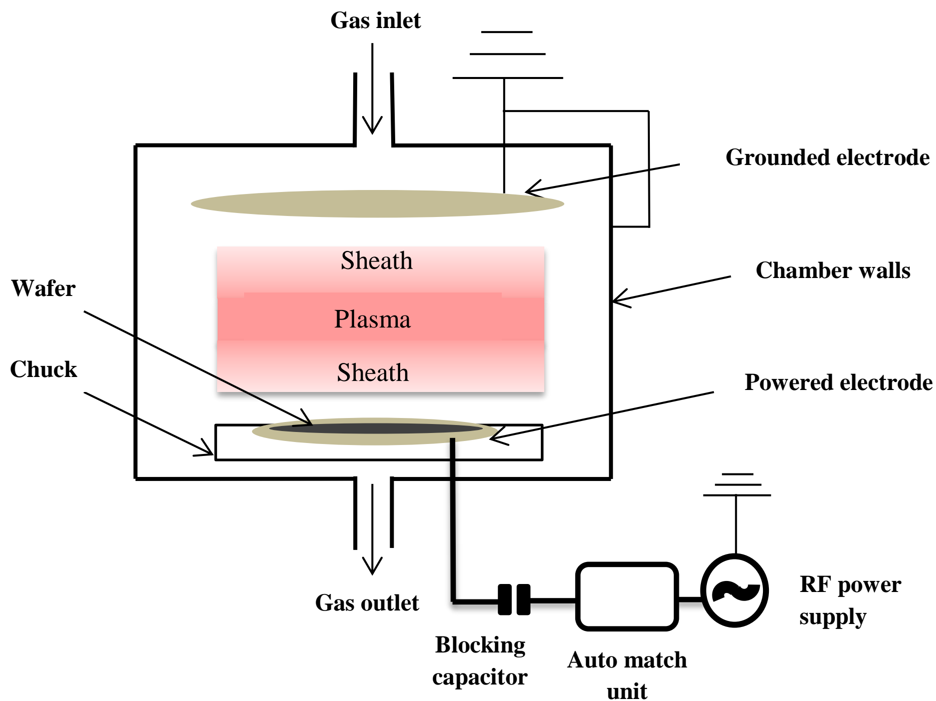

Figure 1.1 Schematic of asymmetric capacitively coupled RF discharge

For more than a decade, capacitively-coupled rf discharges have been commonly used for dry plasma etching in the semiconductor industry. A capacitively-coupled plasma (CCP) reactor usually contains two parallel plate electrodes in a vacuum chamber separated by a finite distance. One of the two electrodes, the driven/powered electrode, would be connected to a power supply and the other grounded electrode as shown in figure 1.1. Reactor walls, usually made from aluminum or stainless steel, would be grounded. CCP discharges are commonly operated at 13.56 MHz driving frequency for anisotropic etching applications with relatively low plasma densities (10^{15}- 10^{17} m^{-3}) [1].

In capacitive discharge, plasma electrons are influenced by electric field produced by applied rf voltage [2]. However, ions are usually less influenced by electric field due to its higher mass and also it would cause electrons to

reach walls or electrode faster than ions. For time varying rf cycle, electrons tends to oscillate to and fro within net positively charged region known as sheath formed near each electrode as shown in figure 1.1. This positive space charge would also prevent the leakage of electrons to the electrode. In CCP discharge, ions from the plasma bulk are accelerated by strong electric field (time-averaged) within the sheath to produce high energetic ions responsible for ion bombardment at the substrate.

CCP discharges usually have two orifices, which would serve as inlet and outlet for the process gas. In this work, the process gas is fed to the reactor through the shower head on the grounded electrode. The flow of gas into the reactor is controlled by mass flow controller during plasma operation. A CCP discharge can be asymmetric if the area of the grounded electrode is different to that of the powered electrode. In the present case, area of the powered electrode area was smaller than the grounded electrode together with walls, resulting in large DC bias voltage at the powered electrode. Such a configuration was known to be "reactive ion etching" (RIE) system involving bombardment of energetic ions and reactive neutral species on a wafer surface placed on powered electrode to obtain high anisotropy and better physical etch. Moreover, CCP used in this work was with RIE configuration. Other configuration used with CCP was "plasma etching" (PE), where substrate to be processed would be placed on grounded electrode. In this plasma dry etching configuration, etching mechanism would be driven by radicals and etching would be in all direction with undercut beneath the mask layer due to Brownian motion of radicals. Thus, it is referred as isotropic etching. For instance, dry etching of Si etching using CF_4 plasma [3].

Most common etching tool used with CCP source would be RIE system and was first investigated by Coburn *et al*., in 1979 [4]. The plasma etch rate was found to increase using RIE configuration due to the influence of energetic positive ions arrive at the surface of the material to be processed along with

reactive free radicals, responsible for chemical etching. Positive ions, which arrive at plasma sheath regions, would be accelerated towards the electrode (where wafer would be located) due to negative DC potential. These influential ions would cause ion bombardment at the surface of the material and etching mechanism by this technique can be described as ion bombardment enhanced etching. However, the ion bombardment depends on ion density in the plasma and also on the ion energy, which would be determined by DC bias voltage. For example, J.W. Coburn *et al.*, [5] experimentally observed Si etch rate was found to be higher using XeF_2 gas with Ar^+ ion beam at 450 eV compared to radical etch (XeF_2 gas only) or physical sputtering with Ar^+ ion beam. Unlike in PE mechanism, RIE etching mechanism would reduce undercut of mask layer to provide high anisotrophy and also good selectivity can be assured. However, effects of etching using RIE can vary depending on the combinations of material to be etched and etch gases employed [6]. Some of the attributes of incoming energetic ions to influence various steps of etching mechanism through ion bombardment would be [7]:

1. Dissociation of molecule adsorbed on surface to provide reactive radicals
2. Provide active sites by breaking Si-Si bond for reactive radicals.
3. Provide energy for chemisorption of reactive radicals with silicon.
4. Rearrange structure of Si atoms to form bonds with reactive radicals.
5. Removal of volatile product formed at the processed surface.

Even though CCP rf discharges are simple to design and manufacture to achieve high density plasma, they suffer from certain limitations. Usually in CCP sources, the energy of the plasma ions and ion flux to the surface of the substrate cannot be varied independently and the ion energy is coupled with the reactive particle density. So, these plasmas would be inadequate for chemical etching process, which would require dense reactive particles in plasma with low ion bombardment. Moreover, at low pressures (to obtain high aspect ratio),

with high mean free path for electrons, CCP discharges would not strike a plasma due to less generation of electrons as there would be very low or no collisions of electrons. However, the value for low pressures depends various parameters like reactor design, gas flow, applied power, feedstock gas etc.

1.2 Plasma sheath

In a plasma discharge, the temperature of electrons would be higher compared to ions temperature and the mass of electrons would be smaller to the mass of ions. Consider quasi-neutral plasma, where electron density (n_e) and ion density (n_i) are nearly the same ($n_e \approx n_i$), confined by absorbing walls. In this situation more electrons would be rapidly accelerated towards the walls than ions and can be lost. This is because of high energy (gained by electric field) and smaller mass of electrons, and obviously, the electrons would have larger thermal velocity than the ions. This consequently would lead to imbalance in their fluxes, whenever the plasma comes in contact with the electrode, which would be charged negatively. A positive potential would be produced in the bulk due to rapid loss of electrons to the walls. And now the bulk of the plasma would be quasi-neutral and a region found adjacent to the electrode where $n_i \gg n_e$. This dark region would usually be termed as sheath. The plasma contacts the wall surfaces across the sheath, which would be positively charged thin layer. The sheath region potential continues to grow until a steady state is reached and a balance is established between electron and ion fluxes. In this region, the quasi-neutrality condition is violated as only more energetic electrons can enter the sheath. Close to the wall surface, the positive potential falls sharply because of an imbalance of charged particle in sheath region.

In a lower pressure RF discharge the behavior of the sheath would be different from DC discharge. When an RF voltage or current was applied to an electrode, quasi-neutrality would be violated near the electrode within the sheath. Electrons, being lighter, respond to time varying electric field produced by RF

driving voltage and the ions, being heavier, can only respond to time-averaged potential [1]. This would result in a net positive charge in the sheath region on each electrode when averaged over oscillation period. In the sheath, the current that flows can be entirely displacement current due to time varying electric field. And it can be true because plasma bulk was sustained by conduction current carried mainly by electrons and within the time varying sheath, the electron density would be approximately zero.

Electrons can reach the electrode only if the sheath voltage was low and this would happen at a fraction of RF cycle. In this situation, quasineutrality is maintained as the escaped electrons were balanced by the ions lost to the walls. Sheath oscillations, typical in RF discharge, can be important to sustain the discharge at low-pressures [1] and also create an important source of energy for the electrons. At low-pressures, the sheath tends to expand and contract; on average there will be energy gain by the electrons in the sheath. The energy gained by these electrons cause further ionization to sustain the discharge. This would be an important collisionless electron heating mechanism in low pressure plasmas and has been investigated elsewhere [8-10].

1.3 Radical species in plasma etch process

Reactive plasma discharges are most widely used in semiconductors industries for various plasma based applications in manufacturing the large scale integrated circuits [1]. For example, sub-micrometer features on a large area wafer surface with high aspect ratios are being developed using high density plasma reactors through plasma etch processes. Some of the other challenges in plasma etch process can be process uniformity, selectivity and etch profile (anisotropic/isotropic). In recent decade, anisotropic profile currently being essential in etch process because of reduction in feature sizes and spacings; also, undercut would be no longer acceptable which would be common in

isotropic profile. These parameters are studied through the etch rate, which primarily depend on density of radical species in the plasma.

Radicals are neutral particles (no net charge) and can exist in a state of incomplete chemical bonding. They are mostly formed by dissociation of their parent molecule on colliding with energetic electrons. The radicals in the plasma are responsible for dry etching process. They react with the substrate, yielding a volatile etch product, so that it can be removed by pumping. The density of these radicals (reaching the substrate) controls the etching, which can be monitored through a parameter called etch rate. The density of the radical species in the plasma can be controlled through the gas flow, gas pressure and RF power. The concentration of the radical species depends on the wall sticking co-efficient. The sticking co-efficient can be defined as the ratio of atoms reaching the wall surface that adsorb or recombine to all atoms striking the walls. The sticking co-efficient primarily depends on the wall surface material, surface/gas temperatures and surface impurities. During plasma etching processes (wafer after wafer), the reactor walls would usually get coated with etched products and can cause "non-perfect reproducible" reactor walls conditions [11]. Thus changes in reactor wall conditions are an important cause of process drifts [12-14], which cause significant negative impact on etch rates, etch profile, selectivity or uniformity across a wafer to be processed. The modified chamber wall conditions due to deposition of etch products will lead to decrease in reactive species in the plasma, which can be lost to the walls [15, 16]. Thus, insight into on variations in reactive particle density in the plasma chamber can provide better understanding about the performance of the plasma etch processes.

1.4 Motivation of this work

Production of broad range of species such as charged particles and free radicals has made reactive plasmas attractive for nanoscale applications. Fluorocarbon,

SF_6, O_2 and other halogenated gas molecules were most common process gases used in reactive plasmas due to their high reactivity. Major developments in plasma etching technology for semiconductor device fabrication had been reviewed by H. Abe *et al*., [17]. Need for reactive etching and their applications along with advantage over conventional wet etching were analyzed. Basic features of reactive plasmas and their potential importance in nanofabrication processes were discussed by K. Ostrikov [18] using "cause and effect" approach. Based on the above reviews in reactive plasmas, production of neutrals along with charged species were found to be crucial in plasma-assisted etching processes and knowledge on their individual concentrations were indispensable to improve capability of nanofabrication for high anisotropy, high selectivity, high uniformity and profile control of the wafer. Fluorocarbon plasmas involving gases such as CF_4, C_2F_6, C_4F_8 and CHF_3 are mostly preferred to etch dielectric materials in the manufacture of silicon ICs. Oxygen was often added with any of these gases to promote CO_2 formation through which the degree of polymerization, essential for process selectivity, can be controlled. Over the years, numerous investigations were performed in fluorocarbon plasmas in various sources to understand the behavior of radicals like F, CF, CF_2 and charged species using different diagnostic tools [19-23]. Unfortunately, fluorocarbon plasmas can result in excess deposition of residual fluorocarbon film on the substrate and this could significantly affect the rate of etching in Si/SiO_2 [24]. An obvious alternative for fluorocarbon to produce fluorine-rich environment would be SF_6, which was known to provide better etch rates than CF_4 [25] and no residual film formation [1, 26] on the substrate. Also for deep Si etching applications, SF_6 or SF_6 based plasmas were commonly used to fabricate micro-electro-mechanical systems (MEMS) [27-30]. Fluorine atoms produced in SF_6 discharges are found to be vital in governing the etch rate, as they react with Si to form volatile SiF_4 molecule in the etch process. Thus, fluorine atom concentration critically affects the etching process.

Several experimental diagnostic approaches have been employed to measure the variation of fluorine atom density as a function of various discharge conditions. K. Sasaki *et al*., [31, 32] determined the ground state fluorine atom concentration in reactive plasmas using vacuum ultraviolet (VUV) absorption spectroscopy. This technique requires a light source to generate fluorescence at ≈ 95 nm for probe emission. Due to unavailability of commercial light source to generate ultraviolet radiation at ≈ 95 nm, a low power, and low pressure electron-cyclotron resonance plasma was used as light source for this absorption measurement. K. Tachibana *et al*., [33] also measured absolute F atom density using vacuum-ultraviolet laser absorption technique in inductively coupled radio-frequency (400 kHz) discharge. A VUV tunable laser was used as light source to generate F atom resonance lines around 95 nm using Xe gas by a two-photon resonance four-wave-mixing technique. However, VUV absorption technique was not extended to investigate F atom density in SF_6 plasmas, probably due to (a) large uncertainties in transition probability, (b) large errors associated with assumption of emitting F atoms temperature from light source, (c) underestimation of F atom densities due to distortion of spectral distribution due to self-absorption and excitation of F atoms through dissociative process in the light source [34]. J. W. Coburn *et al*., [35] investigated the discharge condition dependence on F atom density in fluorocarbon discharge using emission spectroscopy. Only relative F atom density was monitored using emission lines of fluorine and argon with certain limitations. Another well-known diagnostic technique to measure ground state fluorine atom was using mass spectrometry. Fortunately, this technique was not limited by energy level like optical diagnostics. However, this technique can attract large background signals due to production of radicals through dissociative ionization and decomposition by filaments with high temperatures [36]. K. Nakumura *et al*., [37] showed that signal to noise ratio can be improved with help of cooling liquid nitrogen trap installed in a mass spectrometer. Mass spectrometers operated with different pumping stages and

mechanical chopper were also found to improve beam to background signal ratio [36, 38]. With improved beam to background signal ratio, ground state fluorine atom concentration was measured with great reliability in fluorocarbon discharges using mass spectrometer [37, 39, 40]. However, measurement of absolute F atom density calibrated using dissociative ionization signal can attract significant error due to Frank-Condon effect [41]. Fortunately, knowledge on mass dependent instrument response parameters of mass spectrometer obtained using different gases of known density can serve an alternate calibration procedure for absolute measurements [42, 43].

Numerous experimental [44-50] and numerical [51-56] investigations have been performed in SF_6 or SF_6 based plasmas. However, only limited studies on SF_6 or SF_6 based plasmas can be found in the literature using capacitively coupled plasma source [57, 58] and no absolute F atom density measurement was reported in both these studies. Only recently, S. Kechkar *et al.*, [59] investigated the power variation of absolute F-atom density in capacitively coupled reactor (used in this work) using SF_6/Ar and SF_6/O_2/Ar feedstock mixtures. The primary motivation was to investigate variation of absolute F atom concentration using reliable diagnostics like mass spectrometry in capacitively coupled SF_6/O_2/Ar discharge under various operating conditions such as gas pressure, effect of O_2 concentration and applied rf power. With this knowledge on atomic fluorine density in capacitive discharge, optimization of etching process in deep Si etch can be supportive. This work also aimed to develop a non-invasive, low foot print diagnostic tool to monitor real time variation of F atom density to account for any process drift in an industrial environment.

Knowledge on electron kinetics would be essential, especially in low pressure discharges to understand the variations of plasma parameters like electron density, electron temperature and electron energy distribution. Electrical probes are common diagnostic tools to investigate kinetic behavior of electrons.

Godyak *et al*., [60] insisted that determination of plasma parameters in a typical low pressure discharge with assumption of Maxwellian energy distribution may lead to significant error in measurements, as these plasmas usually in non-equilibrium, can exhibit non-Maxwellian characteristics. S. Kechkar *et al*., [61] carried out an extensive investigation of electron kinetics in O_2 capacitive discharge (used in this work) using Langmuir probe diagnostic tool. Rate of ionization was found to increase, beyond a threshold condition, with gas pressure due to enhancement in tail of electron energy distribution and this unusual electron behavior was not obvious. Such uncharacteristic distribution function of electrons motivated to carry out further investigation in O_2 capacitive discharge to understand the exact mechanism responsible for enhancement of ionization tail with gas pressure.

1.5 Thesis outline

This section briefly outlines the thesis structure comprised of seven chapters in total. Basic fundamentals of plasma are discussed in chapter 1. In addition to this, an introduction to CCP discharges is provided and importance of RIE is discussed. This chapter also provided basic knowledge on plasma sheath and role of radical species in plasma. Motivation of this research work was discussed in the last part of this introduction chapter.

Different plasma diagnostic tools employed in this work are presented in chapter 2. Basic principle of operation and experimental arrangements were discussed for each diagnostic technique used in this work. Calibration procedure, wherever necessary, for diagnostic technique was provided in this work.

Role of O_2 addition to SF_6 discharge was discussed in chapter 3. Absolute fluorine atom density was studied as function of O_2 content in the discharge using reliable diagnostic technique. For applicability of industrial sensor,

variations of fluorine density measured with sensor for conditions investigated in this chapter were compared to reliable diagnostic method.

A variation of absolute fluorine density as function of gas pressure was investigated in chapter 4 and for sensor validation; absolute measurements were compared to optical based diagnostic technique. Also discussed are pressure dependent discharge characteristics studied using I-V probe. Based on discharge characteristic, dissociative excitation contribution to fluorine emission line was investigated and improvement to fluorine actinometry was proposed.

Power variation of absolute fluorine density is investigated in chapter 5 and also the validity of fluorine actinometry was verified. The proportionality constant required for fluorine actinometry was investigated and its dependence on different discharge condition is discussed.

Kinetic behavior of electrons as function of pressure in O_2 discharge was investigated in chapter 6 and plasma parameters were computed from measured electron energy distribution function. Investigation was further extended to understand the exact mechanism responsible for unusual structure in measured electron energy probability function. The last part of this chapter investigated the variation of absolute oxygen density as function of gas pressure measured in O_2/Ar discharge using improved oxygen actinometry with excitation rates obtained from measured electron energy distribution function using Langmuir probe measurements.

Concluding remarks of this research work was presented in chapter 7 along with the scope of future work.

1.6 References

[1] Lieberman, M.A. and Lichtenberg, A.J., (2005), *Principles of Plasma Discharges and Materials Processing, 2nd Edition, .*

[2] Raizer, Y.P., Shneider, M.N.and Yatsenko, N.A., (1995*), Radio-frequency capacitive discharges,* , CRC Press,.

[3] Horiike, H. 1981,*Proc. 19th Semiconductor Technology Seminar,* 193.

[4] Coburn, J.and Winters, H.F., (1979), "Plasma etching—A discussion of mechanisms", *Journal of Vacuum Science & Technology,* Vol.16 (2), pp. 391-403.

[5] Coburn, J.and Winters, H.F., (1979), "Ion-and electron-assisted gas-surface chemistry—An important effect in plasma etching", *J.Appl.Phys.,* Vol.50 (5), pp. 3189-3196.

[6] Nojiri, K., (2014*), Dry etching technology for semiconductors,* , Springer,.

[7] Joosten, G., et al. (1994), "Dynamics of ion-assisted etching in the Si (100)/XeF2/Ar system on a time scale 100 μs–1000 s", *Journal of Vacuum Science & Technology A,* Vol.12 (3), pp. 636-647.

[8] Turner, M. (1993), "Collisionless electron heating in an inductively coupled discharge", *Phys.Rev.Lett.,* Vol.71 (12), pp. 1844.

[9] Turner, M. (1995), "Pressure heating of electrons in capacitively coupled rf discharges", *Phys.Rev.Lett.,* Vol.75 (7), pp. 1312.

[10] Turner, M.M. (2009), "Collisionless heating in radio-frequency discharges: a review", *J.Phys.D,* Vol.42 (19), pp. 194008.

[11] Cunge, G., et al. (2005), "New chamber walls conditioning and cleaning strategies to improve the stability of plasma processes", *Plasma Sources Sci.Technol.,* Vol.14 (3), pp. 599.

[12] Xu, S., et al. (2001), "Characteristics and mechanism of etch process sensitivity to chamber surface condition", *J.Vac.Sci.Technol.B,* Vol.19 (1), pp. 166-171.

[13] Ullal, S.J., et al. (2002), "Effect of chamber wall conditions on Cl and Cl-2 concentrations in an inductively coupled plasma reactor", *Journal of Vacuum Science & Technology A-Vacuum Surfaces and Films,* Vol.20 (1), pp. 43-52.

[14] Cunge, G., Joubert, O.and Sadeghi, N., (2003), "Enhancement of the recombination rate of Br atoms by CF 4 addition and resist etching in HBr/Cl 2/O 2 plasmas", *J.Appl.Phys.,* Vol.94 (10), pp. 6285-6290.

[15] Joubert, O., et al. (2004), "Monitoring chamber walls coating deposited during plasma processes: Application to silicon gate etch processes", *Journal of Vacuum Science & Technology a,* Vol.22 (3), pp. 553-563.

[16] Ullal, S.J., et al. (2002), "Formation and removal of composite halogenated silicon oxide and fluorocarbon films deposited on chamber walls during plasma etching of multiple film stacks", *Journal of Vacuum Science & Technology B,* Vol.20 (5), pp. 1939-1946.

[17] Abe, H., Yoneda, M.and Fujiwara, N., (2008), "Developments of plasma etching technology for fabricating semiconductor devices", *Japanese Journal of Applied Physics,* Vol.47 (3R), pp. 1435.

[18] Ostrikov, K. (2005), "Colloquium: Reactive plasmas as a versatile nanofabrication tool", *Reviews of modern physics,* Vol.77 (2), pp. 489.

[19] Mogab, C., Adams, A.and Flamm, D.L., (1978), "Plasma etching of Si and SiO2—the effect of oxygen additions to CF4 plasmas", *J.Appl.Phys.,* Vol.49 (7), pp. 3796-3803.

[20] d'Agostino, R., et al. (1981), "Spectroscopic diagnostics of CF4-O2 plasmas during Si and SiO2 etching processes", *J.Appl.Phys.,* Vol.52 (3), pp. 1259-1265.

[21] Cunge, G.and Booth, J., (1999), "CF2 production and loss mechanisms in fluorocarbon discharges: fluorine-poor conditions and polymerization", *J.Appl.Phys.,* Vol.85 pp. 3952-3959.

[22] Booth, J., et al. (1999), "CFx radical production and loss in a CF4 reactive ion etching plasma: fluorine rich conditions", *J.Appl.Phys.,* Vol.85 pp. 3097-3107.

[23] Singh, H., Coburn, J.and Graves, D.B., (2001), "Measurements of neutral and ion composition, neutral temperature, and electron energy distribution function in a CF4 inductively coupled plasma", *Journal of Vacuum Science & Technology A,* Vol.19 (3), pp. 718-729.

[24] Chabert, P., Boswell, R.and Davis, C., (1998), "Investigation of a SF 6 helicon plasma", *Journal of Vacuum Science & Technology A: Vacuum, Surfaces, and Films,* Vol.16 (1), pp. 78-86.

[25] Tachi, S., Tsujimoto, K.and Okudaira, S., (1988), "Low-temperature reactive ion etching and microwave plasma etching of silicon", *Appl.Phys.Lett.,* Vol.52 (8), pp. 616-618.

[26] Eisele, K. (1981), "SF 6, a preferable etchant for plasma etching silicon", *J.Electrochem.Soc.,* Vol.128 (1), pp. 123-126.

[27] Khan, F.and Adesida, I., (1999), "High rate etching of SiC using inductively coupled plasma reactive ion etching in SF~ 6-based gas mixtures", *Appl.Phys.Lett.,* Vol.75 (15),.

[28] Chabert, P., et al. (2000), "High rate etching of 4H–SiC using a SF6/O2 helicon plasma", *Appl.Phys.Lett.,* Vol.76 (16), pp. 2310-2312.

[29] Aachboun, S.and Ranson, P., (1999), "Deep anisotropic etching of silicon", *Journal of Vacuum Science & Technology A,* Vol.17 (4), pp. 2270-2273.

[30] Marcos, G., Rhallabi, A.and Ranson, P., (2004), "Topographic and kinetic effects of the SF6/O2 rate during a cryogenic etching process of silicon", *Journal of Vacuum Science & Technology B,* Vol.22 (4), pp. 1912-1922.

[31] Sasaki, K., Kawai, Y.and Kadota, K., (1999), "Determination of fluorine atom density in reactive plasmas by vacuum ultraviolet absorption spectroscopy at 95.85 nm", *Rev.Sci.Instrum.,* Vol.70 (1), pp. 76-81.

[32] Sasaki, K., et al. (1998), "Absolute density and reaction kinetics of fluorine atoms in high-density c-C_4F_8 plasmas", *J.Appl.Phys.,* Vol.83 (12), pp. 7482-7487.

[33] Tachibana, K.and Kamisugi, H., (1999), "Vacuum-ultraviolet laser absorption spectroscopy for absolute measurement of fluorine atom density in fluorocarbon plasmas", *Appl.Phys.Lett.,* Vol.74 (16), pp. 2390-2392.

[34] Sasaki, K., Kawai, Y.and Kadota, K., (1997), "Vacuum ultraviolet absorption spectroscopy for absolute density measurements of fluorine atoms in fluorocarbon plasmas", *Appl.Phys.Lett.,* Vol.70 (11), pp. 1375-1377.

[35] Coburn, J.and Chen, M., (1981), "Dependence of F atom density on pressure and flow rate in CF 4 glow discharges as determined by emission spectroscopy", *Journal of Vacuum Science and Technology,* Vol.18 (2), pp. 353-356.

[36] Agarwal, S., et al. (2004), "Measurement of absolute radical densities in a plasma using modulated-beam line-of-sight threshold ionization mass spectrometry", *Journal of Vacuum Science & Technology A,* Vol.22 (1), pp. 71-81.

[37] Nakamura, K., Segi, K.and Sugai, H., (1997), "Absolute fluorine atom densities in fluorocarbon high-density plasmas measured by appearance mass spectrometry", *Japanese journal of applied physics,* Vol.36 (4A), pp. L439.

[38] Singh, H., Coburn, J.W.and Graves, D.B., (1999), "Mass spectrometric detection of reactive neutral species: Beam-to-background ratio", *Journal of Vacuum Science & Technology A,* Vol.17 (5), pp. 2447-2455.

[39] Schwarzenbach, W., et al. (1997), "Mass Spectrometric Detection of F Atoms and CFx Radicals in CF 4 Plasmas", *Japanese journal of applied physics,* Vol.36 (7S), pp. 4644.

[40] Tserepi, A., et al. (1997), "Kinetics of F atoms and fluorocarbon radicals studied by threshold ionization mass spectrometry in a microwave CF4 plasma", *Journal of Vacuum Science & Technology A,* Vol.15 (6), pp. 3120-3126.

[41] Singh, H., Coburn, J.and Graves, D.B., (2000), "Appearance potential mass spectrometry: Discrimination of dissociative ionization products", *Journal of Vacuum Science & Technology A,* Vol.18 (2), pp. 299-305.

[42] Benedikt, J., et al. (2005), "Threshold ionization mass spectrometry of reactive species in remote Ar/ C2H2 expanding thermal plasma", *Journal of Vacuum Science & Technology A,* Vol.23 (5), pp. 1400-1412.

[43] Pulpytel, J., Arefi-Khonsari, F.and Morscheidt, W., (2005), "Threshold ionization mass spectrometry study of singlet molecular oxygen in the deposition of SnO2 by PACVD", *J.Phys.D,* Vol.38 (9), pp. 1390.

[44] Picard, A., Turban, G.and Grolleau, B., (1986), "Plasma diagnostics of a SF6 radiofrequency discharge used for the etching of silicon", *J.Phys.D,* Vol.19 (6), pp. 991.

[45] d'Agostino, R.and Flamm, D.L., (1981), "Plasma etching of Si and SiO2 in SF6–O2 mixtures", *J.Appl.Phys.,* Vol.52 (1), pp. 162-167.

[46] Petrović, Z.L., et al. (1993), "Spatiotemporal Optical Emission Spectroscopy of rf discharges in SF6", *J.Appl.Phys.,* Vol.73 (5), pp. 2163-2172.

[47] Wagner, J.J.and Brandt, W.W., (1981), "DC plasma etching of silicon by sulfur hexafluoride. Mass spectrometric study of the discharge products", *Plasma Chem.Plasma Process.,* Vol.1 (2), pp. 201-215.

[48] Rudenko, K., Myakon'kikh, A.and Orlikovsky, A., (2007), "Plasma etching of poly-Si/SiO2/Si structures: Langmuir-probe and optical-emission-spectroscopy monitoring", *Russian Microelectronics,* Vol.36 (3), pp. 179-192.

[49] Saloum, S., Akel, M.and Alkhaled, B., (2009), "Diagnostic and processing in SF6 RF remote plasma for silicon etching", *J.Phys.D,* Vol.42 (17), pp. 175206.

[50] Pessoa, R., et al. (2010), "Study of SF6 and SF6/O2 plasmas in a hollow cathode reactive ion etching reactor using Langmuir probe and optical emission spectroscopy techniques", *Plasma Sources Sci.Technol.,* Vol.19 (2), pp. 025013.

[51] Ryan, K.and Plumb, I., (1990), "A model for the etching of silicon in SF6/O2 plasmas", *Plasma Chem.Plasma Process.,* Vol.10 (2), pp. 207-229.

[52] Kline, L. (1986), "Electron and chemical kinetics in the low-pressure RF discharge etching of silicon in SF6", *IEEE Trans.Plasma Sci.,* Vol.14 (2), pp. 145-155.

[53] Anderson, H., Merson, J.and Light, R., (1986), "A kinetic model for plasma etching silicon in a SF6/O2 RF discharge", *IEEE Trans.Plasma Sci.,* Vol.14 (2), pp. 156-164.

[54] Riccardi, C., et al. (2000), "Modeling and diagnostic of an SF 6 RF plasma at low pressure", *IEEE Trans.Plasma Sci.,* Vol.28 (1), pp. 278-287.

[55] Kokkoris, G., et al. (2009), "A global model for SF6 plasmas coupling reaction kinetics in the gas phase and on the surface of the reactor walls", *J.Phys.D,* Vol.42 (5), pp. 055209.

[56] Lallement, L., et al. (2009), "Global model and diagnostic of a low-pressure SF6/Ar inductively coupled plasma", *Plasma Sources Sci.Technol.,* Vol.18 (2), pp. 025001.

[57] Kopalidis, P.M.and Jorne, J., (1992), "Langmuir Probe Measurements and Characterization of Silicon Etching in SF 6/O 2 Discharges", *J.Electrochem.Soc.,* Vol.139 (3), pp. 839-844.

[58] Khairallah, Y., Khonsari-Arefi, F.and Amouroux, J., (1994), "Decomposition of gaseous dielectrics (CF4, SF6) by a non-equilibrium plasma. Mechanisms, kinetics, mass spectrometric studies and interactions with polymeric targets", *Pure and applied chemistry,* Vol.66 (6), pp. 1353-1362.

[59] Kechkar, S., et al. (2014), "Investigation of absolute atomic fluorine density in a capacitively coupled SF6/O-2/Ar and SF6/Ar discharge", *Plasma Sources Science & Technology,* Vol.23 (6), pp. 065029.

[60] Godyak, V., Piejak, R.and Alexandrovich, B., (1993), "Probe diagnostics of non-Maxwellian plasmas", *J.Appl.Phys.,* Vol.73 (8), pp. 3657-3663.

[61] Kechkar, S. (2015), "Experimental investigation of a low pressure capacitively-coupled discharge", *PhD Thesis, School of Physical Sciences, Dublin City University,* .

Chapter 2- Experimental tools and diagnostic techniques

In the previous introductory chapter, the role of radical species in plasma based surface processes for nano-fabrication of ICs was discussed. For precise control of surface processes, it is always vital to quantify atomic radical species concentration in any plasma based discharges. As mentioned in previous chapter, this research work mainly focuses to quantify densities of atomic fluorine and oxygen in SF_6 and O_2 based discharges respectively. Several diagnostic techniques have been successfully employed to investigate atomic radical concentration in fluorine and oxygen based plasma discharges.

Absolute measurement of fluorine atom concentrations has been investigated using VUV absorption spectroscopic technique in fluorocarbon plasma discharges [1-3]. However, this technique was not extended to measure atomic fluorine density in SF_6 based discharges and could be due to large errors associated with measurements [2, 3]. Herring *et al* [4] measured atomic fluorine concentration using two-photon absorption laser-induced fluorescence spectroscopy (TALIF), by combining commercial dye lasers with stimulated Raman scattering in H_2 to generate probe radiation at 170 nm region for fluorine atom detection. But Herring investigated fluorine atoms generated by laser photolysis of F_2 using TALIF and not in plasma discharge [4]. Another diagnostic technique successfully been used to measure absolute fluorine atom density is appearance potential mass spectrometry (APMS) [5-8]. At some instances, signal to noise ratio monitored using this technique can be large due to significant contribution from dissociative ionization of the parent specie [5]. However, S. Kechkar *et al* [9] had successfully investigated variations of absolute atomic fluorine density with applied rf power in capacitively coupled SF_6 based discharge. Unfortunately for an industrial application, this tool has certain drawbacks such as intrusive nature, large foot print and time consumption. Optical emission spectroscopy (OES) is most commonly used non-intrusive, low foot print tool in industry for real time monitoring of radical density variations in plasma discharge. However, only relative variations of

atomic species density can be monitored using OES and for absolute measurements, OES has to be combined with other diagnostics like Langmuir probe, Interferometer.

In this research work, APMS technique was used to investigate variations of absolute atomic fluorine density in SF_6 based capacitively coupled plasma (CCP) discharge (discussed in section 2.1) at different operating conditions. These absolute fluorine density measurements were used as benchmark results for OES measurements. In this chapter, basic principles and operation of mass spectrometer was discussed in section 2.2 and theory of APMS technique along with calibration procedure to obtain absolute density of atomic fluorine atoms was presented in section 2.2.1. Section 2.3 includes basic theory of OES, actinometry and operations of sensors used in this work. In the final section of this chapter, different probe techniques used in this work to study kinetic behaviour of electrons in this discharge was discussed.

2.1 Reactive ion etcher - Plasmalab system 100

An Oxford instruments Plasmalab system 100 [10] was used in this work to investigate the behavior of radical species and electron kinetics. Figure 2.1 shows the schematic of rf excited (13.56 MHz) parallel plate capacitively-coupled plasma, CCP source used in this work. It consists of lower powered/driven electrode and grounded electrode of diameters 205 mm and 295 mm respectively with a 50 mm separation gap (without quartz plate). The wafers to be processed were placed on the powered electrode and can process 200 mm wafers. The RF voltage, from the RF power supply, was applied to the powered electrode through an auto-match unit. This unit balances the impedance between the power supply output and the load and ensures an effective power transfer between the power supply and plasma. The feedstock gases from the mass flow controller (MFC) unit were fed to the chamber through the shower-head provided on the grounded electrode. The reactor walls

and electrodes are made of aluminium alloy (6082) with aluminium in large proportion. An automatic variable throttle valve was located beneath the powered electrode to maintain input pressure. An Alcatel (ATP400HPC) turbo-molecular pump, with a pumping speed of 400 l/s, was used to evacuate the chamber and it was backed by an Alcatel rotary pump with a pumping speed of 6 l/s. The MKS (627B-15968) capacitance manometer and Edwards cold cathode ionization (Edwards AIM-S-NW25) pressure gauges were used with this chamber to measure the process pressure and the base pressure (4.5×10^{-5} to 5×10^{-6} Torr) respectively. Efficient rf power coupling to the plasma was ensured by automatic matching network located between the rf generator and electrode. Four UV graded optical view ports made of quartz were provided; of which, three, with 40 mm diameter, were located on the radial inner bore of the chamber and one, with 10 mm diameter was located on axial center of the chamber.

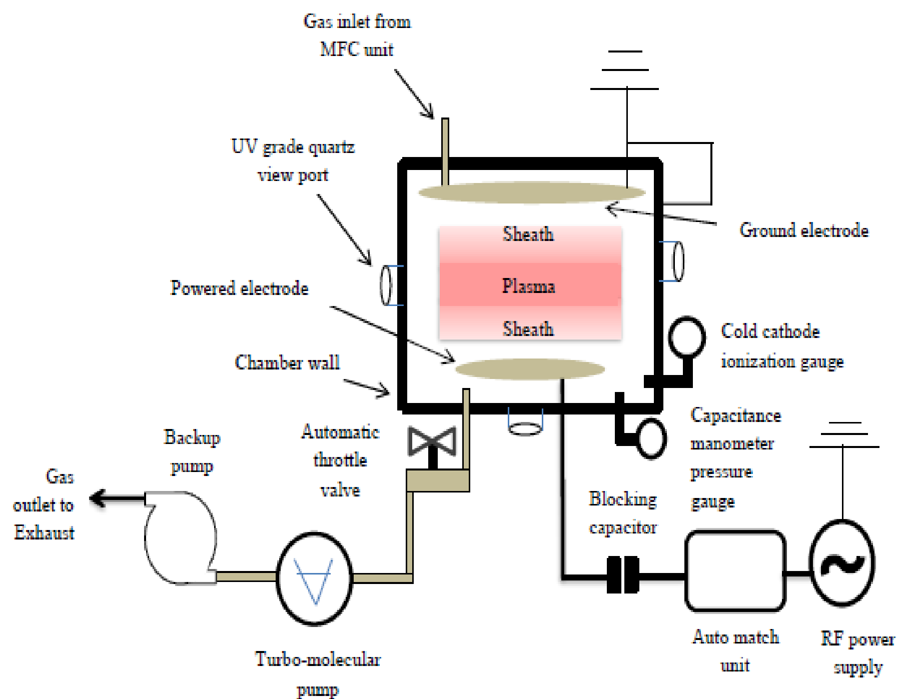

Figure 2.1 Schematic of Oxford instruments Plasmalab system 100

2.2 Mass spectrometry

Mass spectrometry (MS) is one of the powerful diagnostic tools for measuring density of radicals (neutrals) specie and charged species in the plasma. It measures the composition of unknown gas by ionizing the gas and detects it based on their mass to charge ratios. A typical mass spectrometer will consist of an ionizing chamber, mass analyzer and detector. Neutral species enter the ionizing chamber through a small orifice and are ionized through the filaments, which produce an electron beam in the ionization chamber. These filaments can be operated at fixed or variable energies depending on operation type. A mass spectrometer can also be called residual gas analyzer (RGA) if operated in this manner. Ionized species were transferred to the mass analyzer through an electrostatic lens and separated based on their mass to charge (*m/z*) ratios. Quadrupole mass filter can be used as the mass analyzer to identify species based on their masses. A quadrupole mass filter consists of four parallel metal rods (electrodes). A potential of $(U+V\cos(\omega t))$ is applied to two opposite rods and potential of $-(U+V\cos(\omega t))$ to the other two rods, where U is a dc voltage and $V\cos(\omega t)$ is a ac voltage. The trajectories of ions in the filter can be altered by varying the ac and dc voltages. Only selected ions with a certain mass to charge ratios can pass through the mass filter and reach the detector; other ions would move out of trajectory and collide with the rods. This kind of mass spectrometer is known as quadrupole mass spectrometer (QMS). Ions passing successfully the mass analyzer will reach the secondary electron multiplier (SEM) for detection. SEM was operated at high voltage and resulting current was converted to mass spectrometer signal. Figure 2.2 shows the schematic of mass spectrometer used in RGA mode.

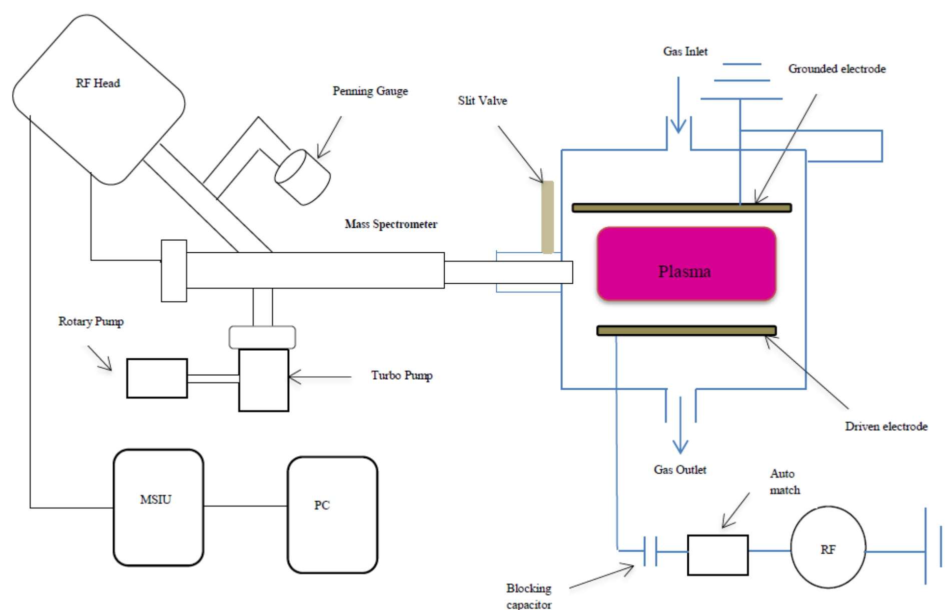

Figure 2.2 Schematic of Hiden Analytical mass spectrometer EQP 300

The mass spectrometer used in this work was an EQP 300 from Hiden Analytical. It was a commercial mass spectrometer with a quadrupole type filter. It can be used to detect neutral and ion (positive/negative) species by switching between RGA and Secondary ion mass spectrometry (SIMS) mode respectively. The sampling head of the MS can be inserted directly into the plasma region in this series of mass spectrometer. As the sensitive probe was enclosed within a metal enclosure, this arrangement allowed the sampling head to be inserted directly into the plasma region. The ionization source was located ≈ 2 – 3 cm behind the orifice; this would reduce the background signal for good sensitivity. The orifice on the sampling head was 150 μm in diameter. Plasma was generated using 13.56 MHz RF excited capacitively-coupled plasma source. A variable gate valve was used to control the chamber pressure. Neutrals generated in the plasma enter the mass spectrometer through the orifice and then pass into the ionization chamber. Filaments generated an electron beam to ionize the neutrals. These ionized species were directed to triple filter quadruple mass analyser using electrostatic lenses where they were

filtered with respect to their mass to charge ratio. Secondary electron multiplier (SEM) was used to detect the ions.

2.2.1 Appearance potential mass spectrometry and calibration procedure

The appearance potential mass spectrometry (APMS) technique was used to measure the density of neutral species based on their threshold ionization potential. In this work, APMS was used to measure the atomic fluorine and argon densities in the plasma discharge. APMS ionizes neutrals with selective electron energies whereas fixed electron energy (usually 70 eV) was used in RGA mode to ionize neutrals. The atomic fluorine density was measured based on the production of atomic fluorine ions, F^+ ions (*m/e = 19*) created within the ionization source of the mass spectrometer. F^+ ions can be created by various processes and each has different appearance potentials, ε_x. as shown below:

$$F + e \rightarrow F^+ + 2e, \quad \varepsilon_1 = 15.5 \text{ eV [11]} \qquad (2.1)$$

$$F_2 + e \rightarrow F^+ + F + 2e, \quad \varepsilon_2 = 21.0 \text{ eV [12]} \qquad (2.2)$$

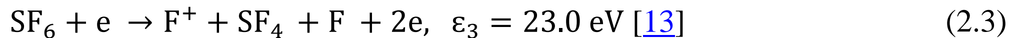

$$SF_6 + e \rightarrow F^+ + SF_4 + F + 2e, \quad \varepsilon_3 = 23.0 \text{ eV [13]} \qquad (2.3)$$

In this work, the interest was on the density of ground state fluorine atom density and that can be measured using F^+ ions produced by direct ionization of fluorine atom as in process 2.1. F^+ ions produced by processes 2.2 and 2.3 is usually termed as dissociative ionization. In case of fixed electron energy (70 eV in RGA), it would be difficult to measure absolute ground state fluorine atom density. In APMS, atomic fluorine species were ionized with selective electron energies and which allowed direct measurement of ground state fluorine atom density. The electron energy scans were performed between the threshold energies of processes 2.1 and 2.2 as the energy separation between these potentials was sufficiently large with respect to FWHM of the Gaussian energy distribution of the ionizing electrons. In figure 2.3, three F^+ ion signals vs electron energy were shown with 0.1 eV energy resolution for reliable

measurements; plasma on signal, M_{ON} (ε), background or plasma off signal, M_{OFF} (ε), and the residual signal, M_{RES} (ε). As fluorine atoms or fluorine containing molecules usually be reactive in nature and can get adsorbed by reacting with inner surfaces of the mass spectrometer. It is possible that F^+ ion signals can be detected, with no gas flow, due to desorbed fluorine atoms from the inner surfaces. This signal can be referred as residual signal, M_{RES} (ε). These adsorbed fluorine atoms or fluorine containing molecules can be a primary source of contamination in the mass spectrometer. Due to this contamination and the nature of experiments, the residual signal can increase. The signal obtained for discharge operated at 40 mTorr $SF_6/O_2/Ar$ (85/10/5 %) with the RF power off was referred as background or plasma off signal, M_{OFF} (ε). There can be many possibilities for this background F^+ ion signal. One such can be caused by thermal pyrolysis of SF_6 molecules on the filaments, which could produce fluorine radicals that can be ionized and detected as F^+ ion signal. This background signal superimpose on the signal produced by fluorine atoms emanating from the plasma. Neutral dissociation from SF_6 can also contribute to background signal i.e. $\mathrm{SF_6 + e \rightarrow F + SF_5 + e}$ and $\mathrm{SF_6 + e \rightarrow 2F + SF_4 + e}$ [11]. Fluorine atoms produced from these neutral dissociations can contribute to background F^+ ion signals because the threshold energies for these reactions were 9.6 eV and 12.1 eV respectively and lower than the ionization energy of fluorine atoms (15.5 eV). Thus background signal was found to increase with SF_6 partial pressure. Due to these processes, the plasma-on signal (M_{ON} (ε)) measured under same discharge condition as in background signal but with applied rf power i.e., 300 W for case in figure 2.3, would have contributions from residual and background signal apart from fluorine atom contributions originating from the plasma. As seen in figure 2.3, slope of F^+ ion signal changed for electron energy above 21 eV and which indicated significant additional contribution to F^+ ion signal was from process 2.2. Thus electron energy scans were performed between ε_1- ε_2 because above 21.0 eV process 2.2

contributes to F^+ ion signal where some of the F^+ ions would be from F_2 and SF_6 in the discharge

The fluorine atom density was calculated from the fluorine ion signal, $M^{F \to F^+}$ and was given by

$$M^{F \to F^+} = M_{ON}(\varepsilon) - cM_{OFF}(\varepsilon) \tag{2.4}$$

where c is the correction factor. When the discharge was switched on, the neutral gas density tends to reduce due to gas heating based on ideal gas law. In order to account for this reduction in neutral gas density, this correction factor was applied for background signal. Assuming a proportional relation between neutral gas density of SF_6 and $M_{OFF}(\varepsilon)$, correction factor was calculated as 0.78 for assumed gas temperature of 365 K based on previous gas temperature measurements in this plasma reactor chamber using TALIF and thermocouple [14]. The inclusion of correction factor does not considerably affect the fluorine atom density measurements because the difference between the plasma on and background signal was adequately large as shown in figure 2.3.

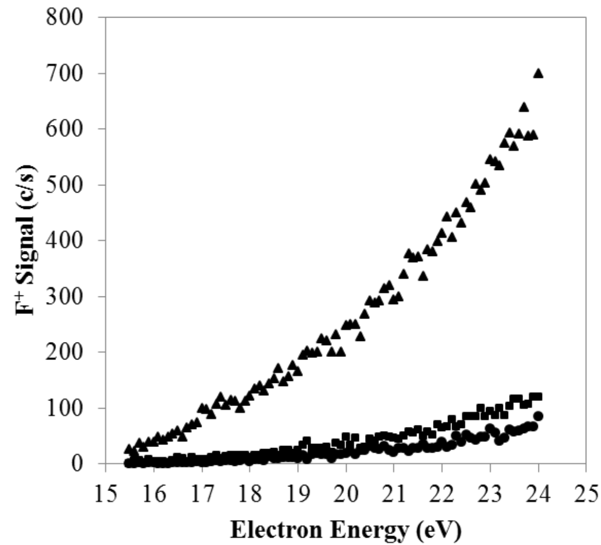

Figure 2.3 Electron energy scan of fluorine ions; signals shown were residual signal (●), background signal (■) and plasma on signal (▲).

The ion signal, $M^{X^+}(\varepsilon)$, proportional to the [X] in the ionizer can be written as

$$M^{X^+}(\varepsilon) = \alpha I_e \sigma(\varepsilon) [X] \tag{2.5}$$

where I_e is the electron emission current from the ionizer; $\sigma(\varepsilon)$ is the electron energy dependent ionization cross section; α is the product of extraction efficiency of the ions, β, species mass dependent transmission efficiency of the quadrupole,$T(m_{X^+})$, species mass dependent sensitivity of the SEM detector, $\theta(m_{X^+})$ and the length of the ionizer, l_{ion}; [X] is the number density of the neutral species in the ionizer. An appropriate reference signal is required to calculate the number density of unknown species. In traditional APMS technique, dissociative ionization signal was used as reference signal and it resulted in over-estimation of the number density of radicals [15]. Due to this reason, argon ion signal, $M^{Ar \rightarrow Ar^+}$, was used as reference signal to calculate the number density of fluorine atoms from fluorine ion signal, $M^{F \rightarrow F^+}$. The [F] in the ionizer was calculated from both ion signals as [15]

$$\frac{[F]}{[Ar]} = \left(\frac{S^{F \rightarrow F^+}}{S^{Ar \rightarrow Ar^+}}\right)\left(\frac{\lambda^{Ar \rightarrow Ar^+}}{\lambda^{F \rightarrow F^+}}\right)\left(\frac{T(m_{Ar^+})\,\theta(m_{Ar^+})}{T(m_{F^+})\,\theta(m_{F^+})}\right) \tag{2.6}$$

where [Ar] was the number density of argon in the ionizer (plasma off); $S^{F \rightarrow F^+}$and $S^{Ar \rightarrow Ar^+}$ were the slopes of the linear fits to the F^+ and Ar^+ as a function of electron energy; $\lambda^{F \rightarrow F^+}$and $\lambda^{Ar \rightarrow Ar^+}$were the slopes of the linear fits to the cross section of fluorine direct ionization and argon ionization as a function of electron energy. Since experiments were performed involving chemically reactive species like SF_6 & O_2, the electron emission current was fixed at 100 μA for longer filament lifetime as recommended by the manufacturer. Assuming negligible space charge effects, $M^{X^+}(\varepsilon)$ would be proportional to I_e [16] and fortunately, no space charge effects was found in this plasma chamber for < 200 μA. In the equation 2.6, β was assumed to be unity [15] for process involving direct ionization and l_{ion} can be ignored as emission current was fixed.

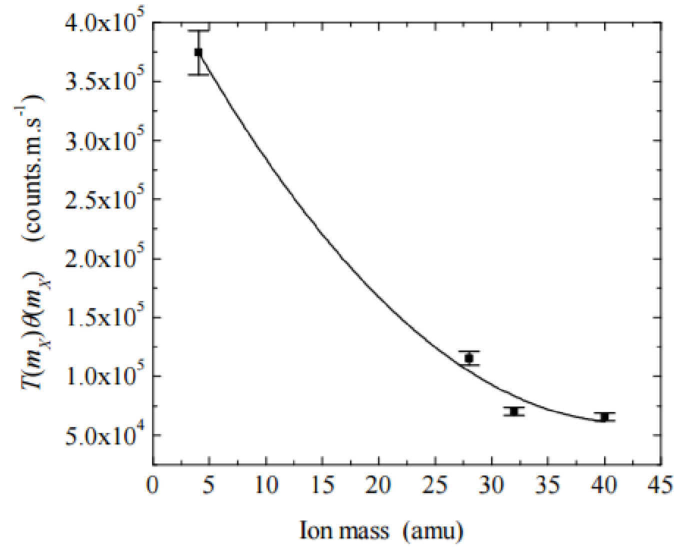

Figure 2.4 Instrument response function for Hiden EQP 300 mass spectrometer [17]

Mass dependent instrument parameters such as $T(m_{X^+})$ and $\theta(m_{X^+})$ in equation 2.6 were evaluated using several gases of known density using

$$T(m_{X^+})\theta(m_{X^+}) = \frac{S^{X\rightarrow X^+}}{\lambda^{X\rightarrow X^+}[X]} \tag{2.7}$$

Helium, nitrogen, oxygen and argon gases were used at known pressure of 40 mTorr and slopes of linear fits of individual gases as function of electron energy was measured. Ionization cross sections for helium, argon were adopted from [18] and for nitrogen and oxygen were from [19]. And also the neutral gas densities of each species were calculated using ideal gas laws with an assumption on gas temperature of 300 K. $T(m_{X^+})\theta(m_{X^+})$ was plotted against singly charged ion mass, m_i as shown in figure 2.4 and a fit was made to the calculated values using power law as shown in figure 2.4 to determine $T(m_{X^+})\theta(m_{X^+})$ for any single charged specie whose mass should be between 4- 40 amu. Based on data fit, dependence of $T(m_{X^+})\theta(m_{X^+})$ was found to be $m_i^{-0.75}$ for this mass spectrometer and this value agreed well with

measurements of $T(m_{X^+})\theta(m_{X^+})$ dependence as $m_{\mathrm{i}}^{-0.85}$ [20] and $m_{\mathrm{i}}^{-0.81}$ [15] in other similar mass spectrometers.

2.3 Optical emission spectroscopy

Optical emission spectroscopy (OES) is a well-established diagnostics tool to monitor radical and charged species in plasma discharges. OES often gains attractiveness and ideal to use in the semiconductor industry because of its low-cost, passive, non-intrusive nature and can be easily mounted on to an existing plasma reactor. Numerous OES based diagnostics techniques were used to provide insight knowledge about the plasma behavior which include:

1. Knowledge on electron density, electron temperature, EEDF can be obtained using line ratio method and trace gas optical emission spectroscopy (TRG-OES) [21, 22].
2. Gas temperature measurements can be investigated by monitoring line broadening mechanism of optical emission lines using high resolution OES [23] and TRG-OES [24].
3. Temporal and spatial behavior of electrons can be studied using phase resolved optical emission spectroscopy [25-28].
4. End point detection to gain information on plasma process completion [29].

Main analysis component measured by OES based technique was emission line, which was emitted light from the plasma as the function of wavelength and would be specific for any specie involved in the plasma process. The high energy plasma electrons would excite the atoms or molecules to upper electronic state by electron impact and then relaxation to a lower energy state or ground state with spontaneous emission in the form of photon and which results in optical line emission. This photon possesses energy equal to the difference between the two electronic states. The optical emission of atoms would be easy to analyze than that of molecules. In case of atoms only one electronic state can

occur whereas in molecules, vibrational and rotational states accompany the large number of electronic states.

2.3.1 Actinometry

Actinometry, one of the popular OES based plasma diagnostics technique used to determine the radical densities in the plasma process was employed in this work. This technique, first proposed by Coburn and Chen [30], uses the emission line intensity ratios to monitor the density of ground state species. To be specific, the ratio of emission line intensities of an unknown species (species of interest) to the known species (called as actinometer) usually an inert gas, which is added in small quantity (≈ 1-10%) to the discharge. The density of actinometer (inert gas) must be known and can be computed using ideal gas law. Variation of ground state species density can be monitored with classical actinometry using emission line ratio of unknown specie to actinometer with certain limitations as follows:

1. Electron impact excitation cross-section of unknown specie and actinometer must have similar shape, especially close to threshold energies.
2. Excitation of unknown specie and actinometer must be from direct electron-impact excitation of ground states and other excitation mechanisms such as dissociative excitation, cascade excitation and excitation via metastables must be negligible.
3. Quenching of populated states must be less significant.
4. Energy distribution of electrons and density of actinometer must remain constant.

Consider a excited state species, promoted from ground state by electron impact excitation, tends to relax to ground state with spontaneous emission. The intensity of the optical emission line of unknown species X was given by

$$I_X = c_X \, h\upsilon_X \, A_{ij}^X \, n_e \, k_e^X \, [\mathrm{X}] \left(\sum_j A_{ij}^X \right)^{-1} \quad (2.8)$$

Population from upper electronic levels and non-radiative de-excitation of the upper electronic levels were ignored. The intensity of optical emission of actinometer (A) was given by

$$I_A = c_A \, h\upsilon_A \, A_{ij}^A \, n_e \, k_e^A \, [\mathrm{A}] \left(\sum_j A_{ij}^A \right)^{-1} \quad (2.9)$$

where quantity c is the factor which accounts for all optical and geometrical parameters such as solid angle and transmissions; hv is the energy of photon of the respective transition; A_{ij} is the Einstein coefficients for spontaneous emission; $\sum_j A_{ij}^X$ is the sum of all the de-excitation processes through spontaneous emission of the ith level; k_e is the direct excitation rate coefficient and can be determined using

$$k_e = \int_0^\infty f(\epsilon) \, \sigma \sqrt{\frac{2\epsilon}{m_e}} \, d\epsilon \quad (2.10)$$

where m_e is the mass of electron; σ is the electron impact excitation cross section; $f(\epsilon)$ is the normalized electron energy distribution function. From the classical actinometric conditions of applicability described before and using equations 2.8 and 2.9, variation of unknown specie density, [X] would be proportional to actinometric signal ratio, I_X/I_A. However to obtain absolute [X] can be obtained using equation 2.11 provided rates of excitation co-efficients k_e^X and k_e^A for species X and A respectively must be known.

$$[X] = K \, \frac{I_X}{I_A} [A] \quad (2.11)$$

Proportionality constant, K was given by

$$K = \frac{k_e^A c_A \, v_A \, A_{ij}^A \, \sum_j A_{ij}^X}{k_e^X c_X \, v_X \, A_{ij}^X \, \sum_j A_{ij}^A} \tag{2.12}$$

Also [X] obtained using equation 2.11 would be invalid if it involves any of these processes - the excitation from higher levels, quenching of the considered excitation states and electron impact dissociative excitations of atomic species. However, to monitor the relative changes in densities of unknown species, the ratio of excitation rate constants, k_e^A/k_e^X, must be constant and [A] must be fixed. Value of k_e^A/k_e^X, would remain constant provided the EEDF remain unchanged. This method for determining the ground state atom densities was termed as the classical actinometric model.

Furthermore, if the plasma process involves quenching of the excited states and dissociative excitation then the rates of de-excitation (k_q) and dissociative pathway (k_{de}) should be taken into account. And equation 2.11 can be rewritten to account for these additional processes. If M was assumed to be the parent molecule which contributes to [X] through dissociative excitation mechanism and also quenching of excited states, then equation 2.11 can be rewritten as

$$[X] = \frac{k_e^A}{k_e^X} \, [\mathrm{A}] \, \frac{I_X}{I_A} \frac{1}{\gamma} - \frac{k_{de}^X}{k_e^X} \, [M] \tag{2.13}$$

with

$$\gamma = \frac{c_X \, v_X \, A_{ij}^X \left(k_q^A \, [M] + \sum_j A_{ij}^A\right)}{c_A \, v_A \, A_{ij}^A \left(k_q^X \, [M] \, + \sum_j A_{ij}^X\right)} \tag{2.14}$$

and [M] was the concentration of parent molecule, from which X excited to upper electronic level through electron impact dissociative excitation.

Variation of relative fluorine atom density was monitored in this work using classical actinometry model. Figure 2.5 described the excitation mechanism

using in this work and corresponding threshold and emission equations were as follows

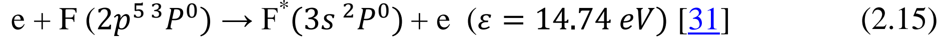

$$e + F\,(2p^{5\;3}P^0) \rightarrow F^*(3s\;^2P^0) + e\;\;(\varepsilon = 14.74\;eV)\;[31] \tag{2.15}$$

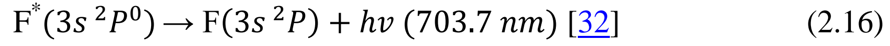

$$F^*(3s\;^2P^0) \rightarrow F(3s\;^2P) + hv\;(703.7\;nm)\;[32] \tag{2.16}$$

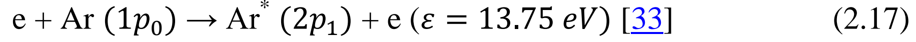

$$e + Ar\;(1p_0) \rightarrow Ar^*\;(2p_1) + e\;(\varepsilon = 13.75\;eV)\;[33] \tag{2.17}$$

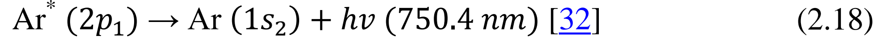

$$Ar^*\;(2p_1) \rightarrow Ar\;(1s_2) + hv\;(750.4\;nm)\;[32] \tag{2.18}$$

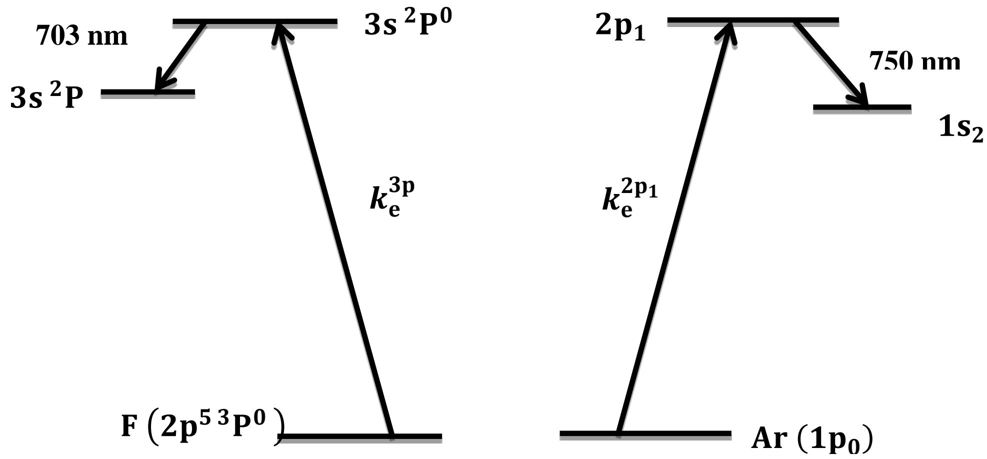

Figure 2.5 Schematic diagrams of the excited states involved in fluorine (left) and argon (right) used to monitor the density of ground state atoms by actinometry.

The time-averaged optical emission intensities of fluorine and actinometer, argon were measured using OES at 703.7 nm and 750.4 nm wavelengths respectively. Ratio of emission intensity at 703.7 nm, I_F and at 750.4 nm, I_{Ar} was used to monitor relative changes to fluorine density assuming investigated conditions where under the limitations of classical actinometry. In this work, relative variations of fluorine density were compared to absolute measurements investigated using APMS for validation for fluorine classical actinometry. Using classical actinometry, relation between fluorine atom density, [F] and actinometric signal can be written as

$$[F] \propto (I_F/I_{Ar}) \tag{2.19}$$

$$[\mathrm{F}] = K(\frac{I_F}{I_{Ar}})[\mathrm{Ar}] \tag{2.20}$$

As mentioned before, above relation would be invalid if any of classical actinometric assumption was violated. In this work, relative variation of [F] measured using APMS technique was compared with normalized actinometric signal for validation of fluorine classical actinometry. In case if equation 2.19 was satisfied, proportionality constant, K in equation 2.20 can be obtained from the slope to a plot of [F] versus $(I_F/I_{Ar})[\mathrm{Ar}]$, which would yield a straight line through origin. This value of K can be used to compute absolute fluorine atom density using classical actinometry. However, value of K can be discharge specific and also was found to vary based on discharge operating conditions in fluorine based discharges [34].

Also in this work, absolute atomic oxygen was investigated using actinometry and for population due to electron impact excitation of ground state oxygen can be written as

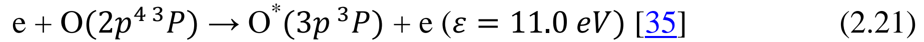

$$\mathrm{e} + \mathrm{O}(2p^4\,{}^3P) \rightarrow \mathrm{O}^*(3p\,{}^3P) + \mathrm{e}\ (\varepsilon = 11.0\ eV)\ [35] \tag{2.21}$$

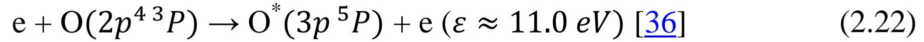

$$\mathrm{e} + \mathrm{O}(2p^4\,{}^3P) \rightarrow \mathrm{O}^*(3p\,{}^5P) + \mathrm{e}\ (\varepsilon \approx 11.0\ eV)\ [36] \tag{2.22}$$

And population through dissociative electron impact excitation of O_2 molecule can be written as

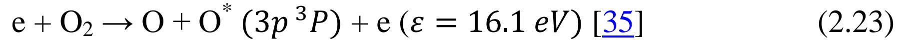

$$\mathrm{e} + \mathrm{O}_2 \rightarrow \mathrm{O} + \mathrm{O}^*\ (3p\,{}^3P) + \mathrm{e}\ (\varepsilon = 16.1\ eV)\ [35] \tag{2.23}$$

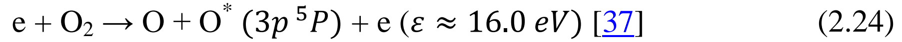

$$\mathrm{e} + \mathrm{O}_2 \rightarrow \mathrm{O} + \mathrm{O}^*\ (3p\,{}^5P) + \mathrm{e}\ (\varepsilon \approx 16.0\ eV)\ [37] \tag{2.24}$$

Radiative de-excitation of populated states can be written as

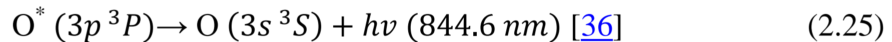

$$\mathrm{O}^*\ (3p\,{}^3P) \rightarrow \mathrm{O}\ (3s\,{}^3S) + hv\ (844.6\ nm)\ [36] \tag{2.25}$$

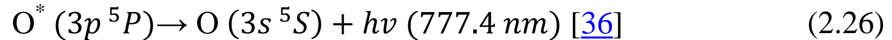

$$\mathrm{O}^*\ (3p\,{}^5P) \rightarrow \mathrm{O}\ (3s\,{}^5S) + hv\ (777.4\ nm)\ [36] \tag{2.26}$$

The time-averaged plasma emission intensities of atomic oxygen at 844.6 nm and 777.4 nm were recorded using OES and actinometric signals $I_O^{844.6}/I_{Ar}^{750.4}$ and $I_O^{777.4}/I_{Ar}^{750.4}$ were used to monitor variations in atomic oxygen density, [O] in various plasma discharges. However, only $I_O^{844.6}/I_{Ar}^{750.4}$ ratio was mostly

considered to compute absolute [O] using actinometry because 844.6 nm oxygen emission line was found to have significantly less contribution from dissociative excitation in comparison to 777.4 nm emission line [32, 38, 39]. So, in this work 844.6 nm oxygen emission line was used to monitor absolute [O] variations in the discharge. Actinometric model essential to compute absolute [O] had been chosen based on EEDF measurements using Langmuir probe and rates of direct and dissociative excitation.

2.3.2 Optical sensor for actinometry

One of the optical detection system used in this work was an Ocean optics HR4000 series high resolution spectrometer [40]. This optical sensor was predominately used in fluorine actinometry to record atomic optical emission lines from the plasma discharge and schematic of Ocean optics optical bench was shown in figure 2.6. Plasma emissions were transmitted to optical bench through a premium grade optical fiber with 600 μm core diameter. Length of the fiber was 2 m and the fiber cover was made using stainless-steel BX with long term bend radius of 24 cm and short term bend radius of 12 cm. Other end of the fiber was secured to optical bench using sub-miniature version A (SMA) connector and which served as an input to spectrometer. The spectral resolution was controlled by the size of aperture, located behind SMA connectors and which optimized the amount of light for analysis. Before the light can enter the spectrometer, it was allowed to pass a filter to restrict optical emission to pre-defined wavelength regions. Then the diffracted light from collimating mirror was focused onto grating of the spectrometer, where wavelength range and resolution can be specified based on groove densities. The reflected light from grating was focused onto charge-coupled device (CCD) detector with the help of focusing mirror. Toshiba TCD 1304AP linear CCD array was used as detector with this spectrometer to convert optical signal to digital signal with signal to noise of 300:1. Finally, the digital signal from detector was transmitted to spectrometer operating software, SpectraSuite [41] for data

acquisition and analysis. The integration time of the spectrometer can be varied between 3.8 ms to 10 s and was controlled through SpectraSuite. Data acquisition was performed using high-speed acquisition mode where integration time, number of scans across wavelength range and total number of scans to average at a particular wavelength were specified for analysis.

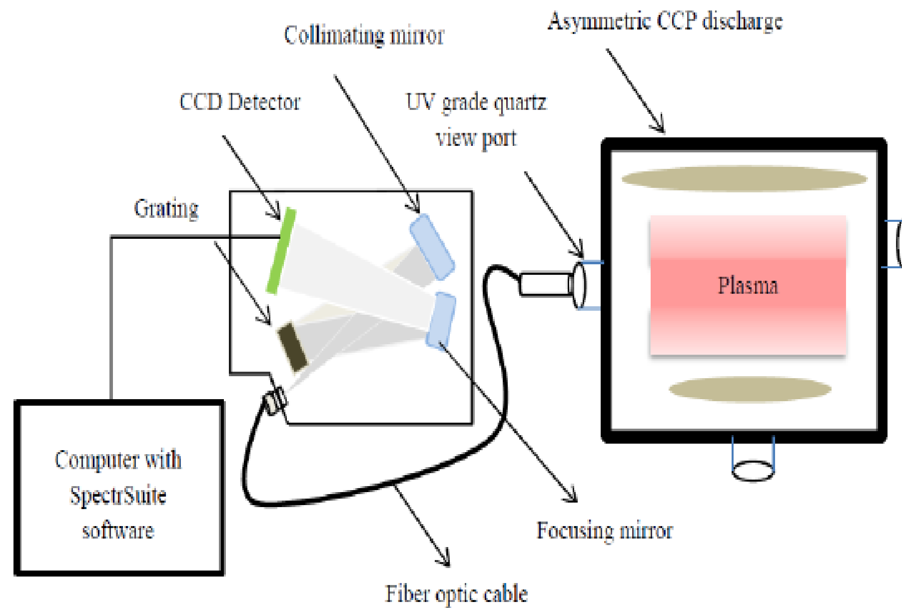

Figure 2.6 Schematic of an Ocean optics HR 4000 spectrometer with plasma discharge for actinometry.

Horiba Jobin Yvon spectrometer (MicroHR) [42] with 140 mm focal length was other optical sensor used in this work for oxygen actinometry. It contained 32 mm x 32 mm diffraction gratings with 1200 grooves mm^{-1} each. It was equipped with an automated scanning monochromator in the CzernyTurner optical pattern along with a Toshiba TCD1304AP CCD detector. The emission from the plasma was directed towards the 10 μm width entrance slit of the monochromator through UV grade quartz optical viewport. The scanning range of the monochromator was fixed in this work between 600 – 850 nm with 0.25 nm spectral resolution. Both optical sensors were calibrated using technique

described elsewhere [43-45] with a Heraeus Tungsten halogen lamp LSB 020. This lamp was placed on lamp mount LSA 367 which was connected to a stabilized power supply LSL 111 and only relative spectral response correction was applied to essential line intensities required for actinometry to account for any dependence due to spectral response of the detection system.

2.4 Probe diagnostics

2.4.1 Langmuir probe

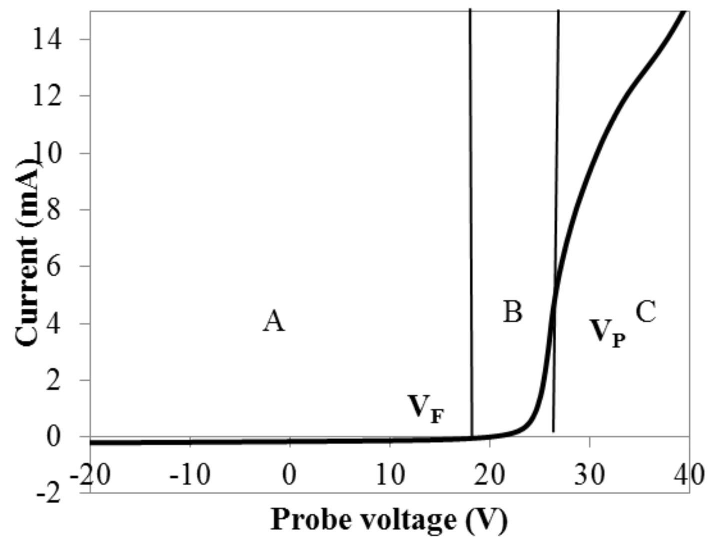

Figure 2.7 Typical I-V characteristics measured using Langmuir probe in Ar discharge at 20 mTorr and 200 W. 'A' denotes ion saturation region, 'B' denotes electron retardation region and 'C' denotes electron saturation region.

Langmuir probe is one of the most commonly used plasma diagnostics and was invented by Nobel Laureate Langmuir [46]. The key plasma parameters like electron density, ion density, electron temperature, plasma potential, floating potential and electron energy distribution function (EEDF) can be measured using a Langmuir probe. These parameters can be used to investigate rates of electron impact ionization and dissociation of the reactive specie in plasma

process. Knowledge on these rates is very important for actinometry (2.4.1) which can be used to monitor atomic specie concentration in the plasma.

2.4.2 Principle of Langmuir probe

A conducting electric probe can be immersed into the plasma to aid in diagnostic applications to measure plasma parameters. This probe tends to collect electrons and ions depending upon the bias voltage applied to probe tip. This principle was first demonstrated by Langmuir [46, 47] and also named after him; hence referred as Langmuir probe. Large fluxes of electrons would incident on the probe because of large difference in electron and ion mobilities. A sheath would be formed between the plasma and the probe tip which compensates for the loss of electrons to the probe. The current drawn through the probe tip from the plasma as a function of applied voltage was referred as current (I) – voltage (V) trace. The analysis of this measured current-voltage (I-V) characteristics aid to provide information about the plasma parameters. A typical I-V characteristic can be divided into three main regions as shown in figure 2.7. The bias potential at which the electron and ion current would be equal was referred as floating potential (V_F). This negative potential developed on the probe relative to the plasma would tend to repel adequate electrons to balance the ion and electron fluxes so that the net current flow through the probe would be zero. The probe biased at a potential drains a current from the plasma, due to thermal electrons and ions, even though there would be no potential difference between the probe and the plasma and this potential was referred as plasma potential (V_P). V_P would also be a measure of potential of the plasma at a given location within the plasma with respect to the walls of the chamber. An inflection on the measured I-V characteristic across probe voltage reveals potential of the plasma. Plasma potential can be measured either by first and second derivatives of current with respect to voltage. At the plasma potential, the first derivative goes through maximum and the second derivative would be equal to zero. As pointed before, I-V characteristic of the probe is

obtained by sweeping probe bias voltage (V_B) from a negative to a positive potential as shown in figure 2.7. When the probe voltage was biased negative with respect to plasma potential ($V_B < V_P$), no electrons reach the probe and only positive ions were collected. Here the current would be referred as *ion saturation current* as the total current was only due to positive ions and the region can be termed as *ion saturation region*. When the probe voltage was biased positively with respect to floating potential ($V_B \geq V_F$), electrons (and negative ions) with high energy reach the probe along with few positive ions. This region would be called *electron retarding region* and the total current would be predominantly due to electrons. In this region, the probe would still repel some electrons which do not have enough energy to overcome the potential barrier. Hence the current in this region can be termed as *electron repelling current*. An increase in probe bias voltage would cause only fewer electrons gets repelled and the total current (predominantly due to electrons) would increase exponentially. With further increase in probe bias voltage, it would reach the plasma potential and where no longer the electrons get repelled by the probe. When probe bias voltage increases beyond plasma potential ($V_B > V_P$), the total current would only be due to electrons and negative ions and current can be termed as *electron saturation current*. This region would be referred as *electron saturation region*.

2.4.3 Procedure to determine plasma parameters

It was clear that an I-V characteristic would provide some facts about the plasma but more precise information about plasma parameters would require further quantitative analysis. Numerous techniques were employed to probe characteristics to determine plasma parameters such as electron density (n_e), effective electron temperature (T_{eff}), plasma density, and plasma potential (V_P). The following were some of those techniques:

Langmuir method: This procedure was applied to the region where probe bias voltage was large compared to floating potential of plasma and also current drawn was predominantly due to electrons. Maxwellian EEDF was assumed to compute plasma parameters.

Orbital motion limit theory for the collection of electrons [47-49]: This theory was applied in a regime with thick collisionless sheath where ratio of the probe radius to the Debye length was very much less than unity. Again Maxwellian EEDF was assumed to compute electron current obtained from electron saturation region of the probe characteristic.

Orbital motion limit theory for the collection of ions [47, 49, 50]: This theory was applied to ion saturation region and electron temperature (in ion rich region) was measured from the slope of I-V characteristics close to floating potential of plasma. Ion density of the plasma was obtained using extrapolation of ion saturation region either with linear or parabolic approximation.

Radial ion motion theory [49, 51-53]: There could be situations where orbital ion motion was destroyed due to ion-ion collision, ion-atom collision or disruption caused by finite cylindrical probe length [54]. In such cases, radial ion motion theory was adopted and it requires knowledge on sheath voltage of the probe to compute ion current. Probe sheath voltage was calculated from floating potential of plasma with Maxwellian EEDF assumption.

Most of these conventional theories assume Maxwellian EEDF for measurements of electron and ion currents obtained from probe characteristics. However, low pressure plasma discharges would usually be characterized by non-Maxwellian electron distribution [49]. Assumption of Maxwellian electron distribution in low-pressure discharges can lead to large uncertainty in the measured plasma parameters and Godyak *et al*., [49] evidently discussed errors involved with such assumptions. One method which gained significant attraction in low-pressure discharge was Druyvesteyn method [55] since no

assumption on electron distribution was required. It was successfully adopted in low-pressure discharges and other plasma discharges [53, 56-60] for measurements of EEDFs. Since this method was independent on the shape of the EEDF and can relate directly to the second derivative of the probe characteristics to determine the EEDF and from that other plasma parameters can be obtained. And also this method would be effective for any isotropic electron velocity distribution and does not depend on the ratio of the probe radius to the Debye length, r_p/λ_D [61]. The EEDF, $f(\varepsilon)$ can be obtained using Druyvesteyn method, was given by

$$f(\varepsilon) = \left(\frac{d^2I}{dV^2}\right)\frac{2m_e}{e^2\mathrm{A}}\left(\frac{2e\varepsilon}{m_e}\right)^{\frac{1}{2}} \tag{2.27}$$

where ε is the electron energy, d^2I/dV^2 is the second derivative of the probe I-V characteristic, m_e is the mass of electron, e is the charge of an electron and A is the surface area of probe. The electron density, n_e, and effective electron temperature, T_{eff}, can be calculated from obtained EEDF and were obtained using equations 2.28 & 2.29. In low pressure capacitive discharges, electrons would rarely be in thermal equilibrium with each other and as said before, electron distribution would usually be characterized by non-Maxwellian distribution [62]. So, temperature of electrons, T_e would usually be described by effective electron temperature [62, 63].

$$n_e = \int_0^\infty f(\varepsilon)\, d\varepsilon \tag{2.28}$$

$$T_{eff} = \frac{2}{3n_e}\int_0^\infty \varepsilon\ f(\varepsilon) d\varepsilon \tag{2.29}$$

In most cases the electron distribution would be represented as electron energy probability function, $f_e(\varepsilon)$,(EEPF), so that it would be appropriate to determine the type of electron energy distribution and it can be calculated using

$$f_e(\varepsilon) = \frac{f(\varepsilon)}{\sqrt{\varepsilon}} \tag{2.30}$$

In order to determine EEDF by Druyvesteyn method, current drawn by the probe must be only from electrons. Practically, total current (I_T) drawn by this probe was made of electron current (I_e) and ion current (I_i). So, any influence of ion current was removed from total current by the procedure described by Steinbruchel [64] to obtain electron current required by Druyvesteyn method to determine EEDF. Steinbruchel adopted Laframboise theory [50] to obtain ion current contribution and parametrized results of Laframboise to obtain arbitrary values of r_p/λ_D [64]. According to Laframboise, ion current for a cylindrical Langmuir probe for a known ion density, n_i was given by

$$\mathrm{I_i} = en_iA(k_BT_e/2\pi m_i)^{1/2}i_i \tag{2.31}$$

Dimensionless correction factor i_i was a function of dimensionless potential, X and also depend on r_p/λ_D value.

$$i_i(X) = a(-X)^b \tag{2.32}$$

$$X = e(\mathrm{V_B} - \mathrm{V_P})/k_BT_e \tag{2.33}$$

Dimensionless parameters a and b depend on r_p/λ_D value and were obtained for a corresponding value of r_p/λ_D value which can be found elsewhere [64]. At first, Druyvesteyn method was applied to initial probe characteristics to obtain initial n_e and T_e along with plasma potential. From these initial values, Debye length was calculated using

$$\lambda_D = (\epsilon_O\ k_BT_e/e^2n_e)^{1/2} \tag{2.34}$$

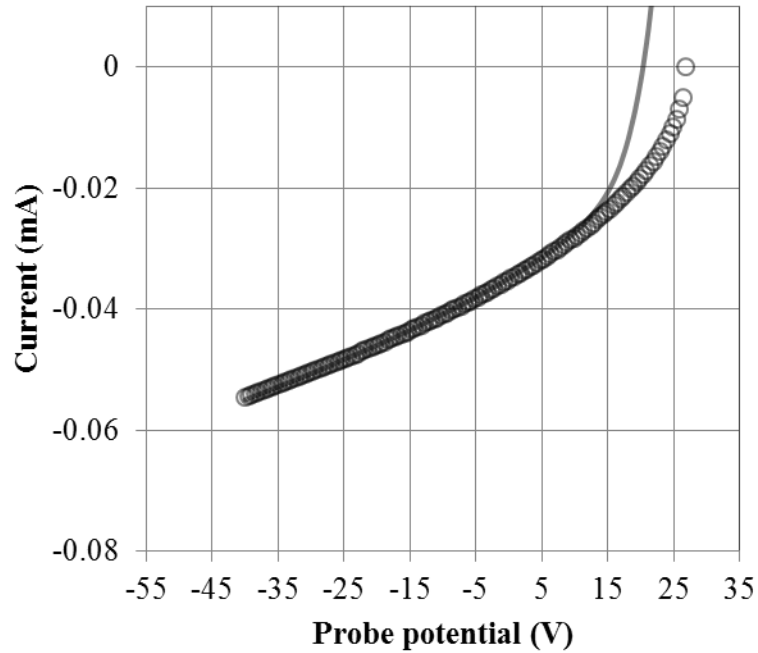

Figure 2.8 Probe I-V characteristics (solid lines) obtained using Smart probe and calculated ion current, i_i^c (○) in 20 mTorr Ar plasma discharge with applied rf power of 200 W. $V_P = 27.3$ V.

Value evaluated from ratio of r_p/λ_D was used to obtain initial values of dimensionless constant *a* and *b* from the plot in [64]. Assuming quasi-neutrality condition in plasma, initial ion density was approximated to initial n_e. Dimensionless potential, *X* from equation 2.33 and dimensionless factor, i_i from equation 2.32 were calculated from initial plasma parameters obtained from initial probe I-V trace and then substituted in equation 2.31 to obtain calculated ion current, i_i^c. It was well know from probe characteristics, only ions were collected at very large negative potential and current drawn would be purely ion current. With this in mind, i_i^c was fitted to obtained probe I-V characteristics across very large negative probe potential till plasma potential. Dimensionless parameters in equation 2.32 and initial ion density was varied slightly to obtain best fit between i_i^c and initial probe I-V trace for most of negative probe

potential as shown in figures 2.8 & 2.9. Close to floating potential, ion current was found to deviate from total current as the electron current contribution becomes significant due to increasing positive probe potential. Therefore, electron current required for Druyvesteyn method to measure EEDF was calculated by subtracting the best fit data of i_i^c from total measured current.

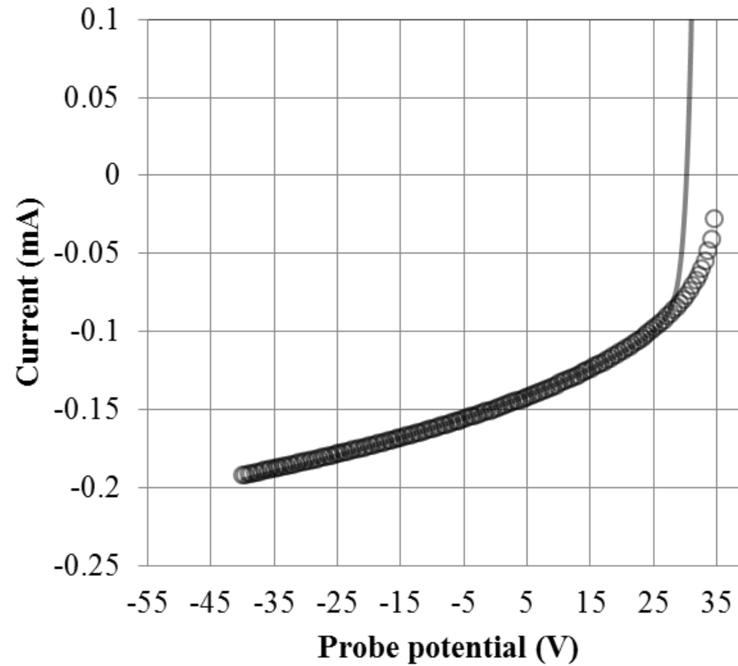

Figure 2.9 Probe I-V characteristics (solid lines) obtained using Smart probe and calculated ion current, i_i^c (○) in 300 mTorr Ar plasma discharge with applied rf power of 200 W. V_P = 34.7 V.

Like other conventional methods, Druyvesteyn methods also got its drawbacks and limitations, especially usage in high pressure plasma discharges to determine EEDF would be highly unreliable. At very high pressures, collisions of electrons with other particles in plasma near probe-plasma region becomes more obvious as the mean free path of electrons approximately equals to probe radius or Debye length and thus it would cause violation in cylindrical probe inequality [61] which could make Druyvesteyn formula invalid. Also validity of

Druyvesteyn method would be unreliable with discharges with increase in magnetic field [61].

2.4.4 Commercial Langmuir probe- The Smart-Probe

The SmartProbe is a commercial Langmuir probe used in this work was developed by Scientific Systems. Figure 2.10 shows the schematic diagram of the Langmuir probe. The SmartProbe consist of the Langmuir probe, Reference probe with Preamplifier, Acquisition Electronic Unit (ACU) and SmartSoft software. The probe tip, which constitutes to be the active part of the Langmuir Probe, was made of platinum wire with 0.15 mm diameter. The length of the probe tip was varied between 3-12 mm depending on the experiments performed. The advantage of using platinum wire was, to minimize the contamination level so that I-V characteristic would be undistorted. The probe tip was connected to the ACU through a coaxial cable. This cable was covered using ceramic shaft, to prevent it from the plasma. As mentioned above, the I-V characteristic was measured using current drawn by varying the probe voltage across the probe tip. The plasma parameters calculated using I-V characteristics assumes that probe-plasma sheath bias contains only direct current (DC) component and no significant RF component. If there is contribution from RF component, then time dependent variation of plasma potential will occur due to RF driving voltage. This would produce distorted I-V data and the plasma parameters measured from this would be incorrect. In order to account for this RF compensation, a compensation electrode along with a set of inductors forms the part of SmartProbe. The function of RF compensation to keep the probe-ground impedance higher compared to plasma- probe sheath impedance. So that majority of the RF potential appears across the probe-ground impedance and thus ensures the probe floats at the plasma potential. The set of self resonant inductors, located close to probe, were tuned to 13.56 MHz and related harmonics and would increase the probe impedance. The inductors were cooled using air through a 4 mm diameter Teflon air inlet and exhaust was built into

the probe shaft. The SmartProbe also consist of reference electrode (reference probe) which tracked and corrected for any low frequency DC shifts in the plasma potential. This reference probe was made of stainless steel and forms a wire loop around the main shaft of the Langmuir probe. The major part of reference probe in the plasma was covered with ceramic shaft for insulation. The other end of the reference probe is connected to ACU through electrical feed-through. In this work the probe voltage was varied from -100 to 100 V and sample per point were chosen between 100 -200. I-V characteristics measured in this work were an average of 10-20 sweeps. The probe tip was cleaned before each sweep to ensure it was free from contamination. To prevent from etching, the probe tip was regularly changed as it was used in chemically reactive (O_2-SF_6) plasma.

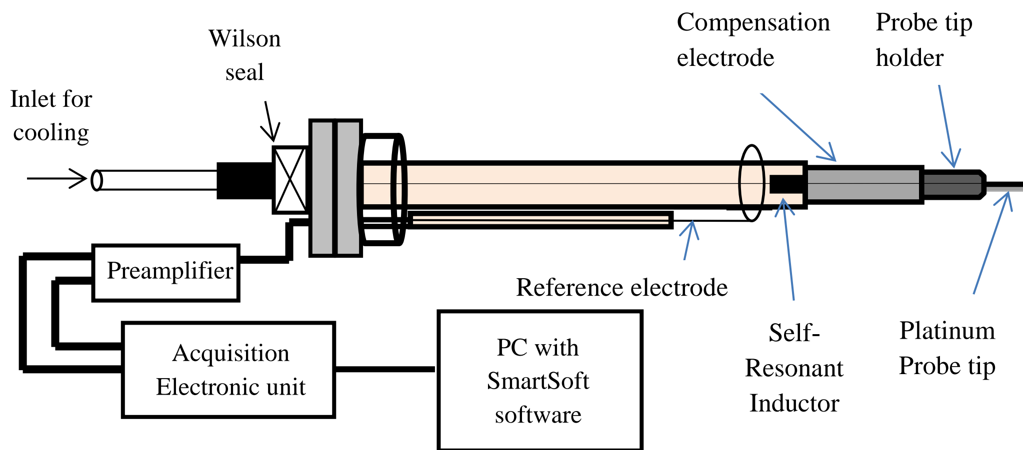

Figure 2.10 Schematic of the Smart-Probe – commercial Langmuir probe system used in this work.

2.4.5 Hairpin probe

Hairpin probe, one of the microwave resonance based probe technique was first proposed by Stenzel [65] and was latter revisited for improvements by Piejak *et al.*, [66] for electron density measurements in low pressure plasma discharge. The hairpin microwave resonator used in this work was designed by Gaman

and more detailed description can be found elsewhere [67]. The theory of hairpin probe was to generate a local electric field through U-shaped (hairpin shaped) quarter wavelength transmission line, whose characteristic resonance frequency depends on the permittivity of the dielectric medium surrounding the wire. Relative shifts in resonance frequency can be observed if the probe was immersed in different medium. Suppose, the resonance frequency, f_r of hairpin probe was given by

$$f_r = \frac{c}{4L\sqrt{\epsilon}} \tag{2.35}$$

where c was the light speed, L was the resonator length and ϵ was the relative permittivity of the medium around the probe. Since ϵ would be unity in vacuum medium, then resonance frequency in vacuum, f_{ro} would become

$$f_{ro} = \frac{c}{4L} \tag{2.36}$$

In plasma state, relative permittivity can be defined as

$$\epsilon = 1 - \frac{f_p^2}{f^2} \tag{2.37}$$

where f_p was resonant frequency of plasma = $(e^2 n_e/\pi m_e)$ and if the probe was immersed in plasma, substituting equation 2.37 into equation 2.35, then, $f_r^2 = f_{ro}^2 + f_p^2$ (with $f_r > f_p$). Electron density was determined using equation 2.38 due relative shift in the resonance frequency from vacuum to plasma medium.

$$n_e = \frac{f_r^2 - f_{ro}^2}{0.81} \tag{2.38}$$

where resonance frequencies were measured in GHz and electron density, n_e was obtained in 10^{10} cm^{-3}.

2.4.6 Octiv VI probe

In this work, the phase shift angle between the plasma current and voltage was measured to corroborate Langmuir probe predictions of changes in electron heating mode. An Octiv VI probe developed by Impedans Ltd [68] is employed here. The inline probe was installed the between powered electrode and automatic matching unit. The probe incorporates capacitive sensing for voltage acquisition with inductive current pickups in combination with analog-to-digital conversion (ADC) circuitry for signal digitisation. The Fast Fourier transform is utilised for frequency domain analysis and extraction of phase data via dedicated logic performing noise reduction.

2.5 Reference

[1] Kawai, Y., Sasaki, K.and Kadota, K., (1997), "Comparison of the fluorine atom density measured by actinometry and vacuum ultraviolet absorption spectroscopy", *Japanese journal of applied physics,* Vol.36 (9A), pp. L1261.

[2] Sasaki, K., Kawai, Y.and Kadota, K., (1999), "Determination of fluorine atom density in reactive plasmas by vacuum ultraviolet absorption spectroscopy at 95.85 nm", *Rev.Sci.Instrum.,* Vol.70 (1), pp. 76-81.

[3] Tachibana, K.and Kamisugi, H., (1999), "Vacuum-ultraviolet laser absorption spectroscopy for absolute measurement of fluorine atom density in fluorocarbon plasmas", *Appl.Phys.Lett.,* Vol.74 (16), pp. 2390-2392.

[4] Herring, G., et al. (1988), "Two-photon-excited fluorescence spectroscopy of atomic fluorine at 170 nm", *Opt.Lett.,* Vol.13 (5), pp. 360-362.

[5] Nakamura, K., Segi, K.and Sugai, H., (1997), "Absolute fluorine atom densities in fluorocarbon high-density plasmas measured by appearance mass spectrometry", *Japanese journal of applied physics,* Vol.36 (4A), pp. L439.

[6] Hikosaka, Y., Nakamura, M.and Sugai, H., (1994), "Free radicals in an inductively coupled etching plasma", *Japanese journal of applied physics,* Vol.33 (4S), pp. 2157.

[7] Schwarzenbach, W., et al. (1997), "Mass Spectrometric Detection of F Atoms and CFx Radicals in CF 4 Plasmas", *Japanese journal of applied physics,* Vol.36 (7S), pp. 4644.

[8] Tserepi, A., et al. (1997), "Kinetics of F atoms and fluorocarbon radicals studied by threshold ionization mass spectrometry in a microwave CF 4 plasma", *Journal of Vacuum Science & Technology A: Vacuum, Surfaces, and Films,* Vol.15 (6), pp. 3120-3126.

[9] Kechkar, S., et al. (2014), "Investigation of absolute atomic fluorine density in a capacitively coupled SF6/O2/Ar and SF6/Ar discharge", *Plasma Sources Sci.Technol.,* Vol.23 (6), pp. 065029.

[10] Oxford Instruments, [online], www.oxfordinstruments.com.

[11] Rao, M.V.V.S.and Srivastava, S.K., (1996), "Cross sections for the production of positive ions by electron impact on F-2", *Journal of Physics B-Atomic Molecular and Optical Physics,* Vol.29 (9), pp. 1841-1848.

[12] Huber, K.and Herzberg, G., (1970), "Molecular Spectra and Molecular Structure, IV. Constants of Diatomic Molecules Litton, New York, 1979. 26 SF Boys and F. Bernardi", *Mol.Phys.,* Vol.19 pp. 553.

[13] Christophorou, L.G.and Olthoff, J.K., (2000), "Electron interactions with SF6", *Journal of Physical and Chemical Reference Data,* Vol.29 (3), pp. 267-330.

[14] Kechkar, S., et al. (2013), "Investigation of atomic oxygen density in a capacitively coupled O2/SF6 discharge using two-photon absorption laser-induced fluorescence spectroscopy and a Langmuir probe", *Plasma Sources Sci.Technol.,* Vol.22 (4), pp. 045013.

[15] Singh, H., Coburn, J.and Graves, D.B., (2000), "Appearance potential mass spectrometry: Discrimination of dissociative ionization products", *Journal of Vacuum Science & Technology A,* Vol.18 (2), pp. 299-305.

[16] Agarwal, S., et al. (2004), "Measurement of absolute radical densities in a plasma using modulated-beam line-of-sight threshold ionization mass spectrometry", *Journal of Vacuum Science & Technology A,* Vol.22 (1), pp. 71-81.

[17] Kechkar, S., et al. (2014), "Investigation of absolute atomic fluorine density in a capacitively coupled SF6/O-2/Ar and SF6/Ar discharge", *Plasma Sources Science & Technology,* Vol.23 (6), pp. 065029.

[18] Wetzel, R.C., et al. (1987), "Absolute cross sections for electron-impact ionization of the rare-gas atoms by the fast-neutral-beam method", *Physical Review A,* Vol.35 (2), pp. 559.

[19] Straub, H., et al. (1996), "Absolute partial cross sections for electron-impact ionization of H 2, N 2, and O 2 from threshold to 1000 eV", *Physical Review A,* Vol.54 (3), pp. 2146.

[20] Pulpytel, J., Arefi-Khonsari, F.and Morscheidt, W., (2005), "Threshold ionization mass spectrometry study of singlet molecular oxygen in the deposition of SnO2 by PACVD", *J.Phys.D,* Vol.38 (9), pp. 1390.

[21] Donnelly, V. (2004), "Plasma electron temperatures and electron energy distributions measured by trace rare gases optical emission spectroscopy", *J.Phys.D,* Vol.37 (19), pp. R217.

[22] Crintea, D., et al. (2009), "Plasma diagnostics by optical emission spectroscopy on argon and comparison with Thomson scattering", *J.Phys.D,* Vol.42 (4), pp. 045208.

[23] Gottscho, R.A.and Donnelly, V.M., (1984), "Optical emission actinometry and spectral line shapes in rf glow discharges", *J.Appl.Phys.,* Vol.56 (2), pp. 245-250.

[24] Schabel, M., et al. (2002), "Determination of electron temperature, atomic fluorine concentration, and gas temperature in inductively coupled fluorocarbon/rare gas plasmas using optical emission spectroscopy", *Journal of Vacuum Science & Technology A,* Vol.20 (2), pp. 555-563.

[25] Gans, T., Schulz-Von Der Gathen, V.and Döbele, H., (2004), "Spectroscopic measurements of phase-resolved electron energy distribution functions in RF-excited discharges", *EPL (Europhysics Letters),* Vol.66 (2), pp. 232.

[26] Abdel-Rahman, M., et al. (2005), "Space and time resolved rotational state populations and gas temperatures in an inductively coupled hydrogen RF discharge", *Plasma Sources Sci.Technol.,* Vol.14 (1), pp. 51.

[27] Schulze, J., et al. (2007), "Space and phase resolved plasma parameters in an industrial dual-frequency capacitively coupled radio-frequency discharge", *J.Phys.D,* Vol.40 (22), pp. 7008.

[28] Schulze, J., et al. (2010), "Phase resolved optical emission spectroscopy: a non-intrusive diagnostic to study electron dynamics in capacitive radio frequency discharges", *J.Phys.D,* Vol.43 (12), pp. 124016.

[29] Yue, H.H., et al. (2001), "Plasma etching endpoint detection using multiple wavelengths for small open-area wafers", *Journal of Vacuum Science & Technology A,* Vol.19 (1), pp. 66-75.

[30] Coburn, J.and Chen, M., (1980), "Optical emission spectroscopy of reactive plasmas: A method for correlating emission intensities to reactive particle density", *J.Appl.Phys.,* Vol.51 (6), pp. 3134-3136.

[31] Morgan, W. (1992), "A critical evaluation of low-energy electron impact cross sections for plasma processing modeling. I: Cl2, F2, and HCl", *Plasma Chem.Plasma Process.,* Vol.12 (4), pp. 449-476.

[32] Walkup, R., Saenger, K.and Selwyn, G., (1986), "Studies of atomic oxygen in O2 CF4 rf discharges by two-photon laser-induced fluorescence and optical emission spectroscopy", *J.Chem.Phys.,* Vol.84 (5), pp. 2668-2674.

[33] Tachibana, K. (1986), "Excitation of the 1 s 5, 1 s 4, 1 s 3, and 1 s 2 levels of argon by low-energy electrons", *Physical Review A,* Vol.34 (2), pp. 1007.

[34] Kawai, Y., Sasaki, K.and Kadota, K., (1997), "Comparison of the fluorine atom density measured by actinometry and vacuum ultraviolet absorption spectroscopy", *Japanese journal of applied physics,* Vol.36 (9A), pp. L1261.

[35] Booth, J., et al. (1991), "Oxygen atom actinometry reinvestigated: Comparison with absolute measurements by resonance absorption at 130 nm", *J.Appl.Phys.,* Vol.69 (2), pp. 618-626.

[36] Laher, R.R.and Gilmore, F.R., (1990), "Updated excitation and ionization cross sections for electron impact on atomic oxygen", *Journal of Physical and Chemical Reference Data,* Vol.19 (1), pp. 277-305.

[37] Erdman, P.and Zipf, E., (1987), "Excitation of the OI (3s5S0–3p5P; λ7774 Å) multiplet by electron impact on O2", *J.Chem.Phys.,* Vol.87 (8), pp. 4540-4545.

[38] Katsch, H., et al. (2000), "Detection of atomic oxygen: Improvement of actinometry and comparison with laser spectroscopy", *J.Appl.Phys.,* Vol.88 (11), pp. 6232-6238.

[39] Pagnon, D., et al. (1995), "On the use of actinometry to measure the dissociation in O2 DC glow discharges: determination of the wall recombination probability", *J.Phys.D,* Vol.28 (9), pp. 1856.

[40] Ocean Optics HR4000, [online], http://oceanoptics.com/product/hr4000cg-uv-nir/.

[41] Ocean Optics SpectrSuite, [online], http://oceanoptics.com/wp-content/uploads/SpectraSuite.pdf.

[42] Horiba Scientific, [online], http://www.horiba.com/us/en/scientific/products/optical-spectroscopy/spectrometers-monochromators/micro-hr/microhr-motorized-208/.

[43] Horiba Jobin Yvon Instrument Response Corrections Technical Note 203 Optical Spectroscopy Division, [online], http://www.horiba.com/fileadmin/uploads/Scientific/Documents/OSD/203_Instrument_Response_Corrections.pdf.

[44] Fantz, U. (2006), "Basics of plasma spectroscopy", *Plasma Sources Science and Technology,* Vol.15 (4), pp. S137.

[45] Gaigalas, A., et al. (2009), "Procedures for wavelength calibration and spectral response correction of CCD array spectrometers", *Journal of Research of the National Institute of Standards and Technology,* Vol.114 (4), pp. 1.

[46] Mott-Smith, H.M.and Langmuir, I., (1926), "The theory of collectors in gaseous discharges", *Physical review,* Vol.28 (4), pp. 727.

[47] I. Langmuir, H.M. (1924), *Gen. Electr. Rev.,* Vol.27 pp. 449, 538, 616, 762, 810.

[48] Verweij, W., (1961)*, Probe measurements and determination of electron mobility in the positive column of low-pressure mercury-argon discharges,* , Philips Research Laboratories,.

[49] Godyak, V., Piejak, R.and Alexandrovich, B., (1993), "Probe diagnostics of non-Maxwellian plasmas", *J.Appl.Phys.,* Vol.73 (8), pp. 3657-3663.

[50] Laframboise, J.G. (1966), *Theory of spherical and cylindrical Langmuir probes in a collisionless, Maxwellian plasma at rest,* .

[51] Allen, J., Boyd, R.and Reynolds, P., (1957), "The collection of positive ions by a probe immersed in a plasma", *Proceedings of the Physical Society.Section B,* Vol.70 (3), pp. 297.

[52] Chen, F.F. (1965), "Numerical computations for ion probe characteristics in a collisionless plasma", *Journal of Nuclear Energy.Part C, Plasma Physics, Accelerators, Thermonuclear Research,* Vol.7 (1), pp. 47.

[53] Kagan, Y.M.and Perel, V., (1963), "Probe Methods of Plasma Characterization", *Usp.Fiz.Nauk,* Vol.81 (3), pp. 409-452.

[54] Shih, C.and Levi, E., (1971), "Effect of collisions on cold ion collection by means of Langmuir probes", *AIAA J.,* Vol.9 (9), pp. 1673-1680.

[55] Druyvesteyn, M. (1930), "The low-voltage arc", *Z.Phys,* .

[56] Kolobov, V.I. (2006), "Striations in rare gas plasmas", *J.Phys.D,* Vol.39 (24), pp. R487.

[57] Golubovskii, Y.B.and Kolobov, V., (1988), "S. H. al Hawat,"Anode region of a low-current glow discharge infineon at low pressures,"", *Sov.Phys.Tech.Phys,* Vol.33 pp. 1046.

[58] Gill, P.and Webb, C., (1977), "Electron energy distributions in the negative glow and their relevance to hollow cathode lasers", *J.Phys.D,* Vol.10 (3), pp. 299.

[59] Kolokolov, N.and Blagoev, A., (1993), "lonization and quenching of excited atoms with the production of fast electrons", *Physics-Uspekhi,* Vol.36 (3), pp. 152.

[60] Amemiya, H. (1990), "Plasmas with negative ions-probe measurements and charge equilibrium", *Journal of physics.D, Applied physics,* Vol.23 (8), pp. 999-1014.

[61] Godyak, V.and Demidov, V., (2011), "Probe measurements of electron-energy distributions in plasmas: what can we measure and how can we achieve reliable results?", *J.Phys.D,* Vol.44 (23), pp. 233001.

[62] Godyak, V., Piejak, R.and Alexandrovich, B., (1992), "Measurement of electron energy distribution in low-pressure RF discharges", *Plasma Sources Sci.Technol.,* Vol.1 (1), pp. 36.

[63] Lieberman, M.A. and Lichtenberg, A.J., (2005), *Principles of plasma discharges and materials processing,* , John Wiley & Sons,.

[64] Steinbrüchel, C. (1990), "A new method for analyzing Langmuir probe data and the determination of ion densities and etch yields in an etching plasma", *Journal of Vacuum Science & Technology A,* Vol.8 (3), pp. 1663-1667.

[65] Stenzel, R. (1976), "Microwave resonator probe for localized density measurements in weakly magnetized plasmas", *Rev.Sci.Instrum.,* Vol.47 (5), pp. 603-607.

[66] Piejak, R., et al. (2004), "The hairpin resonator: A plasma density measuring technique revisited", *J.Appl.Phys.,* Vol.95 (7), pp. 3785-3791.

[67] Gaman, C. , (2011), "Mass-spectroscopy and modeling of capacitive coupled hydrogen plasmas", Dublin City University,.

[68] "Impedans ltd.", [online], https://www.impedans.com/octiv-vi.

Chapter 3- Investigation of fluorine radical concentration in a capacitively coupled $SF_6/O_2/Ar$ discharge as a function of O_2 concentration

Plasma etching is one of the vital processes in modern semiconductor industries responsible for manufacturing micro/nano-sized integrated circuits. The efficiency of plasma etch process would be quantified using parameters like etch rate and aspect ratio. For deep silicon etching, SF_6 or SF_6 based plasma has been widely used to provide high etch rates. Production of radical species in these plasma governs the etch rate and flux of ions to surface controls the etch profile. Thus, it would be essential to monitor or measure radical species in the plasma using reliable diagnostic techniques for understanding plasma assisted processes in modern semiconductor industries.

3.1 Motivation

Plasma etching performed using SF_6/O_2 mixtures were commonly referred as non-Bosch process to obtain anisotropic profile with high-aspect ratio without alternating steps [1] as compared to Bosch process[2]. Experimental investigations on various discharge shows addition of O_2 to SF_6 plasma improved anisotropic etching through enhanced side-wall passivation and selectivity [3-5], reduced sulfur-based deposition on the reactor walls [6] and improved etch rate [7, 8]. Atomic fluorine radical plays major role in etching Si/SiC and etch rate found to vary (atomic fluorine radical density could be varying) with O_2 concentration in the discharge [7, 8]. So, knowledge on fluorine atom density, [F], in reactive ion etching SF_6/O_2 plasma would be vital to understand mechanism of etch and etch rate. Behavior of fluorine atoms in SF_6/O_2 was investigated experimentally [9-11] and numerically [12-14] in various discharges but no published information about absolute [F] could be found in reactive ion etching capacitively coupled plasma as function of molecular oxygen, O_2, content using reliable diagnostic technique apart from actinometry [15]. The primary objective of my work in this chapter is to investigate the variation in absolute [F], which predominantly controls etch rate, as function of O_2 concentration using reliable plasma diagnostic technique.

And also monitor relative density of ground state fluorine atom using a sensor for industrial application.

Role of oxygen on fluorine atom density in SF_6 discharge was investigated in section 3.2 of this chapter. Then absolute [F] was investigated in $SF_6/O_2/Ar$ capacitively coupled plasma by varying partial pressure of O_2 in 100 W rf discharge using appearance potential mass spectrometry (APMS) in section 3.3. Atomic fluorine densities were investigated at two different total gas pressure i.e., 70 mTorr and 200 mTorr. Absolute [F] was found to vary with molecular oxygen content in the discharge and was initially found to increase, reached a maximum value, before decreasing with increase in molecular oxygen concentration. The validity of sensor measurements, monitoring relative [F] using actinometry, was investigated in section 3.4 by comparing with APMS measurements. Dependence on fluorine production rate was investigated in section 3.5 and various findings on this chapter were summarized in section 3.6.

3.2 Role of oxygen radicals in SF_6 discharge

Atomic oxygen produced through molecular dissociation of O_2 in SF_6/O_2 plasma would play an important role as inhibitor for deep anisotropic silicon etching applications. Oxygen radicals would react with Si substrate to form SiO_xF_y passivation layer and can protect side walls from isotropic etching of high density fluorine flux to obtain anisotropy [3-8]. Moreover, enhancement of fluorine atom density with addition of O_2 in fluorine based discharge had been demonstrated in various literatures [9-14].

This section investigated time evolution of fluorine ion signal, F^+ (proportional to [F]) in SF_6 feedstock with and without O_2 as shown in figure 3.1 at 60 mTorr gas pressure with discharge operated at 500 W rf power. Fluorine ion signal was monitored at fixed electron energy of 21 eV using mass spectrometry as the discharge was switched from pure SF_6 to SF_6/O_2 (90/10 %) and back to pure SF_6 for fixed gas pressure and rf power.

An enhancement of F^+ signal was observed when pure SF_6 discharge was diluted with 10% O_2 at ≈190 seconds as shown in figure 3.1. There could be numerous explanations for this rapid increase in F^+ signal, by a factor of ≈ 60 upon addition of O_2 to feedstock gas. Firstly, significant increase in F^+ signal could be due to decrease in fluorine atom loss rate to reactor walls. In the SF_6 discharge diluted with O_2, atomic oxygen radicals would readily be chemisorbed onto Al surface (reactor walls) due to their higher initial sticking coefficient than that of fluorine radicals [16] and thereby, smaller surface coverage for adsorption of fluorine atom to surface. Thus, loss mechanism of F atom through surface recombination of adsorbed fluorine with SF_x (where x =1-6) radicals in the plasma could be limited and rate of surface recombination would reduce with initial dilution of SF_6 discharge with O_2. In addition to this, increase in F^+ signal can be due to formation of passivation layers (SiO_xF_y) which would reduce fluorine atom surface recombination at reactor walls. No silicon wafers were used in this investigation and however, such layers could still be formed due to etching of optical view ports, made of quartz.

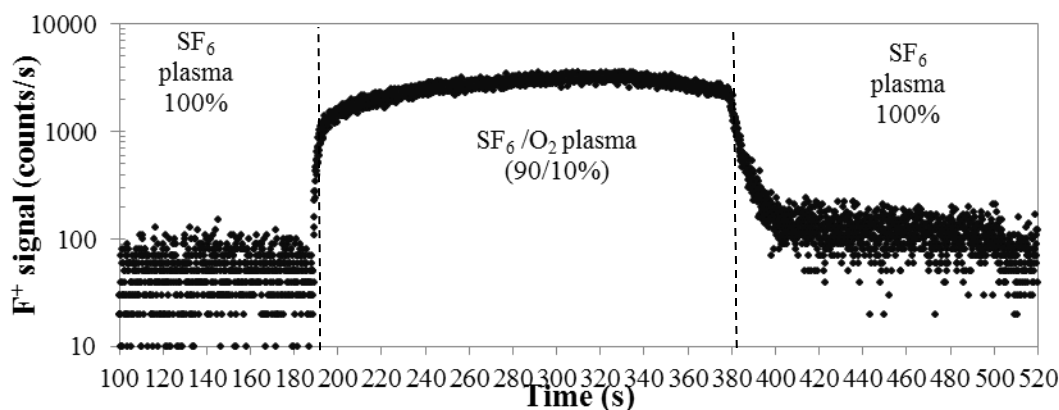

Figure 3.1 Time variation of fluorine signal, F^+ measured using mass spectrometry for fixed electron energy of 21 eV; pressure and RF power were kept constant at 60 mTorr and 500 W respectively. The F^+ signals measured in pure SF_6 plasma for 190 s > time > 380 s and between time 190 – 380 s in SF_6/O_2 (90/10%) discharge.

Another possible explanation for this significant increase in F^+ signal could be production of fluorine atoms due to gas-phase reactions. Fluorine atom production through SF_6-O_2 gas phase reactions were shown in table 3.1 with their corresponding reaction rates [12]. From closer analysis of F^+ signal in figure 3.1, generation of fluorine atom in the discharge through this mechanism could be said as less significant. As O_2 in the discharge was switched off at ≈ 380 seconds, F^+ signal was found to decrease exponentially and initial condition was achieved close ≈ 500 seconds. One possible reason for this behavior of F^+ signal can be long time period required for complete desorption of oxygen atoms from reactor walls. Rapid increase in F^+ signal with addition of O_2 and exponential decrease with long time period to attain initial condition suggest that significant increase in fluorine atom production could be due to decrease in F atom loss rate through surface recombination process. However, further investigation would be required to completely understand the dominant mechanism for enhancement of fluorine atom production with introduction of oxygen in SF_6 discharge.

Table 3.1 Fluorine production through SF_6-O_2 gas-phase reaction and their respective reaction rates co-efficient

Reaction	**Rate co-efficient ($cm^3.s^{-1}$)**	**Reference**
$SF_3 + O \rightarrow SOF_2 + F$	2.0×10^{-11}	[12]
$SF_2 + O \rightarrow SOF + F$	1.1×10^{-10}	[12]
$SF + O \rightarrow SO + F$	1.7×10^{-10}	[12]
$SOF + O \rightarrow SO_2 + F$	7.9×10^{-11}	[12]
$SOF_3 + O \rightarrow SO_2F_2 + F$	5.0×10^{-11}	[12]
$SF_5 + O \rightarrow SOF_4 + F$	1.0×10^{-12}	[12]

3.3 Absolute fluorine atom density in $SF_6/O_2/Ar$ plasma- Effect of O_2 concentration

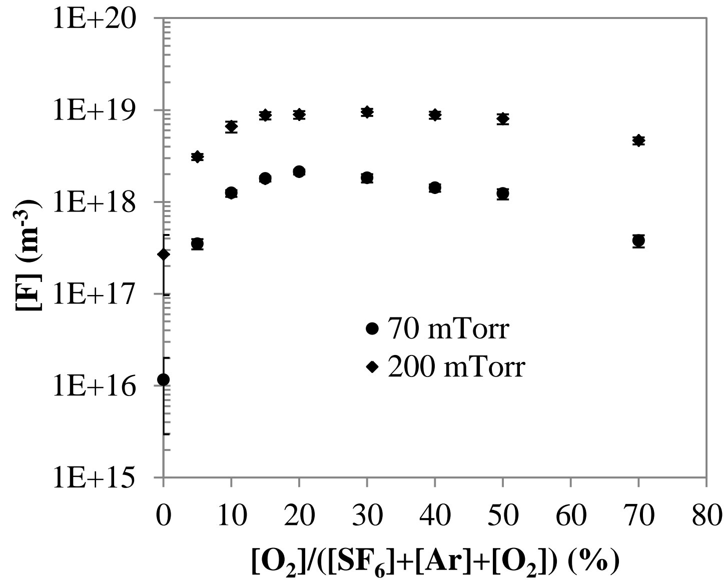

Figure 3.2 Absolute fluorine atom density measured using APMS in $SF_6/O_2/Ar$ plasma by varying O_2 content in feedstock mixture at 70 mTorr (●) and 200 mTorr (♦) gas pressure for 100 W rf power.

F^+ signal was found to increase with introduction of O_2 in SF_6 plasma and possible mechanisms responsible for this behavior of F^+ signal was discussed in previous section. However, to obtain anisotropic profile with perfect vertical sidewalls, knowledge on fluorine atom concentration for given O_2 admixture in SF_6 plasma would be essential. Thus, this section investigated the variations of absolute fluorine atom density as a function of O_2 content in feedstock gas using APMS. Absolute fluorine densities were measured at 70 and 200 mTorr gas pressure at constant discharge power of 100 W as shown in figure 3.2. Linear slopes of fluorine ion signal, F^+, versus electron energy was used to calculate error bars on absolute [F] with 95% confidence interval. Absolute [F] measured at 70 mTorr gas pressure was found to increase initially with addition of O_2 to the discharge and reached a maximum value at 20% O_2. With further

increase in O_2 partial pressure (> 20%), absolute [F] found to decrease. A similar trend of absolute [F] was observed at 200 mTorr but absolute [F] reached a peak value at 30% O_2 under investigated conditions. This difference in peak values of absolute [F] at different O_2 percentage could be due to changes in gas phase reaction coefficients as the discharge was operated at different gas pressures.

Increase in fluorine atom concentration when the discharge was diluted with O_2 can be due to the following reasons. Firstly, additional channel for fluorine atom production can be through gas-phase reactions between fragments of SF_x (where x =1-6) and atomic oxygen [12]. Molecular oxygen in the discharge can dissociate to form atomic oxygen which reacts with fragments of SF_x (where x =1-6) to form oxyfluorides [12] along with fluorine atoms. Secondly, increase in fluorine atom density can be due to change in the rates of surface recombination [9] and which decreases F- atom loss rate with addition of O_2 [17]. Due to formation of oxyfluorides, surface recombination rates of reaction between radicals of SF_x (where x =1-6) and atomic fluorine, F, could be reduced and it would enhance the atomic fluorine density in the discharge. However, the absolute [F] found to decrease for O_2 concentration > 30% for conditions investigated. This decrease in absolute [F] can be mainly due to decrease in SF_6 parital pressure, which was an important source for fluorine atom production through dissociation, as the discharge was diluted with O_2. And also with increase O_2 fractions, the competition between SF_x (where x =1-6) radicals and oxygen to occupy site on the reactor surface could increase, and the recombination reaction rates between SF_x (where x =1-6) radicals and F could increase [13]. Eventually, these gas-phase processes could also account for decrease in fluorine atom density as O_2 concentration increases in the discharge.

3.4 Validation of fluorine actinometry

The validity of sensor measurements through actinometry, to monitor realtive changes in fluorine atom density, was investigated by comparing with absolute variation of [F] measured with APMS technique from previous section. The realtive fluorine atom concentration monitored using actinometric signal ratio, I_F/I_{Ar}, and APMS technique agree qualitatively as shown in figure 3.3 and 3.4. For gas pressure of 70 mTorr (figure 3.3), relative [F] measured using actinometric signal predicted higher value than APMS. However, for gas pressure of 200 mTorr (figure 3.4), the disagreement in realtive [F] measured using two techniques was only found for < 15% O_2 concentration.

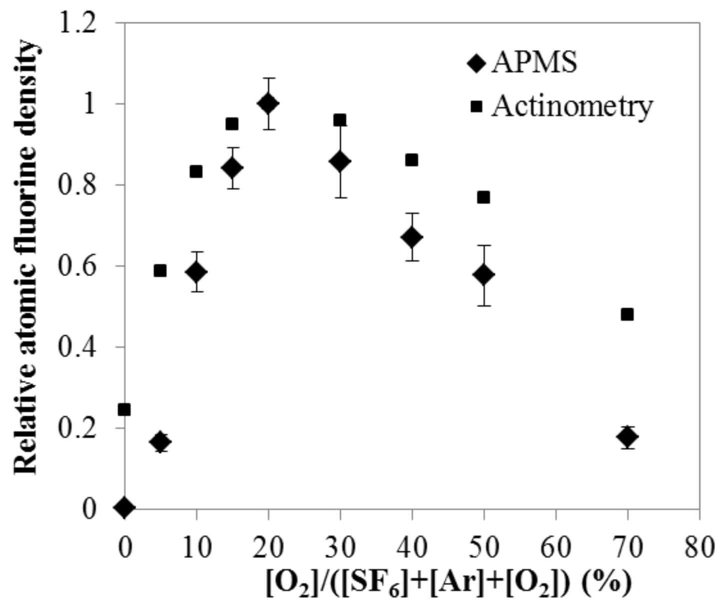

Figure 3.3 Relative fluoirne atom densities measured at 70 mTorr gas pressure using APMS (♦) and actinometry (■) was compared as function of O_2 concentration in a capacitively coupled discharge operated at 100 W rf power.

This discrepancy between relative [F] measured using APMS and actinometric signal, especially at 70 mTorr gas pressure, can be due to following reasons: To monitor actinometric signal, 703.7 nm optical emission line responisble for

fluorine excitation, F^* (703.7 nm), was used. Apart from direct excitation of ground state fluorine atoms, there could be significant additional excitation mechanism contributing to F^*. If such significant process exist, then classical fluorine actinometric model used here to monitor changes in ground state fluorine atom denisty would be unreliable. And the model would require improvement to accommodate such additional excitation process to monitor [F].

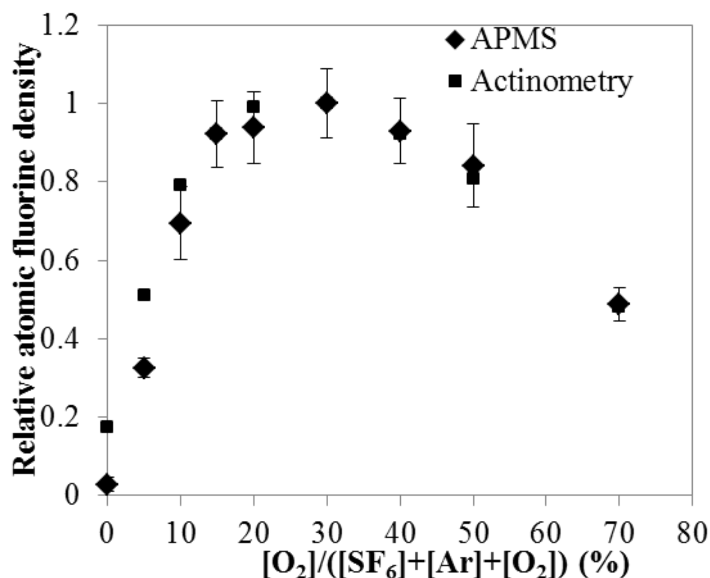

Figure 3.4 Relative fluoirne atom densities measured at 200 mTorr gas pressure using APMS (♦) and actinometry (■) was compared as function of O_2 concentration in a capacitively coupled discharge operated at 100 W rf power.

Assuming additional excitation mechanism was less significant under the conditions investigated here, proportionality constant, K, in actinometry model could be varying with increase in O_2 concentration in the discharge. This variation in K would be violation of one of the assumptions in actinometry model and thus it would make unrealistic to montior relative [F]. With increase in O_2 concentration in the discharge, energy distribution of electrons would change [13] and this would affect the kinectic behaviour of electrons. This would cause significant changes in electron density, n_e, and effective electron

temperature, T_{eff}, in the discharge. SF_6 discharge would be highly electronegative and upon adding O_2, only a marginal increase in n_e was found unitl ≈ 50% O_2 concentration as shown in figure 3.5. Because the discharge would be dominated by SF_x (where x =1-6) and F species, which would involve in electron attachement processes and indeed, would hinder the growth of n_e [10]. Eventually, these processes would affect energy of electrons and lead to decrease in T_{eff} with increasing O_2 concentration [10, 13]. Thus behaviour of electrons would drastically alter electron distribution function as discharge changes from SF_6 to SF_6 diluted with O_2. So any changes in electron distribution function would alter K significantly and lead to violation of actinometry model assumption.

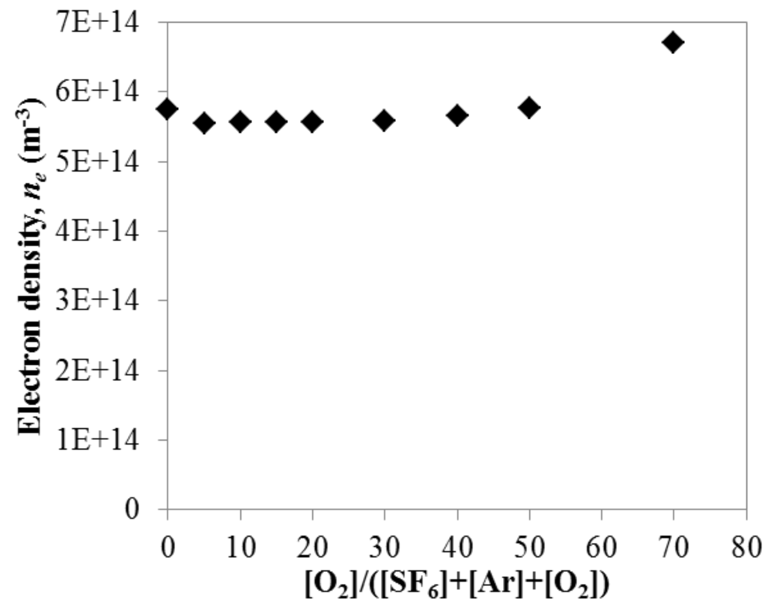

Figure 3.5 Electron density measured using Hairpin probe in a capactively coupled discharge operated at 100 W rf power and 70 mTorr gas pressure in $SF_6/O_2/Ar$ plasma for varying O_2 concentration.

For O_2 concentration ≥ 15%, realtive [F] was found to be in good agreement between two techniques at 200 mTorr than 70 mTorr gas pressure. With increase in discharge gas pressure, mean free path of electrons reduces; high

energy electrons fails to gain energy and decreases as electrons collide with background gas. This kind of change in electron behavior with pressure was observed elsewhere [18] in a similar discharge and also in this discharge with O_2/Ar plasma. Thus, the rate of ionization would decrease and now T_{eff} could be less than electron temperature of high energy tail. Note, with excess addition of O_2 to SF_6 discharge, T_{eff} was expected to drop more signifcantly [10, 13].

3.5 Dissociation fraction and fluorine production efficiency

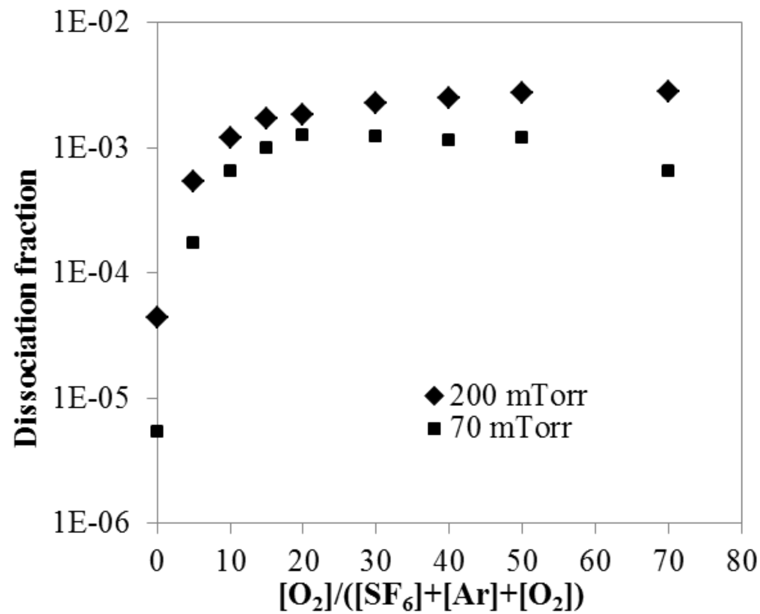

Figure 3.6 Dissociation fractions as a function of O_2 concentration in 70 mTorr (■) and 200 mTorr (♦) gas discharges in SF_6/O_2/Ar plasma operated at 100 W rf power.

As discussed in previous sections, O_2 addition to SF_6 discharge had significant effect on fluorine production. In this section, dependence of fluorine production was investigated and to start with dissociation fraction, D ([F]/[SF_6]) was calculated from absolute APMS measurements. D was found to be higher for 200 mTorr than 70 mTorr as shown in figure 3.6. and it could be due to higher SF_6 paritial pressure in the discharge. In most cases, D would be expected to

increase with increase in O_2 concentration [9, 10, 14, 16] but D was found to drop at 70 mTorr pressure for O_2 concentration > 20 %. For both investigated pressures, D was found to be very low for pure SF_6 discharge; indicating low atomic fluorine production.

With small amount of O_2 (5%) to pure SF_6 discharge, APMS measurements indicated an order increase in fluorine production whereas actinometry predicted an increase by factor of ≈ 3 at both pressures as shown in figure 3.7 and 3.8. Also at 70 mTorr, production efficiency of fluorine was found to increase initially with O_2 content and reached maximum at 20% O_2 concentration. With further increase in O_2 concentration (> 20 %) in the discharge, fluorine production efficiency was found to drop as shown in figure 3.7. For an increase in O_2 concentration in discharge, electronegativity of the discharge would decrease considerably due to increase in concentration of less electronegative species like O and O_2 [10]. In such sceanrios, formation of electron-ion pair formation in the discahrge with high concentration O and O_2 species would be favoured as it would require low energy than in SF_x (where x =1-6) dominated discharge [10] and this would eventually cause conisderable decrease in T_{eff} [10, 14]. It was well known, the main production mechanism of atomic fluorine in low pressure SF_6 discharges would be dissociative processes [12] and for effective dissociation of SF_x (where x =1-6), electrons with energy close to or higher than dissociation reaction threshold energy would be required. Since T_{eff} was expected to decrease with increase in O_2 concentration in discharge [10, 14] and this drop in energy of plasma electrons would significantly affect the dissociation rate which could have caused a certain decrease in fluorine production efficiency. However, actinometry predicted an increase in fluorine production rate with increase in O_2 content at 70 mTorr gas pressure as shown in figure 3.7. Possible reasons for this discrepancy between two techniques at 70 mTorr gas pressure condition was discussed in section 3.4. At 200 mTorr, fluorine production efficiency, defined as atomic fluorine

density over pressure, was found to increase with O_2 content and good agreement was achieved between APMS and actinometric measurements for O_2 concentration > 10 % as shown in figure 3.8. Production rate of fluorine may appear to decrease with increase in SF_6 paritial pressure and it was a mere coincidence. Here the decrease in fluorine production rate could be mainly due to drop in T_{eff} with increase in O_2 concentration in the discharge.

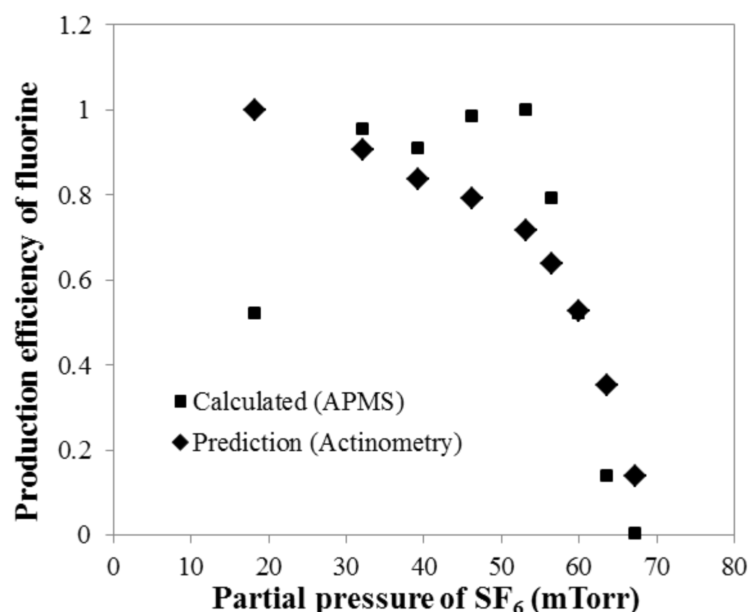

Partial pressure of SF_6 (mTorr)	18.2	32.2	39.2	46.2	53.2	56.6	59.9	63.6	67.2
Equivalent Oxygen content (%)	70	50	40	30	20	15	10	5	0

Figure 3.7 Production efficiency of fluorine calculated from APMS (■) measurements and predicted values from actinometry (♦) measurements were plotted as a function of SF_6 partial pressure in $SF_6/O_2/Ar$ plasma with total gas pressure of 70 mTorr operated at 100 W rf power.

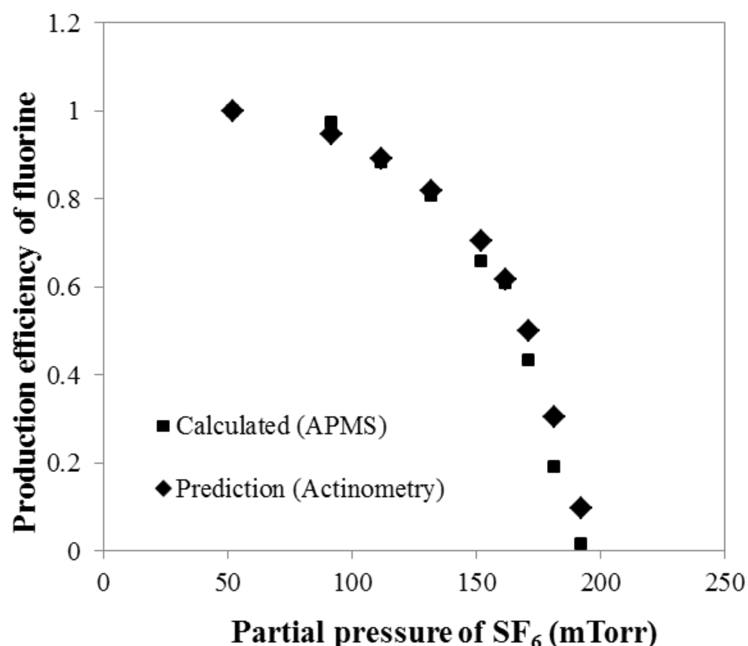

Partial pressure of SF_6 (mTorr)	52	92	112	132	152	162	171	182	192
Equivalent Oxygen content (%)	70	50	40	30	20	15	10	5	0

Figure 3.8 Production efficiency of fluorine calculated from APMS (■) measurements and predicted values from actinometry (♦) measurements were plotted as a function of SF_6 partial pressure in $SF_6/O_2/Ar$ plasma with total gas pressure of 200 mTorr operated at 100 W rf power.

3.6 Conclusion

Absolute atomic fluorine density was investigated in this chapter by varying O_2 concentration in $SF_6/O_2/Ar$ discharge using APMS technique at 70 and 200 mTorr gas pressure for constant rf power of 100 W. With dilution of O_2 in SF_6 discharge, absolute [F] found to increase initially and reached maximum for both investigated gas pressures. This increase in absolute [F] could be mainly

due to decrease in rate of surface recombination of F atom with SF_x (where x =1-6) radicals and gas-phase reaction between SF_x (where x =1-6) and O species, which lead to formation of oxyfluoride compounds along with fluorine atoms. However, absolute [F] found to decrease, after reaching peak, with further increase in O_2 percentage and this could be due to decrease in SF_6 partial pressure in the discharge. Absolute [F] measurements were used to validate optical emission spectroscopy sensor measurements, required for industrial application to monitor relative atomic fluorine density using actinometric techinque. Good qualitative agreements were achieved between both techniques in measuring relative [F] for both investigated gas pressures. However, significant discrepancy in relative [F] measurements was found quantitaively between two techniques for 70 mTorr and 200 mTorr (< 15% O_2) gas pressures. And this poor correlation at these conditions could be due to additional fluorine excitation mechanism apart from direct excitation of ground state fluorine atoms and/or change in kinetic behaviour of electrons within investigated conditions. In addition, good agreement on relative [F] measured using actinometric and APMS technique was achieved at 200 mTorr gas pressure for O_2 concentration ≥ 15%. In addition, any considerable decrease in T_{eff} of high population electrons with increase in O_2 concentration in SF_6 plasma would significantly affect fluorine production efficiency.

3.7 References

[1] Jansen, H., Meint de Boer and Miko Elwenspoek 1996, "The black silicon method. VI. High aspect ratio trench etching for MEMS applications", "The black silicon method. VI. High aspect ratio trench etching for MEMS applications", *Proceedings Micro Electro Mechanical Systems,*: IEEE 250-257.

[2] Laemer,F, Schip,A, (1996), "WO94/14187 (DE93/01129, US patent US5501893)", US5501893.

[3] Aachboun, S.and Ranson, P., (1999), "Deep anisotropic etching of silicon", *Journal of Vacuum Science & Technology A,* Vol.17 (4), pp. 2270-2273.

[4] Boufnichel, M., et al. (2002), "Profile control of high aspect ratio trenches of silicon. I. Effect of process parameters on local bowing", *Journal of Vacuum Science & Technology B,* Vol.20 (4), pp. 1508-1513.

[5] Marcos, G., Rhallabi, A.and Ranson, P., (2004), "Topographic and kinetic effects of the SF6/O2 rate during a cryogenic etching process of silicon", *Journal of Vacuum Science & Technology B,* Vol.22 (4), pp. 1912-1922.

[6] Chabert, P., et al. (2000), "High rate etching of 4H–SiC using a SF6/O2 helicon plasma", *Appl.Phys.Lett.,* Vol.76 (16), pp. 2310-2312.

[7] Khan, F.and Adesida, I., (1999), "High rate etching of SiC using inductively coupled plasma reactive ion etching in SF~ 6-based gas mixtures", *Appl.Phys.Lett.,* Vol.75 (15),.

[8] Chabert, P. (2001), "Deep etching of silicon carbide for micromachining applications: Etch rates and etch mechanisms", *Journal of Vacuum Science & Technology B,* Vol.19 (4), pp. 1339-1345.

[9] Kopalidis, P.M.and Jorne, J., (1992), "Langmuir Probe Measurements and Characterization of Silicon Etching in SF 6/O 2 Discharges", *J.Electrochem.Soc.,* Vol.139 (3), pp. 839-844.

[10] Pessoa, R., et al. (2010), "Study of SF6 and SF6/O2 plasmas in a hollow cathode reactive ion etching reactor using Langmuir probe and optical emission spectroscopy techniques", *Plasma Sources Sci.Technol.,* Vol.19 (2), pp. 025013.

[11] Lim, Y., et al. (2009), "Roles of F and O Radicals and Positive Ions in a SF6/O2 Plasma in Forming Deep Via Structures", *Journal of Korean Physical Society,* Vol.54 pp. 1774.

[12] Ryan, K.and Plumb, I., (1990), "A model for the etching of silicon in SF6/O2 plasmas", *Plasma Chem.Plasma Process.,* Vol.10 (2), pp. 207-229.

[13] Anderson, H., Merson, J.and Light, R., (1986), "A kinetic model for plasma etching silicon in a SF6/O2 RF discharge", *IEEE Trans.Plasma Sci.,* Vol.14 (2), pp. 156-164.

[14] Pateau, A., et al. (2014), "Modeling of inductively coupled plasma SF6/O2/Ar plasma discharge: Effect of O2 on the plasma kinetic properties", *Journal of Vacuum Science & Technology A,* Vol.32 (2), pp. 021303.

[15] d'Agostino, R., et al. (1985), "On the use of actinometric emission spectroscopy in sf6-o2 radiofrequency discharges: Theoretical and experimental analysis", *Plasma Chem.Plasma Process.,* Vol.5 (3), pp. 239-253.

[16] Su, Z. , (2015), "Modelling of Low-Pressure discharges for plasma processing", Dublin City University,.

[17] Hancock, G., Sucksmith, J.P.and Toogood, M.J., (1990), "Plasma kinetic measurements using time-resolved actinometry: comparisons with laser-induced fluorescence", *J.Phys.Chem.,* Vol.94 (8), pp. 3269-3272.

[18] Godyak, V., Piejak, R.and Alexandrovich, B., (1992), "Measurement of electron energy distribution in low-pressure RF discharges", *Plasma Sources Sci.Technol.,* Vol.1 (1), pp. 36.

Chapter 4- Investigation of atomic fluorine density by varying gas pressure in a capacitively coupled $SF_6/O_2/Ar$ discharge

4.1 Motivation

Enhancement of fluorine atom density with small addition of oxygen in SF_6 discharge was evident from previous chapter. Also, atomic fluorine density was found to decrease with excess oxygen content in SF_6 discharge. Apparently, APMS and actinometry measurements agreed well on relative fluorine density variations for different O_2 content in SF_6 discharge operated at 200 mTorr gas pressure. However, only qualitative agreement on variations of relative fluorine density was achieved between both techniques at 70 mTorr gas pressure. Moreover, for pressure increase from 70 to 200 mTorr, inconsistent behavior of fluorine production efficiency was observed with increase in O_2 content. This could be inconclusive as the control variable was not only limited to total gas pressure but also to varying SF_6 and O_2 flow rate. Flow rates of feedstock mixture in the discharge must be fixed along with other control variables for more realistic investigation on fluorine production rate with gas pressure.

One of the most important plasma process parameter to control plasma etching would be gas pressure to influence various discharge phenomena. Some of these phenomena influenced by gas pressure include: sheath voltage drop and sheath thickness [1], fluxes of ions & radical species to surfaces and their ratios through electron energy, and relative rate of gas-phase kinetic processes [2]. These phenomena would control various plasma etching parameters; in particular etch rate [3-5] apart from anisotropy [6, 7] and uniformity [8]. As said before, etch rate would be predominantly driven by radical species produced in the plasma. So, knowledge on radical production with increase in gas pressure in the plasma would be vital for various etching process.

Over the years, various diagnostics technique had been used to investigate the atomic fluorine atom density as a function of different chamber conditions on various discharges in CF_4/CF_4 based [9-11] and SF_6/SF_6 based [12-17] plasmas. P. M. Kopalidis *et al* [18] investigated the effect of pressure and percentage of O_2 on etch rate in a low pressure capacitively coupled SF_6/O_2 reactive ion

etching reactor but no attempt was made in his work and elsewhere so far to experimentally measure the absolute concentration of fluorine atoms as function of chamber pressure in capacitive RIE discharges. Thus, primary motivation in this chapter was to investigate absolute fluorine production as a function of chamber pressure using APMS technique. Moreover, relative variations of atomic fluorine density would be monitored using fluorine actinometry and compared with APMS measurements for sensor validation.

In section 4.2, variation of absolute fluorine atom density was investigated as a function of gas pressure using APMS in $SF_6/O_2/Ar$ discharge operated at 100 W rf power. Based on previous chapter and for higher fluorine production, O_2 content in the discharge was fixed at 26 % for investigated pressures in this chapter. Relative variations of fluorine density were monitored using actinometry in section 4.3 and also relative [F] measured using APMS were used to validate actinometric technique. Electron heating mechanism could change with increase in pressure and apparently can cause changes to electron dynamics. Such discharge transition due to change in electron heating process was verified using I-V probe in section 4.3.1 for investigated pressure range in this chapter. Moreover, improvement to fluorine actinometry with a dissociative term was suggested in section 4.3.2 with adequate knowledge on the electron heating mechanism. Finally, section 4.4 would present the conclusive summary of investigations carried out in this chapter.

4.2 Pressure variation of absolute fluorine atom density in $SF_6/O_2/Ar$ plasma

Variation of absolute ground state fluorine atom density with gas pressure was investigated in $SF_6/O_2/Ar$ (70/26/4%) discharge operated at 100 W RF power using APMS and results were shown in figure 4.1. Absolute [F] was found to increase with pressure and this can be attributed to increase in SF_6 partial pressure in the discharge. Due to pressure restriction in EQP, the plasma

discharge could not be operated beyond total gas pressure of 250 mTorr. The error bar on absolute fluorine atom density measurements were calculated with standard error (corresponds to 95% confidence interval) using slopes of linear fits to fluorine ion signal (F^+) vs electron energy. Increase in absolute fluorine atom density with pressure could be mainly due to dissociation of SF_6 molecules as electrons density was found to be in weak correlation with pressure as shown in figure 4.2 and also elsewhere [11, 14, 18]. Moreover, dissociation fraction was found to increase with gas pressure as shown in figure 4.3 and this indicated rise in fluorine density was significantly due to electron impact dissociation of SF_6. However for pressure > 200 mTorr, dissociation fraction was found to drop and this could be due to decrease in the population of high energy electrons responsible for electronic dissociation of SF_6 molecule.

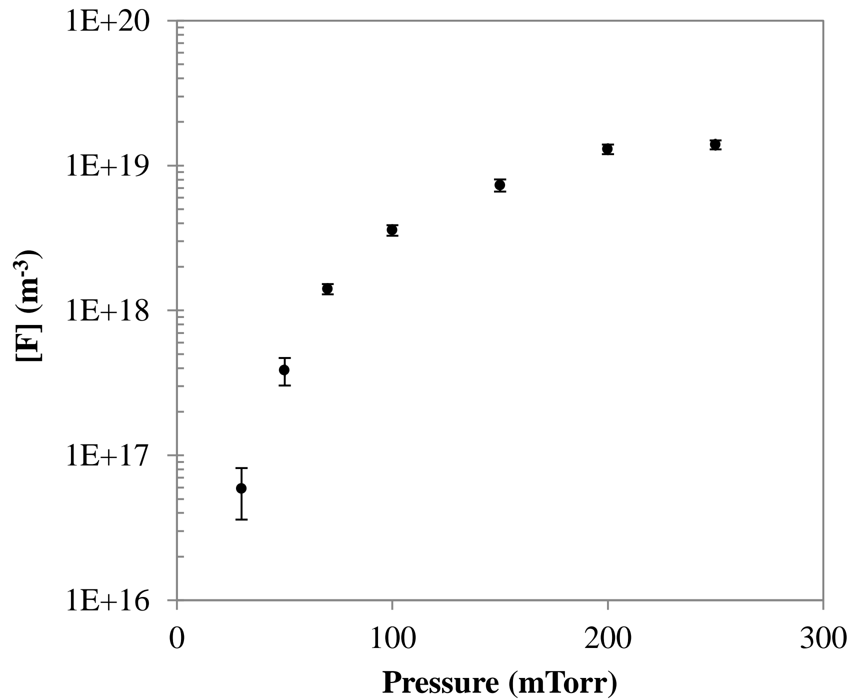

Figure 4.1 Pressure variation of absolute fluorine atom density measured using APMS in $SF_6/O_2/Ar$ (70/26/4%) capacitively coupled discharge operated at 100 W rf power.

Electron heating mechanism can be expected to vary with pressure in capacitive discharges [19, 20] and obviously, this would cause considerable effect on energy of plasma electrons. Furthermore, increase in absolute [F] can also be due to gas phase reactions involving atomic oxygen and SF_x radicals and thereby reducing the loss mechanism of fluorine atoms through recombination reactions [18, 21, 22].

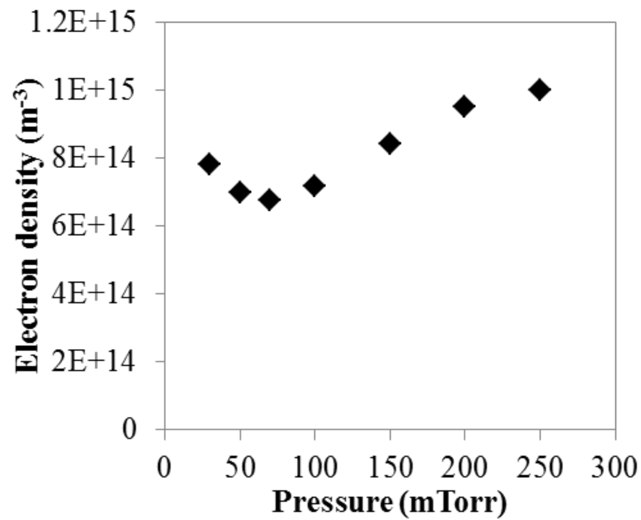

Figure 4.2 Pressure variation of electron density measured using hairpin probe in $SF_6/O_2/Ar$ (70/26/4%) capacitively coupled discharge operated at 100 W rf power.

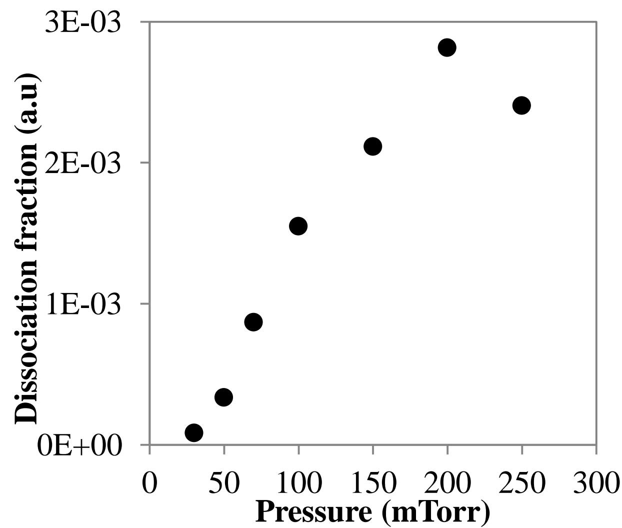

Figure 4.3 Dissociation fraction as a function of gas pressure in in $SF_6/O_2/Ar$ (70/26/4%) capacitively coupled discharge operated at 100 W rf power.

4.3 Relative variation of [F] using actinometry and its validation

In this section, fluorine actinometry was employed to monitor relative [F] using optical emission spectroscopy, widely used industrial sensor to monitor species production in plasma. Absolute [F] measurements using APMS technique was used to validate relative variations of [F] measured using fluorine actinometry. Relative [F], measured using both actinometry and APMS techniques, was found to increase with gas pressure investigated in this work as shown in figure 4.4. However, quantitatively poor correlation between both two techniques on relative [F] measurements was observed for gas pressures > 200 mTorr in this work. Also, actinometry predicted an increase in [F] by a factor of 11 while APMS measurement increased more than two orders of magnitude over the same investigated conditions.

One possible cause for this discrepancy between two techniques in monitoring [F] could be variations in ratio of excitation rate coefficients or proportionality constant, K caused by change in electron heating mechanism. In a typical capacitive rf discharge with increase in gas pressure, the electron heating process would undergo a transition from stochastic (collisionless) electron heating at low pressures (where mean free path for electrons would be similar or greater than discharge length) to ohmic (collisional) electron heating (where mean free path for electrons would be small and thus, electrons collide with neutrals and heated up in bulk plasma rf field). Usually such transition from collisionless to collisional heating will affect electron kinetics due to Ramsauer effect and obviously, change in electron energy distribution function (EEDF) can be observed [23-26]. Such transitions due to changes in electron heating mechanism were also observed in this discharge with argon [20], oxygen [chapter 6] for gas pressure variations. V. Lisovskiy *et al* [27] observed transition due to electron heating in SF_6 and SF_6/O_2 capacitive rf discharge with

increase in gas pressure. If such transition occurs, shape of EEDF would change and the value of K would experience a variation. This variation in K violates one of actinometric limitation, where it assumes of no significant changes to EEDF and in such case, actinometric signal could make erroneous prediction to relative [F] variations.

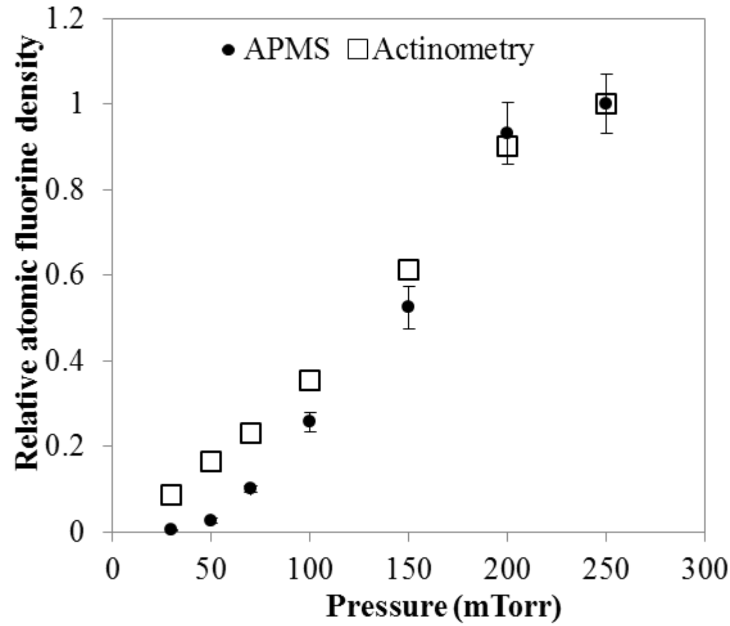

Figure 4.4 Relative fluorine atom densities measured using APMS (●) and actinometry (□) were compared in $SF_6/O_2/Ar$ (70/26/4%) capacitively coupled discharge operated at 100 W rf power.

In addition to above cause for discrepancy between two techniques, relative [F] measured using actinometric signal was found to be higher than APMS measurements, especially for pressures < 200 mTorr. Additional fluorine excitation mechanism apart from direct excitation of fluorine atoms could also be responsible for this poor correlation of actinometric signal with APMS in monitoring relative [F] for pressures < 200 mTorr. If there could be any significant excitation channel [14, 28, 29] to optical emission line at 703.7 nm, then monitoring actinometric signal to predict relative [F] would be unreliable.

Moreover, existence of any additional excitation mechanism apart from direct excitation of ground state fluorine atom was investigated in section 4.3.2.

4.3.1 Electrical characteristics in $SF_6/O_2/Ar$ plasma as function of gas pressure

Variation on relative [F] measured using APMS and actinometry had poor quantitative agreement for investigated pressures and the possible reasons were discussed in section 4.3. One possible explanation was change in discharge characteristics with increase in pressure, which was investigated in this section using current-voltage characteristics (IVCs). Measurements were made with Octiv probe, commercial IV probe from Impedans ltd [30], mounted between match unit and powered electrode of plasma tool used in this work.

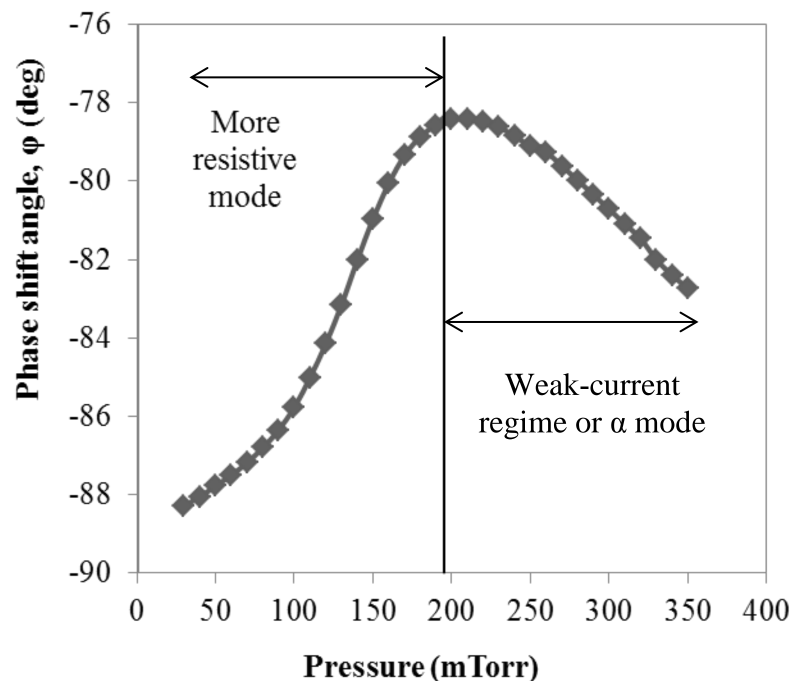

Figure 4.5 Pressure dependence on phase shift angle measured using Octiv probe in $SF_6/O_2/Ar$ (70/26/4%) capacitively coupled discharge operated at 100 W rf power.

IVCs were studied by varying pressures in $SF_6/O_2/Ar$ (70/26/4%) discharge operated at 100 W rf power using Octiv probe to gain knowledge on discharge transition due to change in electron heating mechanism. Phase shift angle (φ) between rf current (I_{rf}) & voltage, rf current, and active rf current, I_{rf} cos(φ) were measured with high precision against varying total gas pressure were shown in figure 4.5, 4.6 & 4.7. With increase in pressure until ≈ 200 mTorr, the discharge was becoming more resistive in the plasma bulk as φ decreased. That indicated voltage drop across plasma bulk would be significant and can be due to low density of electrons in plasma bulk [31]. Consequently, with further increase in pressure, electron-neutral collision frequency increases and low energy electrons in plasma bulk could be heated due to rf electric field in plasma bulk. Thus, electrons in plasma bulk gain energy due to collisional heating with increase in pressure and so φ was approaching $-\pi/2$ as shown in figure 4.5.

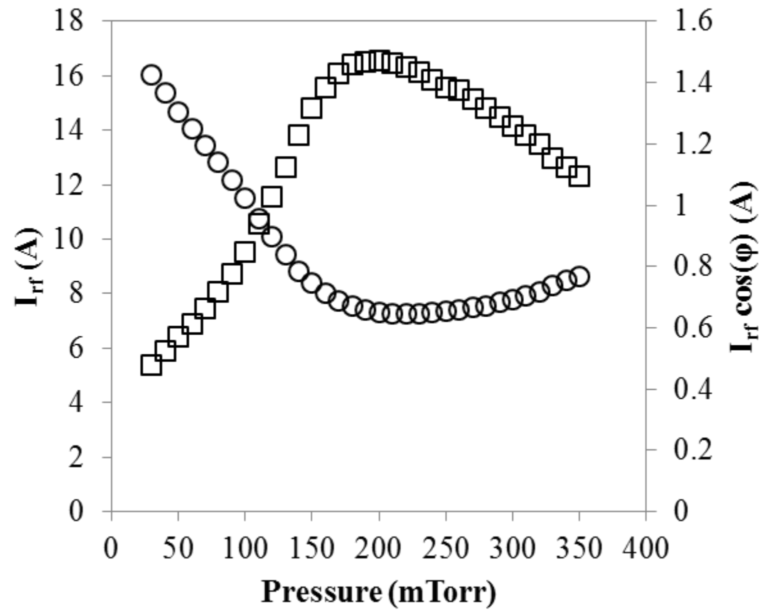

Figure 4.6 Pressure dependence on rf current amplitude (○) and active rf current (□) measured using Octiv probe in $SF_6/O_2/Ar$ (70/26/4%) capacitively coupled discharge operated at 100 W rf power.

In addition, ohmic power transferred to electrons, $P_{ohm} \propto J_o \upsilon_{en}/n_e$ where J_o is the discharge current density, υ_{en} is the electron-neutral collision frequency and n_e is electron density [32]. With increase in pressure, Jo and υ_{en} would be expected to increase and n_e was initially found to decrease as shown in figure 4.2 and this could increase P_{ohm}. For pressures > 70 mTorr, energy transfer to electrons through collisional heating began to increase and rf electric field in bulk also increases as electron density found to increase slowly. Also with increase in gas pressure in electronegative discharge, electrons loss process in the bulk would increase due to electron-ion attachment processes [33]. This could be the reason for slow increase in electron density for pressure > 70 mTorr. Due to complex nature of the discharge studied, further investigation would be essential to gain knowledge kinetic parameters of electrons like electron energy distribution function, effective electron temperature and charged particle densities to clearly understand pressure dependence behavior on electron kinetics in $SF_6/O_2/Ar$ plasma. Nevertheless, change in discharge characteristics, i.e., from resistive to capacitive was evident and contrary to literature reports [12, 31, 34-36]. However, Lisovskiy *et al* [27] found similar behavior (to that reported in this work) in discharge characteristics with variation in gas pressure and observed discharge transition from more resistive to weak-current mode (α-mode) with increase in pressure (figure 5 in [27]). Under investigated pressure in this work, it could be said that discharge transition was apparent and obviously, value of K in actinometry would change as EEDF would be reshaped due to change in electron heating mechanism. This possibly could be the reason for quantitative discrepancy between actinometric signal and APMS measurements on relative [F]. In order to make reliable actinometric model to monitor [F] in such discharge transition, knowledge on EEDF and electron impact excitation cross sections of F & Ar atoms would be essential.

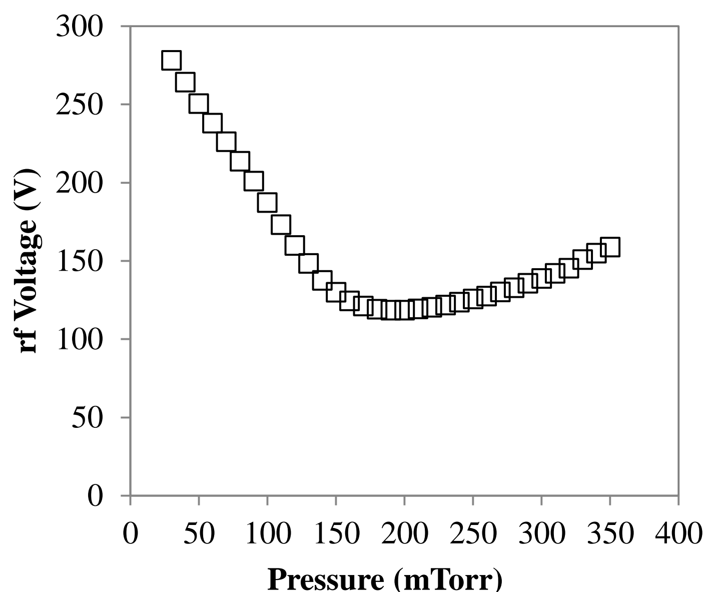

Figure 4.7 Pressure dependence on rf voltage (□) measured using Octiv probe in $SF_6/O_2/Ar$ (70/26/4%) capacitively coupled discharge operated at 100 W rf power.

4.3.2 Dissociative excitation- Improvement to fluorine actinometry

In the previous section, discharge was found to transit to weak-current mode from more resistive behavior with increase in pressure and violated actinometric model assumption. In this section, numerical analysis was carried out to investigate the contribution of additional excitation mechanism contribution to F^* apart from direct electron impact process. Quenching terms were not included due to numerous species production in SF_6-O_2 discharge and with less information on literature about their respective quenching rates on excited fluorine and argon atoms, it would be challenging to incorporate such term in this improved fluorine actinometry.

Both actinometry and APMS measurements established poor quantitative behaviour for pressures < 200 mTorr, where discharge was found to be resistive

according to figure 4.5 and could expect no significant change to EEDF in this regime. So, obviously overestimation of fluorine density variation predicted by actinometry can be predominately due to additional excitation contribution to actinometric signal in this resistive regime. Here, electron impact dissociative excitation was assumed to be dominant additional excitation process [14, 28, 29] as no evidence could be found in literature for any other contribution to fluorine excitation process. According to classical actinometry considered in this study, fluorine density would be proportional to product of ratio of optical emission signals of fluorine and argon atoms, I_F/I_{Ar} and argon density, [Ar] i.e., [F] = K (I_F/I_{Ar}) [Ar], in which proportionality constant, K wouldn't change since the study was limited to gas pressures 30 – 150 mTorr, where no drastic change in EEDF was expected as discharge was in resistive mode. So if fluorine signal measured using actinometry carries significant dissociative contribution then, fluorine density can be written as,

$$[\boldsymbol{F}] = \boldsymbol{K}\left(\frac{\boldsymbol{I_F^{dir}} + \boldsymbol{I_F^{diss}}}{\boldsymbol{I_{Ar}}}\right)[\boldsymbol{Ar}] \tag{4.1}$$

where I_F^{dir} and I_F^{diss} were optical emission signal of F* (703.7 nm) from direct and dissociative excitation respectively and $I_F = I_F^{dir} + I_F^{diss}$. Rearranging

$$[\boldsymbol{F}] = \boldsymbol{K}\left(\frac{\boldsymbol{I_F^{dir}}}{\boldsymbol{I_{Ar}}}\right)[\boldsymbol{Ar}] + \boldsymbol{K}\left(\frac{\boldsymbol{I_F^{diss}}}{\boldsymbol{I_{Ar}}}\right)[\boldsymbol{Ar}] \tag{4.2}$$

Ground state fluorine density measured using APMS, $[F]_{APMS}$ would be proportional to I_F^{dir}/I_{Ar} and so

$$[\boldsymbol{F}] = [\boldsymbol{F}]_{\boldsymbol{APMS}} + \boldsymbol{K}\left(\frac{\boldsymbol{I_F^{diss}}}{\boldsymbol{I_{Ar}}}\right)[\boldsymbol{Ar}] \tag{4.3}$$

Dissociative part of the equation 4.3 can be called as density of fluorine produced through dissociative excitation, $[F]_{diss}$

$$[\boldsymbol{F}] = [\boldsymbol{F}]_{\boldsymbol{APMS}} + [\boldsymbol{F}]_{\boldsymbol{diss}} \tag{4.4}$$

Finally, equation 4.4 was rearranged to verify additional excitation contribution as

$$[F]_{APMS} = K\left(\frac{I_F}{I_{Ar}}\right)[Ar] - [F]_{diss} \tag{4.5}$$

A plot of $[F]_{APMS}\ vs\ (I_F/I_{Ar})[Ar]$ would reveal if any significant additional excitation contribution to measured optical fluorine emission signal. Such a plot was shown in figure 4.8 and it was found the slope had a negative intercept. This suggested that measured optical fluorine emission signal for monitoring relative [F] using actinometry had significant additional excitation mechanism i.e., dissociative excitation apart from direct excitation of ground state fluorine atom for pressures < 200 mTorr. Moreover, fluorine atom production efficiency per unit pressure calculated from dissociative part of actinometric signal and APMS were shown in figure 4.9. As expected, with increase in pressure the rate of atomic fluorine production predicted by dissociative actinometric signal decreased with increase in pressure.

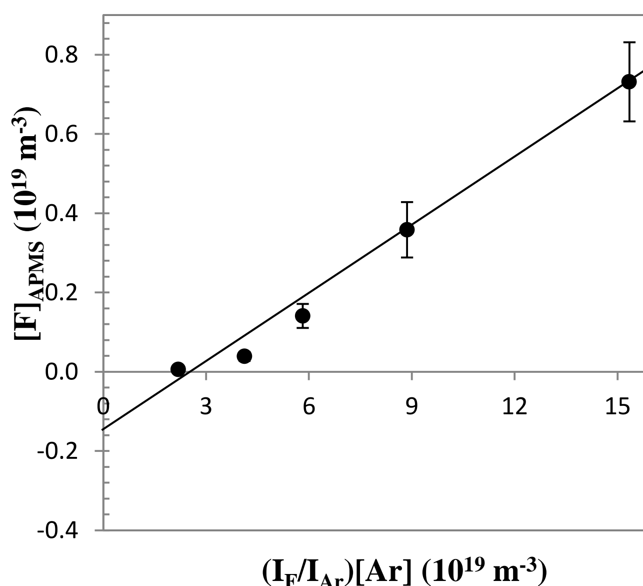

Figure 4.8 Plot of fluorine density measured using APMS, $[F]_{APMS}$ vs actinometric signal, (I_F/I_{Ar}) [Ar] to investigate additional excitation mechanism

contribution to actinometric signal in $SF_6/O_2/Ar$ (70/26/4%) capacitively coupled discharge operated at 100 W rf power.

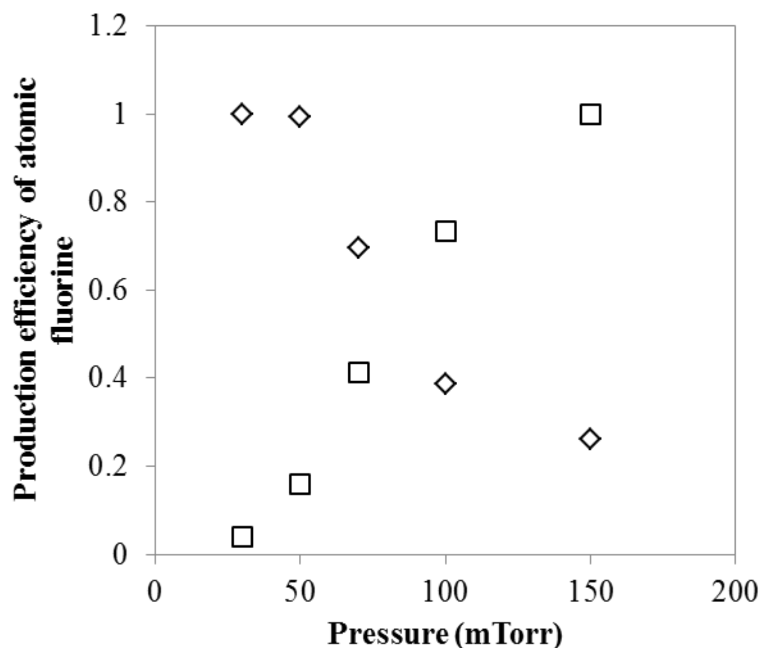

Figure 4.9 Production efficiency of fluorine atom calculated using APMS (□) and dissociative contribution (◊) as function of gas pressure in $SF_6/O_2/Ar$ (70/26/4%) capacitively coupled discharge operated at 100 W rf power.

It should be noted that this section only investigated the existence of additional excitation mechanism to fluorine emission signal apart from direct excitation of ground state fluorine atom and no attempt was made to obtain absolute value for dissociation excitation contribution. Even though EEDF was assumed to be constant at investigated pressures in this section, variation of dissociative excitation contribution is possible due to changes to temperature of high energy electrons (at EEDF tails) with increase in pressure. At low pressures, mean free path of electrons-neutral collision would be large or equivalent or to chamber dimensions and electrons with high temperature would accelerate to sheath, where rf electric field exist. These high energy electrons could be responsible

for various processes like ionization and dissociative excitation close to sheath region in the discharge. Note, optical emission measurements were line averaged between two electrodes and could be heavily contaminated with dissociative signal if such process was dominant. With increase in pressure, electron-neutral collision mean free path would be small and electrons would be cooled due to collisions; electron temperature would decrease. And most ionization will happen in plasma bulk rather than close to sheath. With increase in pressure, the density of high energy electrons in the discharge would also reduce due to cooling through collisions and so does there contribution to favour dissociative excitation process.

In addition, few literatures [14, 28, 29] suggested (irrespective of exact process and threshold energy) SF_6 could be the parent molecule involved in dissociative excitation process. Apparently, this assumption was verified by comparing actinometric signal to that of SF_6 density as shown in figure 4.10. Actinometric signal followed number density of SF_6 for pressures < 200 mTorr under investigated conditions and this verified my assumption made on possible dissociative excitation partner involved. And also strong emphasis was made about significant electron impact dissociation excitation for gas pressures < 200 mTorr. Thus, monitoring actinometric signal without accounting for dissociative excitation process under these conditions (< 200 mTorr) would make relative [F] unreliable using actinometry. So, improvement was made to classical actinometry model to incorporate if any dissociative excitation process through SF_6,

$$[F] = K\left(\frac{I_F}{I_{Ar}}\right)[Ar] - \left(\frac{k_{SF_6}^{de}}{k_F^e}\right)[SF_6] \qquad (4.6)$$

where k_F^e and $k_{SF_6}^{de}$ were excitation rate coefficients for direct and dissociative excitation respectively and $[SF_6]$ was number density of SF_6 molecules.

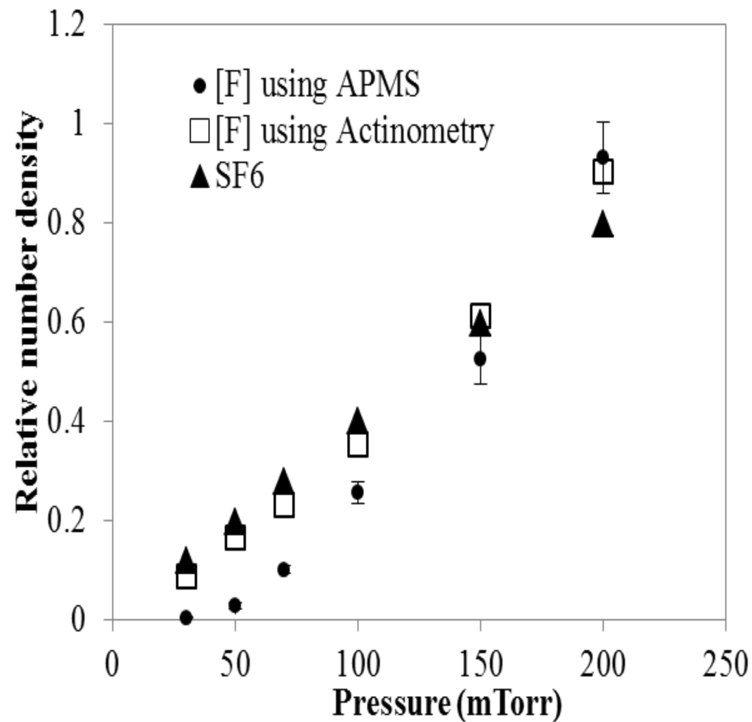

Figure 4.10 Relative number densities of [F] using APMS (●), [F] using actinometry (□) and SF_6 using ideal gas law (▲) in a capacitively coupled discharge.

4.4 Conclusion

Variation of absolute [F] as function of pressure was investigated using APMS in a capacitively coupled $SF_6/O_2/Ar$ (70/26/4%) discharge operated at 100 W rf power. Absolute [F] was found to increase with pressure and could be due to increase in SF_6 partial pressure along with increase in fluorine atom production through reaction between SF_x and O radical species. Fluorine actinometry was validated and quantitatively, poor correlation was observed in relative [F] measurements in comparison to APMS for pressures < 200 mTorr. One of the possible causes for this poor correlation could be change in electron heating mechanism, which would reshape EEDF and could cause variation to *K*, violating actinometry model assumption. This transition behavior in the discharge was investigated using IVCs and was evident as discharge behavior

changed from more resistive to capacitive. However, most significant cause for overestimation of relative [F] by actinometry than APMS measurement, especially for pressures < 200 mTorr was contamination of measured fluorine optical emission signal (703.7 nm), in particular with dissociative excitation. Possible contribution of [F] through dissociative excitation process was calculated for pressures 30 – 150 mTorr with an assumption of no significant change to EEDF, as discharge was found to be resistive from φ measurement of IVCs. Furthermore, with increase in pressure in the resistive regime, production efficiency of fluorine atom predicted by dissociative part of actinometric signal was found to decrease and could be due to change in electron kinetics. Also, number densities of SF_6 closely followed the actinometric signal for pressures < 200 mTorr and this suggested SF_6 could be dissociative partner involved in additional excitation process. Finally, improvement to fluorine actinometry to calculate absolute fluorine atom density was suggested to accommodate dissociative excitation contribution to actinometric signal.

4.5 References

[1] Godyak, V.A., Piejak, R.B.and Alexandrovich, B.M., (1991), "Electrical characteristics of parallel-plate RF discharges in argon", *IEEE Trans.Plasma Sci.,* Vol.19 (4), pp. 660-676.

[2] Sugawara, M., (1998)*, Plasma etching: fundamentals and applications,* , OUP Oxford,.

[3] Chabert, P., et al. (2000), "High rate etching of 4H–SiC using a SF6/O2 helicon plasma", *Appl.Phys.Lett.,* Vol.76 (16), pp. 2310-2312.

[4] Khan, F.and Adesida, I., (1999), "High rate etching of SiC using inductively coupled plasma reactive ion etching in SF~ 6-based gas mixtures", *Appl.Phys.Lett.,* Vol.75 (15),.

[5] Chabert, P. (2001), "Deep etching of silicon carbide for micromachining applications: Etch rates and etch mechanisms", *Journal of Vacuum Science & Technology B,* Vol.19 (4), pp. 1339-1345.

[6] McLaughlin, K., et al. (1991), "Development of Techniques for Real-Time Monitoring and Control in Plasma Etching I. Response Surface Modeling of and Etching of Silicon and Silicon Dioxide", *J.Electrochem.Soc.,* Vol.138 (3), pp. 789-799.

[7] Knizikevičius, R.and Kopustinskas, V., (2004), "Anisotropic etching of silicon in SF 6 plasma", *Vacuum,* Vol.77 (1), pp. 1-4.

[8] Tan, L. , (1994), "Modelling, Simulation and Multivariable control of Plasma Etching of Silicon and Silicon Dioxide", Dublin City University,.

[9] Jenq, J., et al. (1994), "Absolute fluorine atom concentrations in RIE and ECR CF4 plasmas measured by actinometry", *Plasma Sources Sci.Technol.,* Vol.3 (2), pp. 154.

[10] Sasaki, K., et al. (1997), "Kinetics of fluorine atoms in high-density carbon–tetrafluoride plasmas", *J.Appl.Phys.,* Vol.82 (12), pp. 5938-5943.

[11] Singh, H., Coburn, J.and Graves, D.B., (2001), "Measurements of neutral and ion composition, neutral temperature, and electron energy distribution function in a CF4 inductively coupled plasma", *Journal of Vacuum Science & Technology A,* Vol.19 (3), pp. 718-729.

[12] Foest, R., et al. (1996), "Optical and mass spectrometric investigations of ions and neutral species in SF 6 radio-frequency discharges", *Physical Review E,* Vol.54 (2), pp. 1876.

[13] Picard, A., Turban, G.and Grolleau, B., (1986), "Plasma diagnostics of a SF6 radiofrequency discharge used for the etching of silicon", *J.Phys.D,* Vol.19 (6), pp. 991.

[14] Riccardi, C., et al. (2000), "Modeling and diagnostic of an SF 6 RF plasma at low pressure", *IEEE Trans.Plasma Sci.,* Vol.28 (1), pp. 278-287.

[15] Chabert, P., Boswell, R.and Davis, C., (1998), "Investigation of a SF6 helicon plasma", *Journal of Vacuum Science & Technology A,* Vol.16 (1), pp. 78-86.

[16] d'Agostino, R., et al. (1985), "On the use of actinometric emission spectroscopy in sf6-o2 radiofrequency discharges: Theoretical and experimental analysis", *Plasma Chem.Plasma Process.,* Vol.5 (3), pp. 239-253.

[17] Pessoa, R., et al. (2010), "Study of SF6 and SF6/O2 plasmas in a hollow cathode reactive ion etching reactor using Langmuir probe and optical emission spectroscopy techniques", *Plasma Sources Sci.Technol.,* Vol.19 (2), pp. 025013.

[18] Kopalidis, P.M.and Jorne, J., (1992), "Langmuir Probe Measurements and Characterization of Silicon Etching in SF 6/O 2 Discharges", *J.Electrochem.Soc.,* Vol.139 (3), pp. 839-844.

[19] Godyak, V.A., Piejak, R.and Alexandrovich, B., (1992), "Measurement of electron energy distribution in low-pressure RF discharges", *Plasma Sources Sci.Technol.,* Vol.1 (1), pp. 36.

[20] Kechkar, S. , (2015), "Experimental investigation of a low pressure capacitively-coupled discharge", Dublin City University,.

[21] d'Agostino, R.and Flamm, D.L., (1981), "Plasma etching of Si and SiO2 in SF6–O2 mixtures", *J.Appl.Phys.,* Vol.52 (1), pp. 162-167.

[22] Ryan, K.and Plumb, I., (1990), "A model for the etching of silicon in SF6/O2 plasmas", *Plasma Chem.Plasma Process.,* Vol.10 (2), pp. 207-229.

[23] Godyak, V.and Piejak, R., (1990), "Abnormally low electron energy and heating-mode transition in a low-pressure argon rf discharge at 13.56 MHz", *Phys.Rev.Lett.,* Vol.65 (8), pp. 996.

[24] Turner, M., Doyle, R.and Hopkins, M., (1993), "Measured and simulated electron energy distribution functions in a low-pressure radio frequency discharge in argon", *Appl.Phys.Lett.,* Vol.62 (25), pp. 3247-3249.

[25] Deegan, C.M. , (1999), "Characterisation of the heating mechanisms in a capacitively coupled argon rf discharges", Dublin City University,.

[26] Scanlan, J.V. , (1991), "Langmuir probe measurements in 13.56 MHz discharges", Dublin City University,.

[27] Lisovskiy, V., et al. (2007), "Modes of rf capacitive discharge in low-pressure sulfur hexafluoride", *J.Phys.D,* Vol.40 (22), pp. 6989.

[28] Blanks, K., Tabor, A.and Becker, K., (1987), "Absolute cross sections for fluorine 3p→ 3s line emissions following single electron impact on NF3, CF4, and SF6", *J.Chem.Phys.,* Vol.86 (9), pp. 4871-4875.

[29] Forand, J., Becker, K.and McConkey, J., (1986), "Dissociative excitation of SF6 by controlled electron impact", *Can.J.Phys.,* Vol.64 (3), pp. 269-276.

[30] "Impedans ltd.", [online], https://www.impedans.com/octiv-vi.

[31] Gogolides, E., Nicolai, J.and Sawin, H.H., (1989), "Comparison of experimental measurements and model predictions for radio-frequency Ar and SF6 discharges", *Journal of Vacuum Science & Technology A,* Vol.7 (3), pp. 1001-1006.

[32] Lieberman, M.A. and Lichtenberg, A.J., (2005)*, Principles of Plasma Discharges and Materials Processing, 2nd Edition,* .

[33] Kono, A., et al. (1994), "Charged particle densities and kinetics in a radio-frequency SF6 plasma", *J.Appl.Phys.,* Vol.76 (11), pp. 7221-7230.

[34] Bletzinger, P. (1990), "Experimental characteristics of rf parallel-plate discharges: Influence of attaching gases", *J.Appl.Phys.,* Vol.67 (1), pp. 130-138.

[35] Nakano, N., et al. (1994), "Simulations of rf glow discharges in SF 6 by the relaxation continuum model: Physical structure and function of the narrow-gap reactive-ion etcher", *Physical Review E,* Vol.49 (5), pp. 4455.

[36] Kakuta, S., et al. (1993), "Influence of frequency, pressure, and mixture ratio of electronegative gas on electrical characteristics of rf discharges in N2-SF6 mixtures", *J.Appl.Phys.,* Vol.74 (8), pp. 4923-4931.

Chapter 5- Investigation of absolute fluorine atom density as a function of applied rf power in a capacitively coupled $SF_6/O_2/Ar$ discharge

5.1 Motivation

In chapter 4, atomic fluorine density was found to increase with investigated gas pressure in $SF_6/O_2/Ar$ discharge due to increase in SF_6 partial pressure. However, from the values of dissociation fraction, rate of fluorine production was expected to depend on the energy of plasma electrons responsible for dissociation of SF_6 molecule. Also, actinometric signal, monitored for relative variation of [F], had significant dissociative excitation contribution at pressures < 200 mTorr, where the discharge could be in high-current regime. At fixed rf power of 100 W, for pressures ≥ 200 mTorr, discharge could be in α-mode as indicated by measured IVC and also good quantitative agreement was achieved between APMS and actinometry in monitoring relative variations of [F]. Moreover, both techniques had good agreement at similar pressure (200 mTorr) in monitoring relative [F] variations as function of O_2 content in chapter 3. These measurements indicated that discharge could be in weak-current regime or α-mode at pressures close to 200 mTorr with no significant change to EEDF and moreover, at these conditions, relative [F] variations measured using actinometric signal, produced mainly from direct excitation of ground state fluorine atom with very negligible dissociative contribution. Moreover, dissociative excitation contribution to fluorine actinometric signal would be less significant at higher values of D. Thus, the main motivation of this chapter was to investigate the above hypothesis and calculate proportionality constant (K) required for fluorine actinometry.

For fluorine actinometry, knowledge on proportionality constant would be vital to compute absolute fluorine atom density in a plasma discharge. Because fluorine atoms produced in SF_6 based plasma discharges was found to provide superior etching rates due its high reactivity with silicon [1, 2] and also responsible for deep anisotropic trenches along with other charged species [1, 3]. However, absolute fluorine density measured using reliable diagnostic technique would be essential to validate fluorine actinometric measurements

and to compute proportionality constant. Like previous chapters, APMS diagnostic technique was used in this chapter to measure variations of absolute atomic fluorine density as a function of applied rf power.

Several experimental [4-11] and numerical [12-20] investigations were carried out in fluorine based discharges. Unfortunately, no experimental investigation can be found in literatures about absolute fluorine radical measurements using any reliable diagnostic techniques in a capacitively-coupled SF_6 based plasma discharge for actinometry validation. Only in very few studies [21, 22] using global models had been employed on SF_6 based discharges to investigate fluorine atom density in capacitively coupled source. However, those fluorine density measurements were beyond the scope of this investigation. So, this chapter experimentally investigated variation in absolute fluorine atom density as a function of rf power using APMS technique in a capacitive SF_6/O_2 discharge. Using these measurements, validity of fluorine actinometry was verified and constant of proportionality was computed at discharge conditions where both actinometry and APMS techniques had good quantitative agreement.

In this chapter, power variation of absolute fluorine atom density was investigated in section 5.2 using APMS at 40, 70 and 200 mTorr gas pressures with different feedstock mixture of $SF_6/O_2/Ar$ discharge. Absolute [F] measurements from APMS were compared with actinometric values in section 5.3, to verify the validity of fluorine actinometry model at above mentioned discharge conditions. Then proportionality constant was computed in section 5.3.1 for discharge condition where both techniques had good agreement on relative [F] variations. Furthermore, applicability of proportionality constant was investigated at various discharge conditions examined in this work. A collective summary had been presented in section 5.4 based on investigations carried out in this chapter.

5.2 Variation of absolute atomic fluorine density measurements in $SF_6/O_2/Ar$ plasma discharge as a function of rf power

The rf power variation of absolute atomic fluorine density measured using APMS was investigated in this section. These investigations were performed at 40 mTorr, 70 mTorr and 200 mTorr gas pressures with different feedstock proportions of $SF_6/O_2/Ar$ and the input power was varied between 30- 600 W. Absolute fluorine atom density measured at different gas pressures was found to increase with power as shown in figure 5.1. Linear fits of F^+ signal vs energy was used to calculate the standard error bars on absolute [F] with a 95% confidence interval.

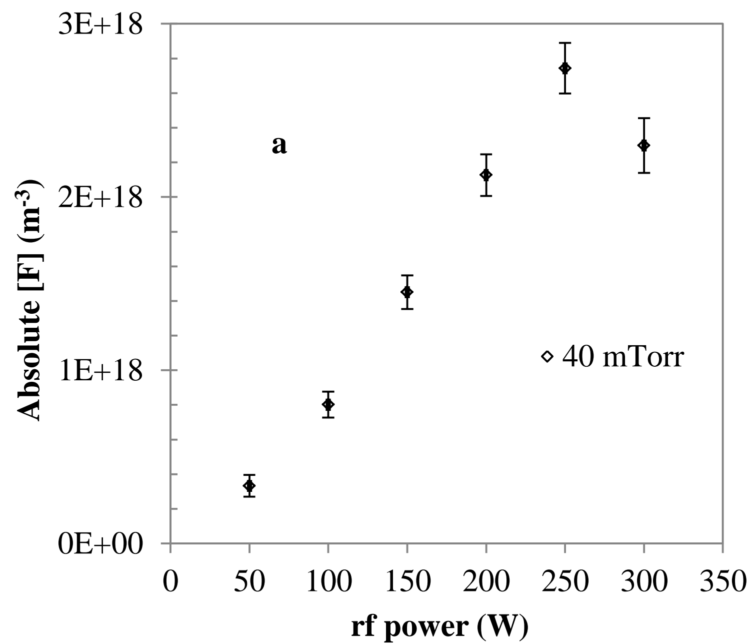

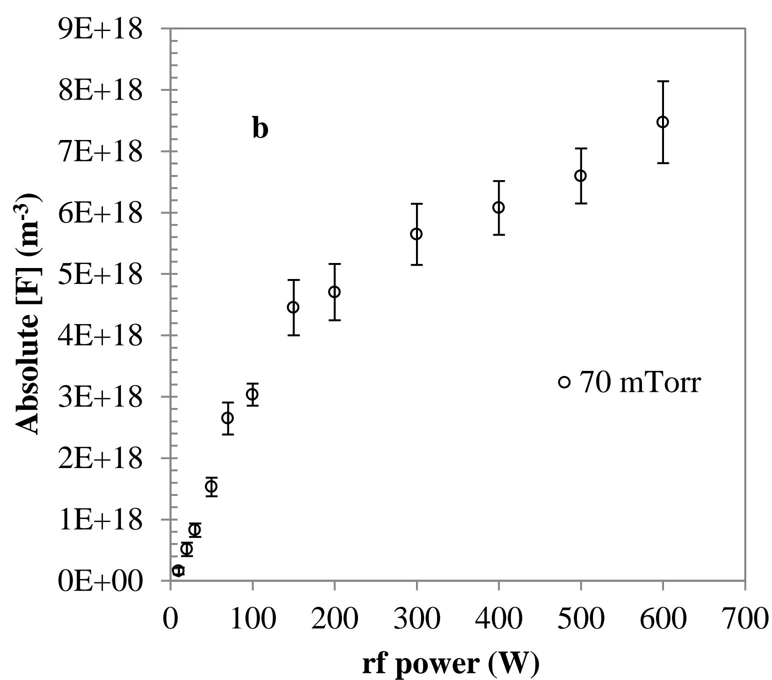

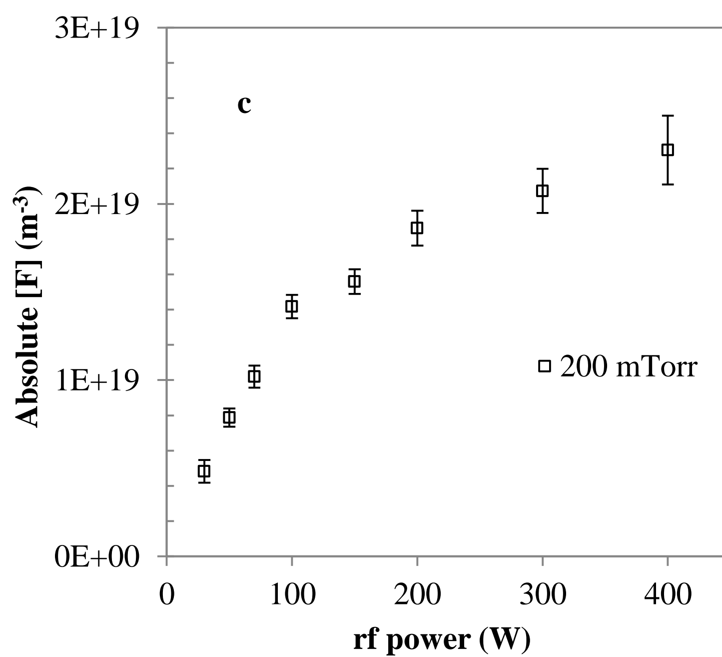

Figure 5.1 Variation of absolute [F] as a function of rf power. The feedstock mixtures were **a**. 85% SF_6, 10% O_2 and 5% Ar at 40 mTorr (◊); **b**. 76% SF_6,

20% O_2 and 4% Ar at 70 mTorr (○); **c**. 66% SF_6, 30% O_2 and 4% Ar at 200 mTorr (□).

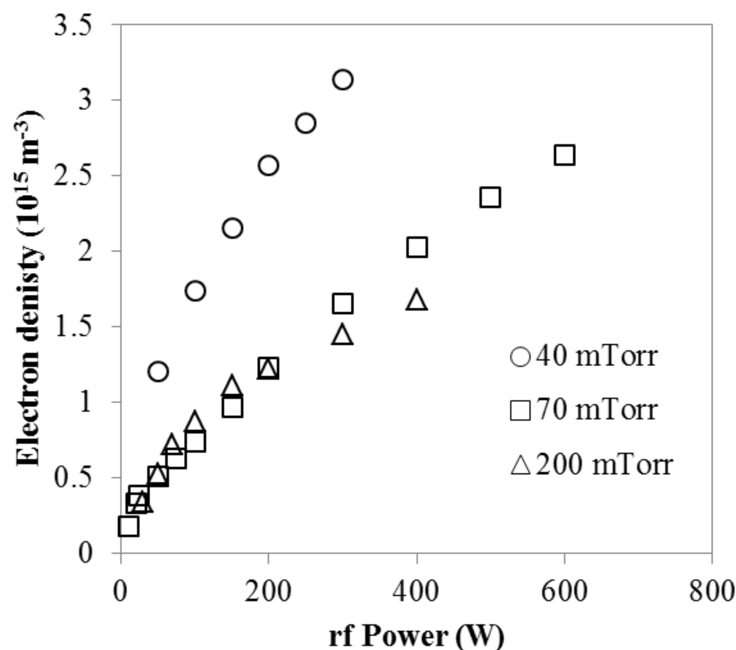

Figure 5.2 Electron density variations as a function of rf power at 40 mTorr (○), 70 mTorr (□) and 200 mTorr (Δ) gas pressures with feedstock mixtures of 85% SF_6, 10% O_2 and 5% Ar, 76% SF_6, 20% O_2 and 4% Ar and 66% SF_6, 30% O_2 and 4% Ar respectively.

Increase in [F] with power can be due to increase in electron density if negligible changes to electron temperature and F-atom loss rate were assumed. This could be a valid assumption as variation of effective electron temperature with power was found to be negligible elsewhere [4, 9, 12, 17] in fluorine based discharges. So, increase in electron density with increasing power, as shown in figure 5.2, would increase production rate of F-atoms through electron-impact dissociation of SF_6 and this obviously would increase fluorine atom density with power with negligible variations to electron temperature and F-atom loss mechanism. However, absolute [F] was found to drop off marginally above 250 W at 40 mTorr gas pressure. One possible reason could to increase in gas

temperature (T_g) with increase in applied rf power [23, 24]. As pressure (P) is constant, this increase in T_g would reduce the number density of SF_6 in the discharge in accordance to ideal gas law ie., $[SF_6] = P / k_B T_g$. Reduction in $[SF_6]$ could have an impact on F-atom production rate and obviously, result in drop in number density of fluorine atoms as observed in previous chapters.

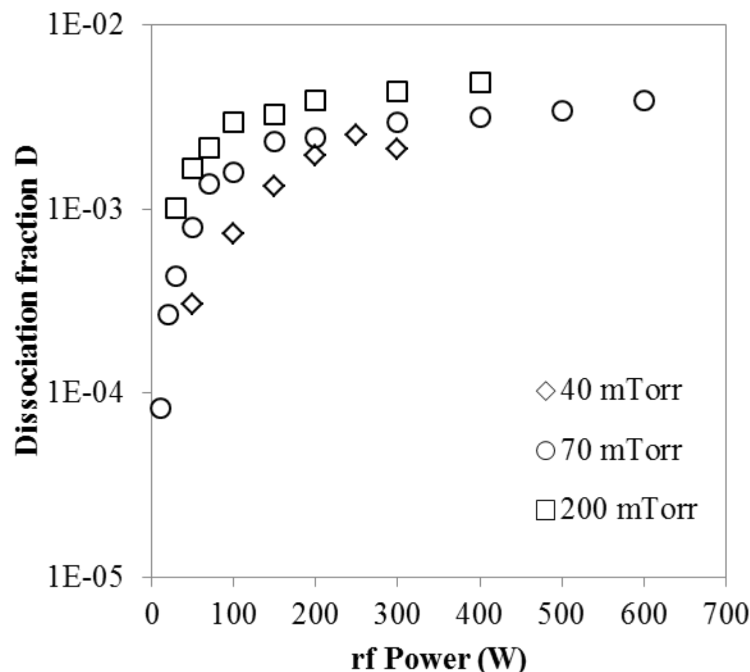

Figure 5.3 Dissociation fraction as a function of rf power at 40 mTorr (◊), 70 mTorr (○) and 200 mTorr (□) gas pressures with feedstock mixtures of 85% SF_6, 15% O_2 and 5% Ar, 76% SF_6, 20% O_2 and 4% Ar and 66% SF_6, 30% O_2 and 4% Ar respectively.

An important plasma process parameter which would play vital role in etch rate was dissociation fraction, $D = [F]/[SF_6]$. Figure 5.3 shows variation of D as a function of rf power at different gas pressures. For all gas pressures investigated in this chapter, D was found to increase with rf power and it was due to increase in production rate of fluorine atoms. As mentioned before, there was no published work on D in capacitively-coupled SF_6/O_2 discharge for comparison.

However, values of D evaluated in this work were in good agreement to other published values in fluorine based discharges elsewhere [25-29]. Note that D dropped marginally above 250 W applied power at 40 mTorr gas pressure. Usually with increase in rf power, electron temperature would drop slowly but would be negligible. Once the electron temperature drop becomes significant with increasing rf power, dissociation degree of SF_6 drops considerably as shown in figure 5.3. This drop in D would also reduce the electron attachment rate to radicals and production of fluorine atoms [30] which obviously led to drop in [F] as shown in figure 5.1.

5.3 Validation of fluorine actinometry- Effect of rf power

Variations of absolute atomic fluorine density as a function of applied rf power was investigated in section 5.2. Using these absolute measurements, validity of fluorine actinometry model was verified in this section to monitor relative variations in fluorine atom density in $SF_6/O_2/Ar$ capacitive discharge as a function of rf power. Relative variations in [F] monitored using actinometric signal, I_F/I_{Ar}, measured with optical emission spectroscopy were compared to absolute APMS measurements for model validation at 40 mTorr, 70 mTorr and 200 mTorr gas pressures as shown in figure 5.4, 5.5 and 5.6 respectively. Error bars on actinometric measurements were too small to indicate due to less significant variation in measured statistical values.

At 40 mTorr gas pressure, both actinometry and APMS measurements indicated increase in atomic fluorine density with increasing rf power as shown in figure 5.4. However, relative [F] increased by a factor of 2 with actinometric measurements while APMS measurements revealed an order increase in [F] over same conditions investigated. With increase in total gas pressure to 70 mTorr along with increase in O_2 partial pressure in feedstock mixture, good qualitative agreement was achieved between actinometry and APMS in monitoring relative [F] over the same rf power as shown in figure 5.5.

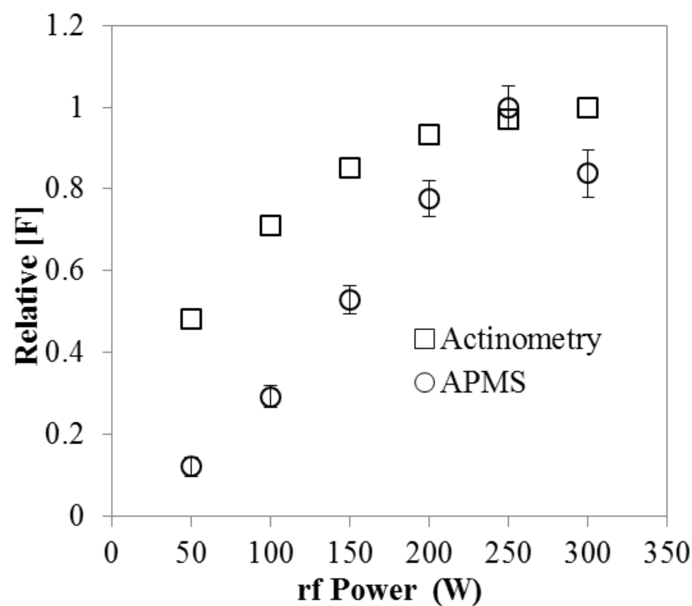

Figure 5.4 A comparison of relative atomic fluorine concentration measured using actinometry (□) and APMS (○) at 40 mTorr gas pressure in $SF_6/O_2/Ar$ (85/10/5%) discharge.

There could be few reasons for this quantitative disagreement between relative [F] monitored using actinometry and absolute [F] measured using APMS, especially at 40 mTorr gas pressure, and they were as follows:

1. Mode transition due to electron heating: In capacitive discharges, operating mode of discharge was expected to change from alpha to gamma (α to γ) mode with increase in rf power due to change in electron heating mechanism [31, 32]. This mechanism will alter energy distribution of electrons and which in turn affect the proportionality constant, *K*, which can be evaluated using electron energy distribution function (EEDF). Any variation in *K* would be violation on one of the classical actinometric model assumptions. Such mode transition was observed in this plasma chamber in argon & oxygen plasmas [33] and elsewhere [34] in similar capacitive SF_6 based discharge. Assuming dissociative excitation contribution was less significant under investigated conditions here; with increase in applied power, *K* could vary due to transition

in discharge heating mode. This could cause unreliable variations in fluorine density monitored using I_F/I_{Ar}. Apparently, this could make the model unreliable to monitor any relative changes on [F]. Also under such scenario, it would be unrealistic to compare model prediction on variations of ground state [F] with measurements made using reliable techniques like APMS. In case of such mode transition, knowledge on EEDF would be essential to account for any variation in K and to improve actinometric model.

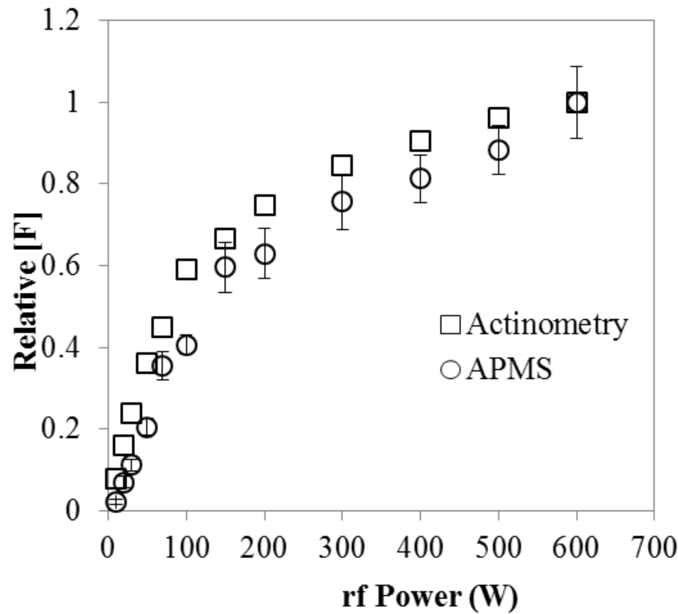

Figure 5.5 A comparison of relative atomic fluorine concentration measured using actinometry (□) and APMS (○) at 70 mTorr gas pressure in $SF_6/O_2/Ar$ (76/20/4%) discharge.

2. Electron impact dissociative excitation: As pointed in previous chapters, there could be additional excitation processes apart from direct excitation of ground state fluorine atom. In those processes, most significant process could be dissociative excitation process [17, 35, 36], which can contribute to optical emission line of fluorine at 703.7 nm. Also, at low pressure conditions, contribution of dissociative excitation could be significant to actinometric signal based on previous chapter investigation. Nevertheless, if dissociative

excitation contributes significantly to emission line at 703.7 nm, then it would contaminate I_F in actinometric signal which was used to monitor variations of ground state [F] but rather it would follow changes in [SF_6]. So, improvement should be made in classical actinometry model to incorporate dissociative channel if there was significant dissociative excitation contribution.

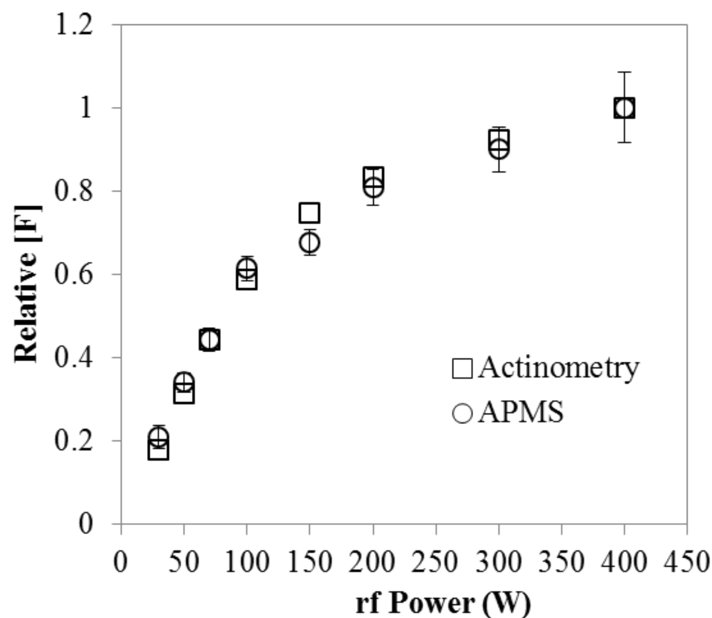

Figure 5.6 A comparison of relative atomic fluorine concentration measured using actinometry (□) and APMS (○) at 200 mTorr gas pressure in $SF_6/O_2/Ar$ (66/30/4%) discharge.

Apparently, dissociative excitation contribution can be suppressed by increasing partial pressure of O_2 in fluorine dominated discharge. This was investigated previously [37] and confirmed by monitoring high resolution emission line shapes of F at 703.7 nm recorded using Fabry-Perot interferometer. Despite this fact, excess dilution of SF_6 discharge with O_2 can reduce [F] due to decrease in SF_6 partial pressure as observed in chapter 3. Assuming EEDF shape was unaltered, increasing the gas pressure of SF_6 dominated discharge, suppressed dissociative contribution as it was investigated and verified in chapter 4. Based on these hypothesis, fluorine atom

concentration was investigated at 200 mTorr gas pressure with feedstock mixture of 66% SF_6, 30% O_2, 4% Ar using APMS for different applied rf power and results were shown in figure 5.1. Relative changes of [F] measured with APMS was compared with actinometric signal as shown in figure 5.6 for same conditions investigated. Relative variations of [F] measured using both techniques had good quantitative and qualitative agreement.

With increasing O_2 content in SF_6 dominated plasma, production rate of fluorine atom increases due to reaction of atomic oxygen with SF_x fragments with decrease in F-atom loss rate through surface recombination as discussed in chapter 3. This increase in F-atom production would mostly contribute to emission line at 703.7 nm through direct excitation of ground state fluorine atom than dissociative excitation of SF_6. Although there could be contribution from dissociative mechanism to emission line at 703.7 nm but it would be very much negligible. Therefore, classical fluorine actinometry model was validated as good agreement was obtained with reliable diagnostic technique i.e., APMS in this case, on relative variations of [F] as shown in figure 5.6.

5.3.1 Proportionality constant for fluorine actinometry and its dependence

As seen from previous section, classical fluorine actinometry model was validated and good agreement was obtained between actinometry and APMS measurements on relative [F] measurements. This model investigation was extended further to evaluate proportionality constant (K) required for classical fluorine actinometry to calculate fluorine atom density. So far, no published value of K can be found in literature in capacitive SF_6 based plasma discharges. However, value of K was evaluated in other fluorine based discharges and results were tabulated in Table 5.1.

Table 5.1 Value of *K* evaluated in fluorine based discharges

S.No.	Discharge type	Gas	Value of *K*	Reference
1	Reactive ion etching/ Electron cyclotron resonance	CF_4	0.56	[6]
2	Capacitively-coupled rf discharge	CF_4	4.1	[25]
3	Helicon-wave plasma discharge	C_4F_8	1.5 (2 mTorr) and 0.9 (7 mTorr)	[29]
4	Helicon-wave plasma discharge	CF_4	4.3 (low power) and 2.0 ~ 2.5 (high power)	[29]
5	Inductively-coupled rf discharge	SF_6/Ar	1.121	[38]

Value of *K* was evaluated using absolute [F] measured with APMS as shown in figure 5.7 using equation 5.1

$$[\mathrm{F}]_{\mathrm{APMS}} = K \frac{I_F}{I_{Ar}} [\mathrm{Ar}] \qquad (5.1)$$

For this investigation, neutral gas temperature, T_g, required to compute argon number density [Ar], was fixed at 340 K. Usually, in low-density capacitive discharges, gas temperature would range between 300 – 500 K as measured using different methods [39, 40]. And also, with increase in applied power, gas temperatures were found to increase in capacitive SF_6 discharge [23]. If there was no significant change in pressure, then number density of species would decrease with increase in gas temperature according to ideal gas law. In contrary, [F] was found to increase in this investigation with increase in applied rf power for fixed feedstock gas pressure. This seems to suggest not much variation in gas temperature can be expected for investigated conditions.

However, further investigation would be required to measure exact gas temperature as it can significantly cause variation in value of *K* as shown in figure 5.8.

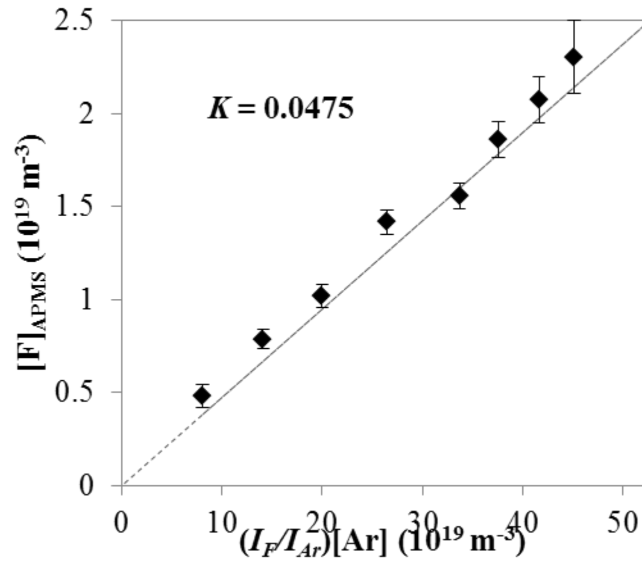

Figure 5.7 Evaluation of proportionality constant for fluorine actinometry in $SF_6/O_2/Ar$ (66/30/4%) discharge operated at 200 mTorr gas pressure.

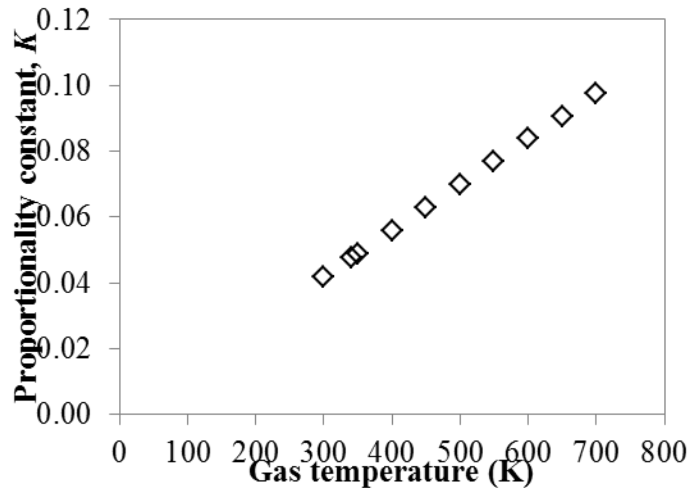

Figure 5.8 Linear dependence of proportionality constant, *K* with gas temperature at fixed pressure of actinometer (argon) for power variation investigation in $SF_6/O_2/Ar$ (66/30/4%) discharge.

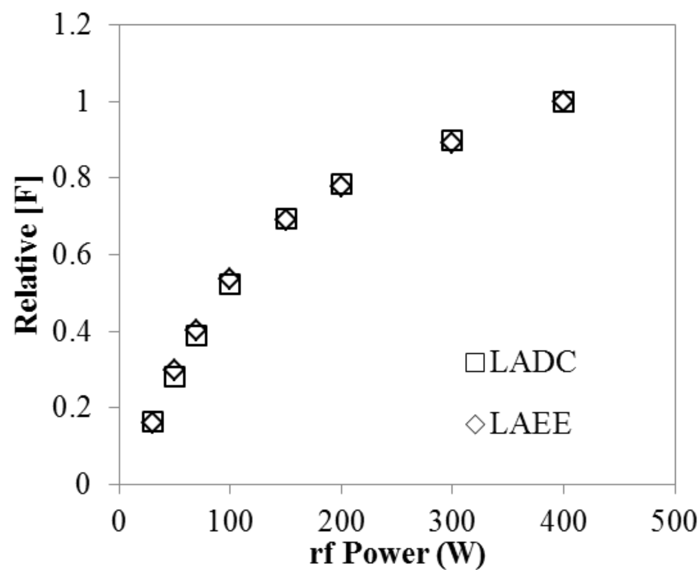

Figure 5.9 Relative variations of [F] measured at LADC (□) and LAEE (◊) as a function of applied power in 200 mTorr $SF_6/O_2/Ar$ (66/30/4%) discharge.

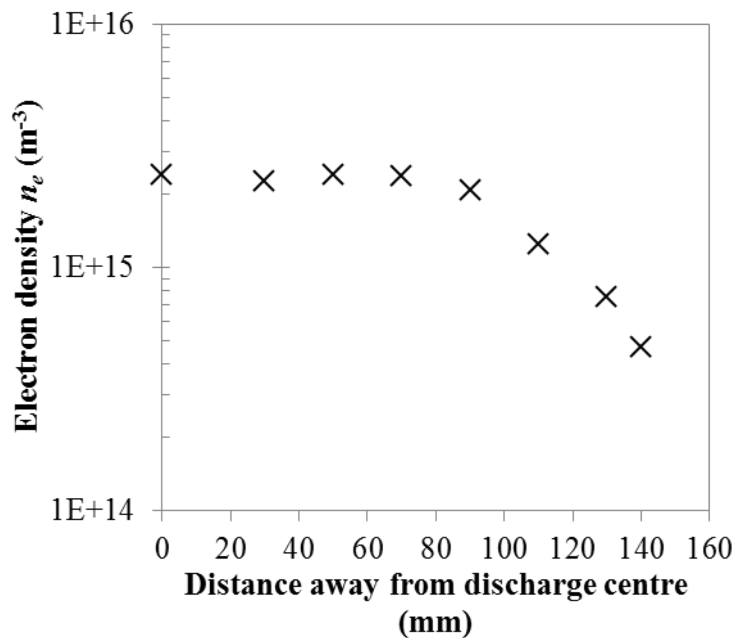

Figure 5.10 Radial variation of electron density measured using hairpin probe in 200 mTorr $SF_6/O_2/Ar$ (66/30/4%) discharge operated at 600 W applied rf power.

In this investigation, value of K evaluated for fluorine actinometry in $SF_6/O_2/Ar$ plasma was lowest in comparison to other measurements evaluated/estimated in fluorine based discharges as shown in table 5.1. As mentioned before, there was no published value of K in SF_6 based discharge for reliable comparison. Low value of K in this work can be due to spatial location of mass spectrometer used to measure absolute [F]. The results of absolute [F] were considered to be lower estimate as orifice head of mass spectrometer in the downstream, was located close to reactor walls. Radially, density of plasma would be low close to reactor walls to that of discharge centre. And this was verified using line averaged optical emissions obtained across discharge centre and edge of an electrode. Even though, line of sight measurements in both cases were not similar, relative variations of [F] would be same. This was verified using optical emission measurements obtained at two different radial positions in the discharge i.e., line averaged across discharge centre (LADC) and line averaged across electrode edge (LAEE) for same operating conditions as shown in figure 5.9. Good agreement between measurements at LADC and LAEE revealed relative variations of [F] would be similar at plasma bulk and walls. Now, fluorine production rate, mainly governed by electron density n_e, may vary between plasma bulk and wall. If fluorine was predominantly produced through electron impact dissociation of SF_6 across the discharge centre to walls, then $[F] \propto n_e$ provided insignificant changes to electron temperature. Radial variations of electron density measured using hairpin probe in 200 mTorr $SF_6/O_2/Ar$ (66/30/4%) plasma discharge were shown in figure 5.10. Due to limitation in probe measurements, applied rf power was maintained at 600 W for radial measurements. As the probe was positioned close to electrode edge i.e., $\approx$ 140 mm away from discharge centre, n_e was found to decrease by a factor of $\approx$ 5. Probe measurements close to reactor walls were not possible due to poor sensitivity of hairpin probe. But it can be expected that n_e could drop further close to reactor walls. In addition, optical fluorine emission lines were monitored at two different radial positions i.e., LADC and LAEE for same

conditions investigated in this work. Fluorine emission was found to be lower for LAEE than LADC measurements and reduced by factor of ≈ 4-14 for applied rf power as shown in figure 5.11. Also for varying gas pressures, LAEE measurements were down by factor of 3-8 to that of LADC as shown in figure 5.12. Obviously, knowledge on electron density, electron temperature and gas temperature between discharge centre and reactor walls can provide better variations of [F] in radial direction. Nevertheless, these observations suggested that fluorine atom density close to walls could atleast be an order magnitude lower than at plasma bulk and value of *K* can increase significantly if accounted for such variations in [F] across plasma bulk to walls.

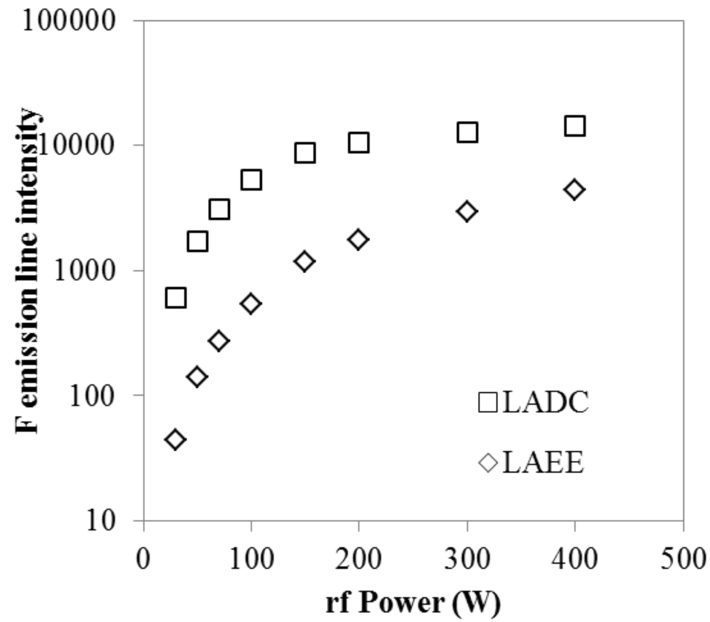

Figure 5.11 F emission line intensity obtained using LADC (□) and LAEE (◊) measurements as a function of applied power in 200 mTorr $SF_6/O_2/Ar$ (66/30/4%) discharge.

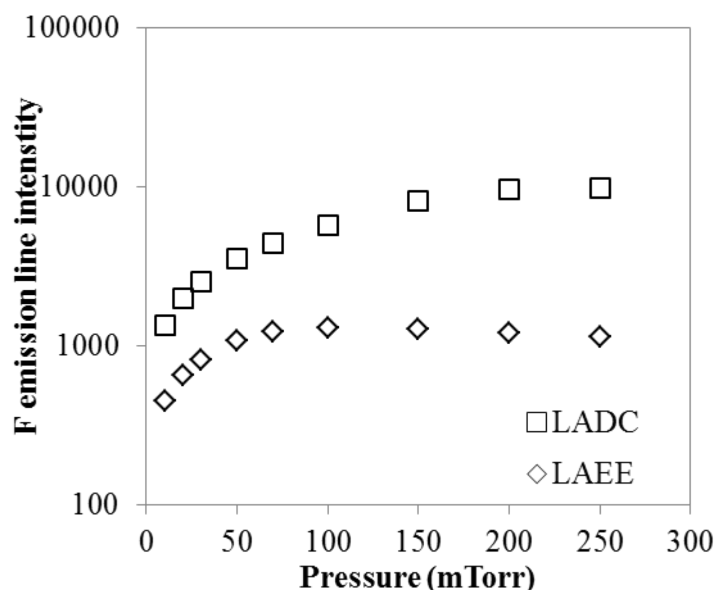

Figure 5.12 F emission line intensity obtained using LADC (□) and LAEE (◊) measurements as a function of gas pressure in $SF_6/O_2/Ar$ (70/26/4%) discharge operated at 100 W rf power.

In most cases, the value of proportionality constant, K required for fluorine actinometry can be specific to plasma discharge and operating conditions. The dependence of evaluated K value in this work was investigated through comparison of [F] with that of absolute value measured using APMS. Since neutral gas temperature was not measured in this work, equation 5.1 was rewritten as in equation 5.2 to make proportionality factor, K/T_g involving neutral gas temperature.

$$[\mathrm{F}]_{\mathrm{APMS}} = \frac{K}{\mathrm{T_g}}\left[\left(\frac{I_F}{I_{Ar}}\right)\frac{\mathrm{P}}{k_B}\right] \tag{5.2}$$

Same measured values used in figure 5.7 to evaluate K, were adopted to compute proportionality factor, K/T_g and the value was found to be 1.4E-4. Actinometric measurements of [F] computed using K/T_g value were compared with APMS measurements for power and pressure variations in $SF_6/O_2/Ar$ discharge as shown in figure 5.13 and figure 5.14. Both values of [F] found to

increase with increase in applied rf power. At low rf power, disagreement was large between experimental and computed values of [F]. Assuming insignificant changes to EEDF, discrepancy could be predominantly due additional excitation contribution to fluorine emission line at 703.7 nm apart from direct excitation mechanism as discussed before. However, discharge transition due to heating mode at low applied rf power was observed with O_2 and Ar plasma in this chamber [33]. In such scenario, *K* value would vary and this needs to be accounted to compute absolute [F] using actinometry.

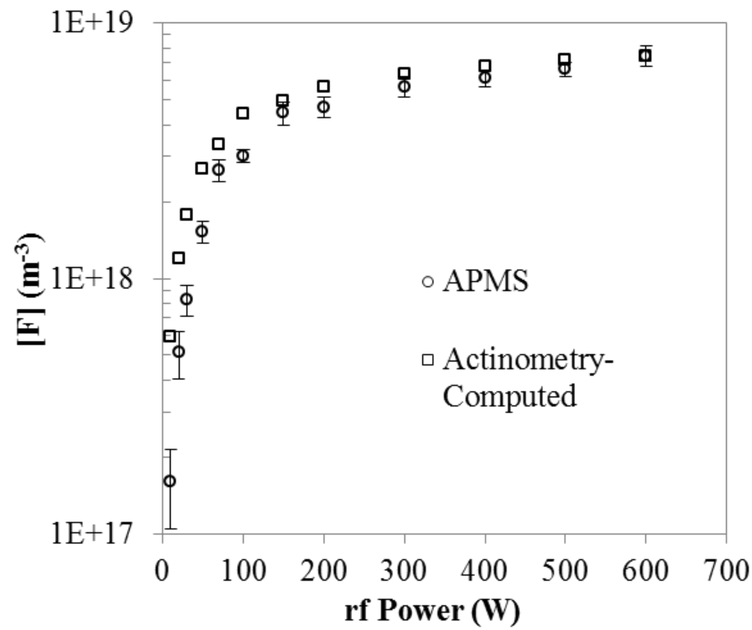

Figure 5.13 Comparison of [F] computed using fluorine actinometry and proportionality factor (□) with absolute [F] measured using APMS (○) in 70 mTorr SF_6/O_2/Ar (76/20/4%) discharge.

Both experimental and computed values of [F] were found to increase with increase in gas pressure as shown in figure 5.14. As said in chapter 4, fluorine emission line at 703.7 nm had significant contamination from dissociative excitation from SF_6 for low pressures (see figure 4.9) and it lead to overestimation of computed [F] using actinometry as shown in figure 5.14.

With increase in pressure, dissociative excitation contribution was expected to decrease and this resulted in good agreement between measured and computed [F] for pressures ≥ 100 mTorr as shown in figure 5.14. So, actinometric prediction of [F] calculated using fixed proportionality factor can be used with good confidence for pressures above 100 mTorr provided dissociative excitation contribution is insignificant.

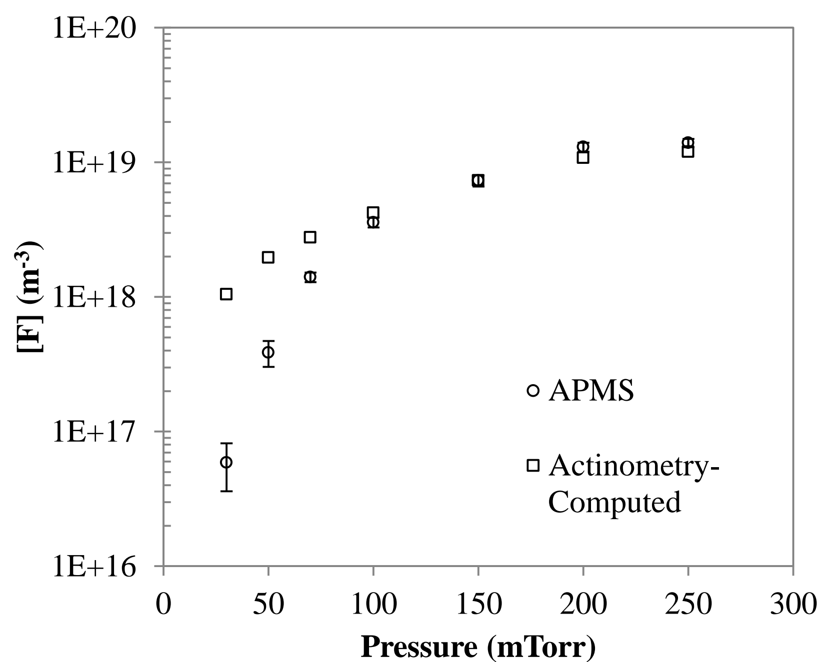

Figure 5.14 Comparison of [F] computed using fluorine actinometry and proportionality factor (□) with absolute [F] measured using APMS (○) for various gas pressure in $SF_6/O_2/Ar$ (70/26/4%) discharge operated at 100 W rf power.

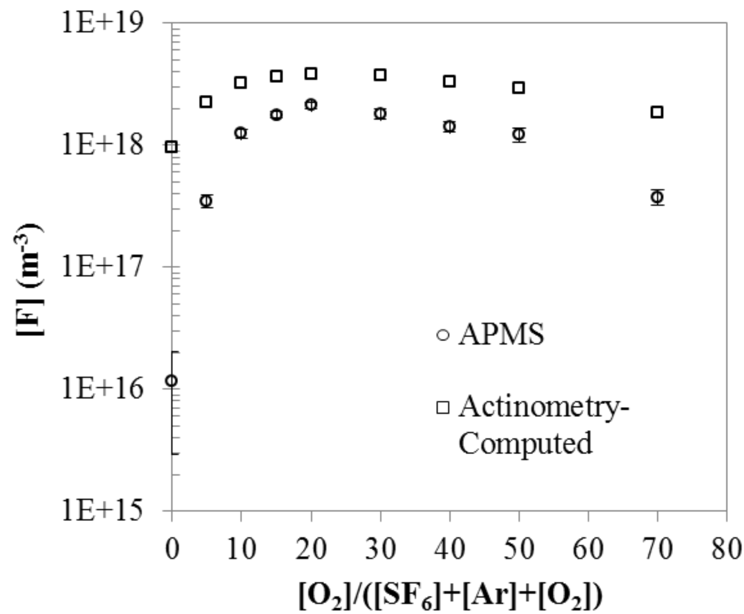

Figure 5.15 Comparison of [F] computed using fluorine actinometry and proportionality factor (□) with absolute [F] measured using APMS (○) for variation of O_2 content in 70 mTorr $SF_6/O_2/Ar$ discharge operated at 100 W rf power.

Computed [F] using actinometry was compared to [F] measured using APMS for variation of partial pressure of O_2 in feedstock mixture of 70 mTorr $SF_6/O_2/Ar$ at 100 W applied rf power as shown in figure 5.15. Overestimation of computed [F] can be again due to significant additional excitation mechanism apart from direct excitation to fluorine actinometric signal, provided EEDF remain unchanged under investigated conditions. However, good agreement was achieved between computed and experimental values of [F] for O_2 content > 10% in feedstock mixture of 200 mTorr $SF_6/O_2/Ar$ at 100 W applied rf power as shown in figure 5.16. For O_2 content > 10%, computed [F] was found to be slightly higher than experimental value and this could be due to spatial location of measurements. As said before, orifice of mass spectrometer was at the reactor walls whereas optical measurements were line averaged across discharge centre. Since relative [F] measured using both

technique had good agreement as shown in figure 3.3 in chapter 3, additional excitation mechanism and discharge transition can be ignored for conditions > 10% O_2 content.

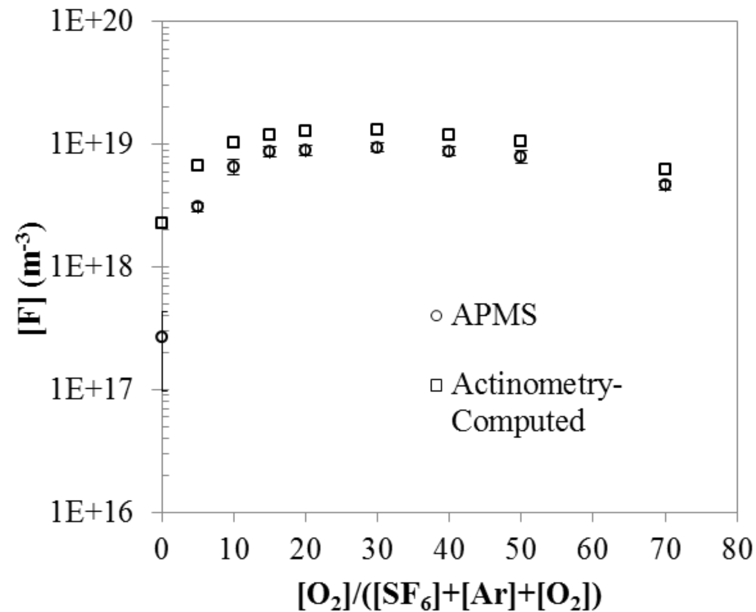

Figure 5.16 Comparison of [F] computed using fluorine actinometry and proportionality factor (□) with absolute [F] measured using APMS (○) for variation of O_2 content in 200 mTorr $SF_6/O_2/Ar$ discharge operated at 100 W rf power.

Finally, validity of factor of proportionality through [F] measurements on different optical sensor was examined and results were shown in figure 5.17. Similar to case discussed above in figure 5.13, significant addition excitation process lead to overestimation of computed [F] than experimental value. Nevertheless, proportionality factor would not vary much if different sensor was used. However, poor calibration of optical emission spectrometer can lead to large errors in measurements and which could cause unreliable absolute [F], measured using fluorine actinometry.

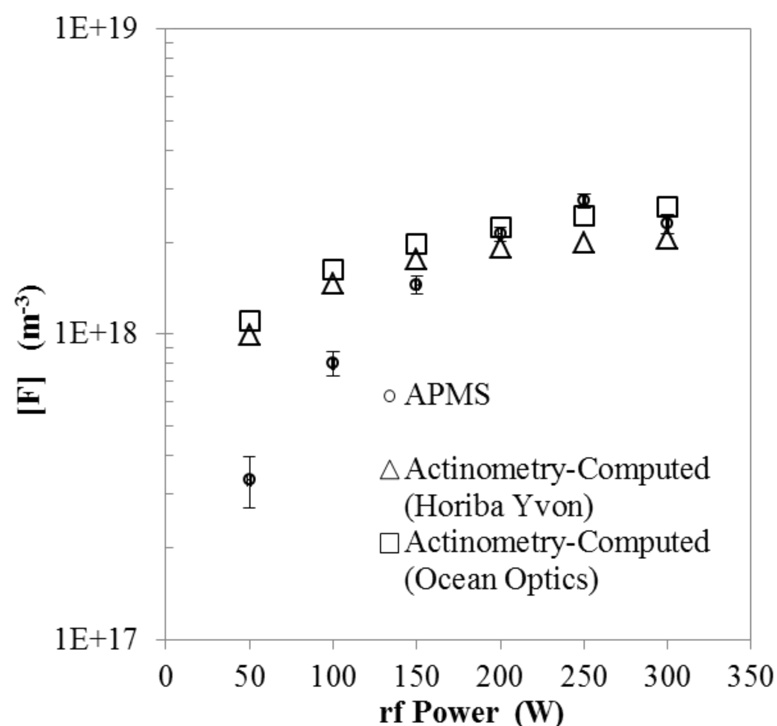

Figure 5.17 Comparison of [F] computed using fluorine actinometry signal measured with Horiba Yvon OES (Δ) and Ocean optics (□) spectrometers, with absolute [F] measured using APMS (○) in 40 mTorr $SF_6/O_2/Ar$ (85/15/5%) discharge for various applied rf power.

5.4 Conclusion

Absolute [F] was measured using APMS technique for various applied rf power was investigated in this chapter. Measurements were examined at 40 mTorr, 70 mTorr and 200 mTorr for different feedstock mixtures of $SF_6/O_2/Ar$ plasma discharge. Absolute [F] was found to increase with applied rf power under investigated conditions. However, absolute [F] decreased slightly for rf power > 250 W at 40 mTorr gas pressure in $SF_6/O_2/Ar$ (85/10/5 %) plasma discharge. This marginal drop in [F] could be due to significant increase in gas temperature or decrease in electron temperature which would decrease fluorine production rate through electronic dissociation process. Relative [F]

measurements between actinometry and APMS had poor quantitative agreement at 40 mTorr gas pressure in $SF_6/O_2/Ar$ (85/10/5 %) discharge and this could be due to additional excitation mechanism apart from ground state fluorine atom excitation process with negligible changes to EEDF. However, good agreement was achieved for relative [F] measurements at 200 mTorr gas pressure in $SF_6/O_2/Ar$ (66/30/4 %) plasma discharge. This agreement validated fluorine actinometry and proportionality constant, K was evaluated as 0.0475. Absolute [F] measurements in this work could be lower estimate as spatial location of orifice head of mass spectrometer was close to chamber walls. Radial variations of fluorine density were verified using optical emission spectrometer and centre to wall density ratio could be close to an order difference for explored conditions in this work. This could be the reason for low K value, in comparison to other values evaluated in fluorine based discharges. Due to limitation in gas temperature measurements in this work, proportionality factor (K/T_g) was evaluated and used for validation. Accounting for centre to wall density ratio, this K value can be used to obtain absolute [F] using fluorine actinometry provided no additional excitation contribution to fluorine actinometric signal and/or negligible changes to EEDF under investigated conditions. Absolute [F] obtained using actinometry would be unreliable when above condition(s) was violated.

5.5 References

[1] Blauw, M., et al. (2003), "Modeling of fluorine-based high-density plasma etching of anisotropic silicon trenches with oxygen sidewall passivation", *J.Appl.Phys.,* Vol.94 (10), pp. 6311-6318.

[2] Khan, F.and Adesida, I., (1999), "High rate etching of SiC using inductively coupled plasma reactive ion etching in SF~ 6-based gas mixtures", *Appl.Phys.Lett.,* Vol.75 (15),.

[3] Aachboun, S.and Ranson, P., (1999), "Deep anisotropic etching of silicon", *Journal of Vacuum Science & Technology A,* Vol.17 (4), pp. 2270-2273.

[4] Pessoa, R., et al. (2010), "Study of SF6 and SF6/O2 plasmas in a hollow cathode reactive ion etching reactor using Langmuir probe and optical emission spectroscopy techniques", *Plasma Sources Sci.Technol.,* Vol.19 (2), pp. 025013.

[5] Kopalidis, P.M.and Jorne, J., (1992), "Langmuir Probe Measurements and Characterization of Silicon Etching in SF 6/O 2 Discharges", *J.Electrochem.Soc.,* Vol.139 (3), pp. 839-844.

[6] Jenq, J., et al. (1994), "Absolute fluorine atom concentrations in RIE and ECR CF4 plasmas measured by actinometry", *Plasma Sources Sci.Technol.,* Vol.3 (2), pp. 154.

[7] Sasaki, K., et al. (1997), "Kinetics of fluorine atoms in high-density carbon–tetrafluoride plasmas", *J.Appl.Phys.,* Vol.82 (12), pp. 5938-5943.

[8] Booth, J.and Sadeghi, N., (1991), "Oxygen and fluorine atom kinetics in electron cyclotron resonance plasmas by time-resolved actinometry", *J.Appl.Phys.,* Vol.70 (2), pp. 611-620.

[9] Singh, H., Coburn, J.and Graves, D.B., (2001), "Measurements of neutral and ion composition, neutral temperature, and electron energy distribution function in a CF4 inductively coupled plasma", *Journal of Vacuum Science & Technology A,* Vol.19 (3), pp. 718-729.

[10] Picard, A., Turban, G.and Grolleau, B., (1986), "Plasma diagnostics of a SF6 radiofrequency discharge used for the etching of silicon", *J.Phys.D,* Vol.19 (6), pp. 991.

[11] Foest, R., et al. (1996), "Optical and mass spectrometric investigations of ions and neutral species in SF 6 radio-frequency discharges", *Physical Review E,* Vol.54 (2), pp. 1876.

[12] Mao, M., Wang, Y.and Bogaerts, A., (2011), "Numerical study of the plasma chemistry in inductively coupled SF6 and SF6/Ar plasmas used for deep silicon etching applications", *J.Phys.D,* Vol.44 (43), pp. 435202.

[13] Kline, L. (1986), "Electron and chemical kinetics in the low-pressure RF discharge etching of silicon in SF6", *IEEE Trans.Plasma Sci.,* Vol.14 (2), pp. 145-155.

[14] Gudmundsson, J. (2002), "Global model of plasma chemistry in a low-pressure O2/F2 discharge", *J.Phys.D,* Vol.35 (4), pp. 328.

[15] Yang, W., et al. (2016), "F-atom kinetics in SF6/Ar inductively coupled plasmas", *Journal of Vacuum Science & Technology A,* Vol.34 (3), pp. 031305.

[16] Anderson, H., Merson, J.and Light, R., (1986), "A kinetic model for plasma etching silicon in a SF6/O2 RF discharge", *IEEE Trans.Plasma Sci.,* Vol.14 (2), pp. 156-164.

[17] Riccardi, C., et al. (2000), "Modeling and diagnostic of an SF 6 RF plasma at low pressure", *IEEE Trans.Plasma Sci.,* Vol.28 (1), pp. 278-287.

[18] Girard, R., et al. (1999), "A two-temperature kinetic model of SF6 plasma", *J.Phys.D,* Vol.32 (22), pp. 2890.

[19] Kokkoris, G., et al. (2009), "A global model for SF6 plasmas coupling reaction kinetics in the gas phase and on the surface of the reactor walls", *J.Phys.D,* Vol.42 (5), pp. 055209.

[20] Pateau, A., et al. (2014), "Modeling of inductively coupled plasma SF6/O2/Ar plasma discharge: Effect of O2 on the plasma kinetic properties", *Journal of Vacuum Science & Technology A,* Vol.32 (2), pp. 021303.

[21] Su, Z. , (2015), "Modelling of Low-Pressure discharges for plasma processing", Dublin City University,.

[22] Kono, A., et al. (1994), "Charged particle densities and kinetics in a radio-frequency SF6 plasma", *J.Appl.Phys.,* Vol.76 (11), pp. 7221-7230.

[23] Cunge, G., et al. (2009), "Gas temperature measurement in CF4, SF6, O2, Cl2, and HBr inductively coupled plasmas", *Journal of Vacuum Science & Technology A,* Vol.27 (3), pp. 471-478.

[24] Haverlag, M., et al. (1996), "Measurement of the gas temperature in fluorocarbon radio frequency discharges using infrared absorption spectroscopy", *Journal of Vacuum Science & Technology A,* Vol.14 (2), pp. 380-383.

[25] Cunge, G., Chabert, P.and Booth, J., (2001), "Absolute fluorine atom concentrations in fluorocarbon plasmas determined from CF {sub 2} loss kinetics", *J.Appl.Phys.,* Vol.89 (12),.

[26] Tserepi, A., et al. (1997), "Kinetics of F atoms and fluorocarbon radicals studied by threshold ionization mass spectrometry in a microwave CF4 plasma", *Journal of Vacuum Science & Technology A,* Vol.15 (6), pp. 3120-3126.

[27] Nakamura, K., Segi, K.and Sugai, H., (1997), "Absolute fluorine atom densities in fluorocarbon high-density plasmas measured by appearance mass spectrometry", *Japanese journal of applied physics,* Vol.36 (4A), pp. L439.

[28] Ninomiya, K., Suzuki, K.and Nishimatsu, S., (1983), "Titration method for measuring fluorine atom concentration in microwave plasma etching", *Japanese Journal of Applied Physics,* Vol.22 (1R), pp. 139.

[29] Kawai, Y., Sasaki, K.and Kadota, K., (1997), "Comparison of the fluorine atom density measured by actinometry and vacuum ultraviolet absorption spectroscopy", *Japanese journal of applied physics,* Vol.36 (9A), pp. L1261.

[30] Kakuta, S., et al. (1993), "Influence of frequency, pressure, and mixture ratio of electronegative gas on electrical characteristics of rf discharges in N2-SF6 mixtures", *J.Appl.Phys.,* Vol.74 (8), pp. 4923-4931.

[31] Godyak, V., Piejak, R.and Alexandrovich, B., (1992), "Evolution of the electron-energy-distribution function during rf discharge transition to the high-voltage mode", *Phys.Rev.Lett.,* Vol.68 (1), pp. 40.

[32] Godyak, V., Piejak, R.and Alexandrovich, B., (1992), "Measurement of electron energy distribution in low-pressure RF discharges", *Plasma Sources Sci.Technol.,* Vol.1 (1), pp. 36.

[33] Kechkar, S. (2015), "Experimental investigation of a low pressure capacitively-coupled discharge", *PhD Thesis, School of Physical Sciences, Dublin City University,* .

[34] Lisovskiy, V., et al. (2007), "Modes of rf capacitive discharge in low-pressure sulfur hexafluoride", *J.Phys.D,* Vol.40 (22), pp. 6989.

[35] Blanks, K., Tabor, A.and Becker, K., (1987), "Absolute cross sections for fluorine 3p→ 3s line emissions following single electron impact on NF3, CF4, and SF6", *J.Chem.Phys.,* Vol.86 (9), pp. 4871-4875.

[36] Forand, J., Becker, K.and McConkey, J., (1986), "Dissociative excitation of SF6 by controlled electron impact", *Can.J.Phys.,* Vol.64 (3), pp. 269-276.

[37] Gottscho, R.A.and Donnelly, V.M., (1984), "Optical emission actinometry and spectral line shapes in rf glow discharges", *J.Appl.Phys.,* Vol.56 (2), pp. 245-250.

[38] Lallement, L., et al. (2009), "Global model and diagnostic of a low-pressure SF6/Ar inductively coupled plasma", *Plasma Sources Sci.Technol.,* Vol.18 (2), pp. 025001.

[39] Davis, G.P.and Gottscho, R.A., (1983), "Measurement of spatially resolved gas-phase plasma temperatures by optical emission and laser-induced fluorescence spectroscopy", *J.Appl.Phys.,* Vol.54 (6), pp. 3080-3086.

[40] Steffens, K.L.and Sobolewski, M.A., (2004), "A technique for temperature mapping in fluorocarbon plasmas using planar laser-induced fluorescence of CF", *J.Appl.Phys.,* Vol.96 (1), pp. 71-81.

Chapter 6- Re-investigation of electron kinetics as a function of gas pressure in O_2 plasma; Measurement of absolute atomic oxygen density using actinometry and Langmuir probe

6.1 Motivation

Knowledge on electron parameters such as electron density (n_e), the effective electron temperature (T_{eff}) and electron energy distribution function (EEDF) are important for understanding rates of various processes within plasma such as dissociation, ionization, excitation and atomic species production. As these parameters are primarily depend on discharge operating conditions, knowledge on kinetic behavior of electrons within plasma will aid in assessing or improving plasma assisted processes such as plasma etching or deposition.

Langmuir probes are most widely used diagnostic tool for investigating behavior of charged species within plasma. Numerous literatures reported the kinetic behavior of electrons in capacitively-coupled discharge using Langmuir probes [1-6]. Moreover, knowledge on electron behavior was investigated using OES based techniques [7-12] and 1D particle-in-cell simulation [13]. But only few experimental studies could be found in literature about the electron kinetic behavior in O_2 plasma which is predominantly used in plasma processing [14, 15]. S. Kechkar *et al* [16] extensively investigated electron heating mechanisms in O_2 and Ar plasmas for various operation conditions in this discharge using Langmuir probe. However, structure was observed on measured electron energy probability function (EEPF) in his study [16] especially during pressure evolution studies. And also, rate of ionization was found to increase with pressure violating particle balance equation mentioned in [17]. These unusual observations motivated to re-investigate electron kinetic behavior in O_2 plasma as function of gas pressure.

In this chapter, possible causes for structure observed in EEPF were discussed in section 6.2. In section 6.3, Langmuir probe arrangement was modified to ensure reference probe was always sampled close to main probe in plasma bulk and investigated its implication on EEPF. Absolute atomic oxygen concentration was investigated as function of pressure in section 6.4 using

actinometry/Langmuir probe measurements was compared with other reliable plasma diagnostics technique for validation. Finally, investigation of O_2 electron kinetics and outcomes were briefly summarized in section 6.5.

6.2 Investigation of kinetic behavior of electrons in O_2 plasma as a function of discharge pressure

Electron heating mechanism was found to vary with gas pressure as discharge undergoes transition and was reported elsewhere [4-6, 14, 15, 18, 19]. Discharge transition due to electron heating usually associated with any abrupt change to electron parameters like EEPF and T_{eff}. Evolution of EEPF with increase in O_2 gas pressure at constant 200 W rf power in capacitively-coupled plasma (CCP) discharge was investigated using Langmuir probe and results were shown in figure 6.1.

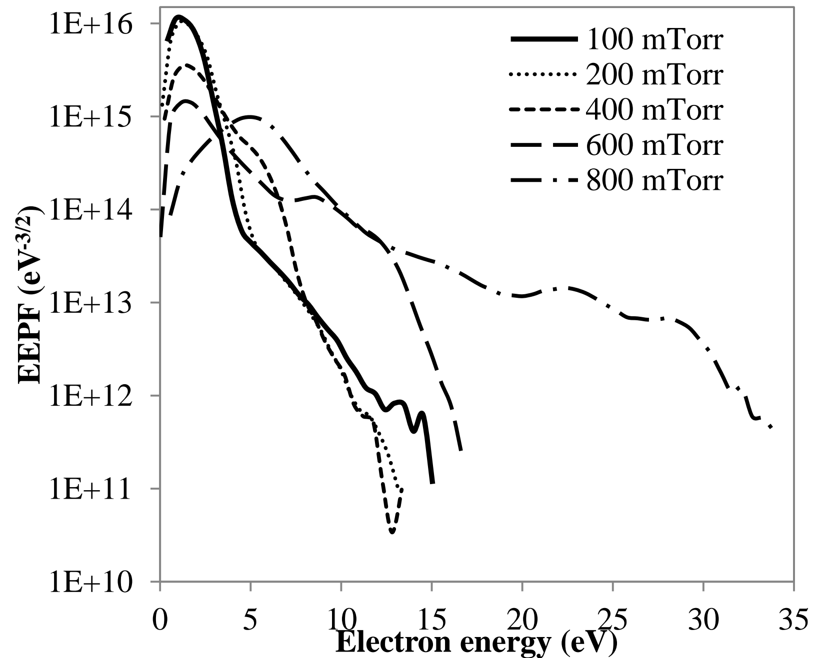

Figure 6.1 Evolution of EEPFs with increase in O_2 pressure at 200 W rf power in capacitively-coupled plasma.

With increase in pressure, electron heating process would change as discharge transition was expected from stochastic (collisionless) to ohmic (collisional) regime. For pressures ≤ 200 mTorr, EEPF was found to bi-Maxwellian, as shown in figure 6.1, with low and high electron energy groups. Similar bi-Maxwellian characterized EEPF was observed in argon [1, 19] at pressure < 300 mTorr and discharge was predominately controlled by stochastic heating, where low energy electrons in the plasma bulk unable to overcome the ambipolar potential barrier whereas high energy electron group (fast electrons) gain energy through interaction with argon atoms through elastic and ionization processes; and balances loss of energy near oscillating plasma-sheath boundary [1]. Further increase in argon pressure (> 500 mTorr), ohmic heating was found to be the dominant electron heating mechanism and Druyvesteyn-like EEPFs were observed [1, 19]. In case of oxygen for pressures > 200 mTorr, shape of EEPF was found to deviate from bi-Maxwellian and thus indicating discharge was in transition mode. Also, electron parameters like n_e and T_{eff} supported such transition with increase in gas pressures as shown in figure 6.2. But for O_2 pressures > 400 mTorr, tail of EEPF was found to increase with gas pressure and structures were observed on measured EEPF.

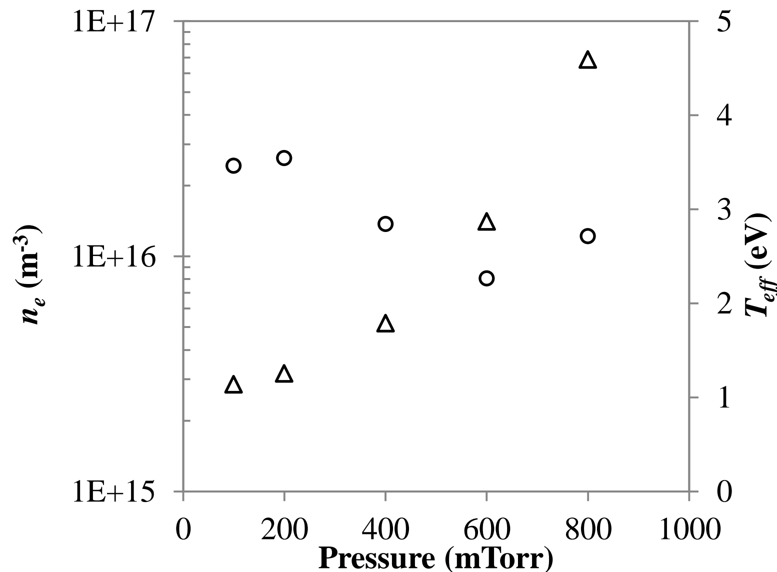

Figure 6.2 Electron density, n_e (○) and effective electron temperature, T_{eff} (Δ) as a function of O_2 gas pressure in a capacitively-coupled plasma operated at 200 W rf power.

6.2.1 Investigation of structure observed on measured EEPF

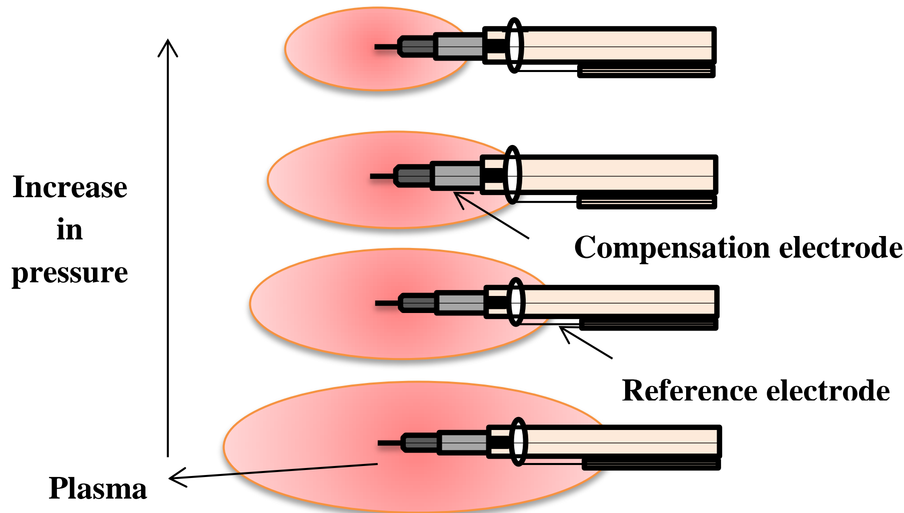

Figure 6.3 Schematic of visually observed plasma confinement with increase in O_2 gas pressure at 200 W rf capacitive discharge.

It was clear from section 6.2, structures were observed in measured EEPF and also enhancement of EEPF tail was evident for pressures > 200 mTorr in O_2 capacitive discharge. Increase in EEPF tail with gas pressure would increase rate of ionization and obviously violating particle balance equation in [17] and was already pointed out by author in [16]. Possible cause for increase in EEPF tail with gas pressure was not understood well as there were only few studies available in literature about EEPFs in capacitively-coupled O_2 discharge. And additional peaks observed on EEPFs, especially at 600 and 800 mTorr pressure, could be due to high energy electrons produced due to super-elastic collision of electrons with O_2 molecules in metastable state [20, 21]. However, additional peak can also appear on EEPF due to distortion in probe current-voltage characteristics (IVCs) [1, 22]. Major distortion in IVCs under these

circumstances can be mainly due to inadequate rf compensation by compensation electrode on the probe [6, 18] and any disturbance to probe offered by plasma sheath resistance [18].

Consider figure 6.3 to further examine this inadequate behavior of compensation and reference electrodes. Position of probe was fixed at radial centre (plasma bulk) and plasma was visually found to confine with increase in O_2 pressure at constant rf power. So, with increase in pressure, reference electrode could be falling out of plasma. Consequently, this could lead to increase in plasma potential and cause distortion in IVCs characteristics, which was verified using second derivative of the IVC [1, 18]. This investigation was extended further with modified reference electrode position as shown in figure 6.4(b). For convenience in this investigation, standard Langmuir probe arrangement was named as “L1” and Langmuir probe with modified reference electrode position was denoted as “L2”. With L2, the reference electrode was always held in plasma bulk to avoid any shift in plasma potential due to plasma sheath resistance. The modified set up, L2 was validated in 20 mTorr and 300 mTorr argon discharge operated at 200 W. Excellent agreement on EEPFs were found between L1 and L2 setups as shown in figure 6.5 and other electron parameters comparison were tabulated in table 6.1.

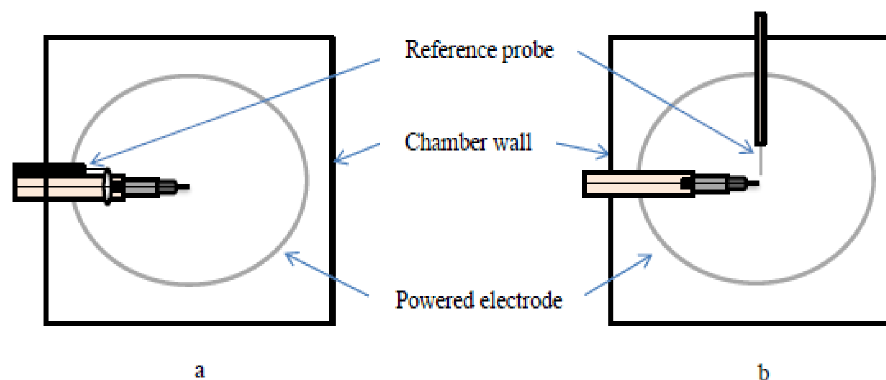

Figure 6.4 Schematics of Langmuir probe with standard setup L1 and (b) Langmuir probe with modified reference electrode position L2

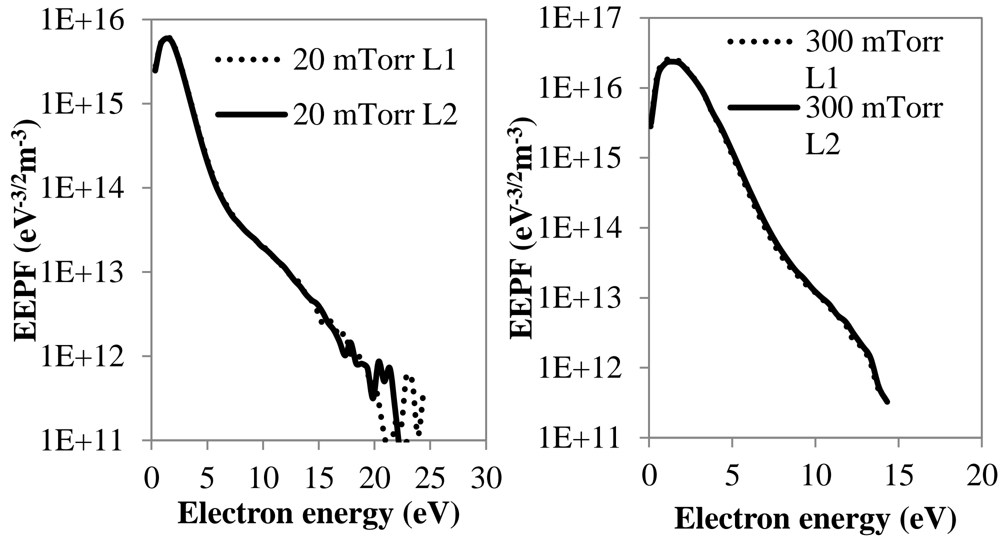

Figure 6.5 EEPFs measured using two Langmuir probe setups, L1 and L2 in 20 mTorr and 300 mTorr argon discharges operated at 200 W rf power.

Table 6.1: Electron parameters measured using two different Langmuir probe arrangements.

Pressure	**20 mTorr**		**300 mTorr**	
Arrangement	**L1**	**L2**	**L1**	**L2**
n_e **(m^{-3})**	1.84E+16	1.80E+16	8.54E+16	8.24E+16
T_{eff} **(eV)**	1.54	1.57	1.49	1.53

6.3 Investigation of heating mode transition in O_2 discharge using Langmuir probe with L2 setup at 200 W rf power.

Kinetics behavior of electrons in O_2 plasma were again investigated in this section with modified Langmuir probe arrangement (L2) for discharge conditions similar to that studied in section 6.2.1. Motivation of these measurements was to verify the hypothesis described in section 6.2.1 using figure 6.3 and to investigate the behavior of measured EEPF with other plasma parameters with modified Langmuir probe setup. EEPFs measured with L2

arrangement in O_2 discharge operated at 200 W at different gas pressures and results were shown in figure 6.6.

With modified Langmuir probe arrangement, L2, the discharge transition due to change in electron heating mechanism, from collisionless to collisional heating regime was observed for increase in O_2 gas pressure. For pressures < 400 mTorr, EEPFs had bi-Maxwellian distribution with low and high energy electron groups as shown in figure 6.6. With increase in pressure beyond 400 mTorr, discharge was found to be in transition regime as high energy electrons in EEPF tail decreased due to collisions with background gas. The discharge was clearly found to be in collisional regime for pressures > 600 mTorr, as EEPFs had Druyvesteyn-like shape accompanied with abrupt changes to electron density and effective electron temperature, would be typical to a capacitive discharge [1, 3], as shown in figure 6.7.

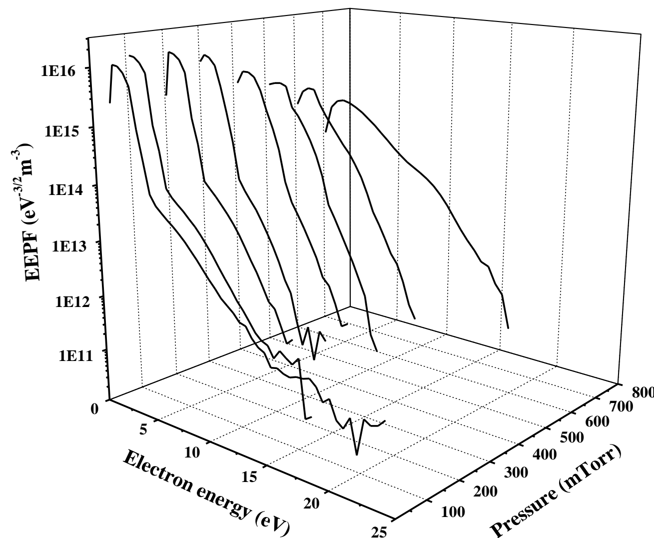

Figure 6.6 Pressure evolutions of EEPFs measured using Langmuir probe with L2 arrangement in O_2 discharge operated at 200 W rf power.

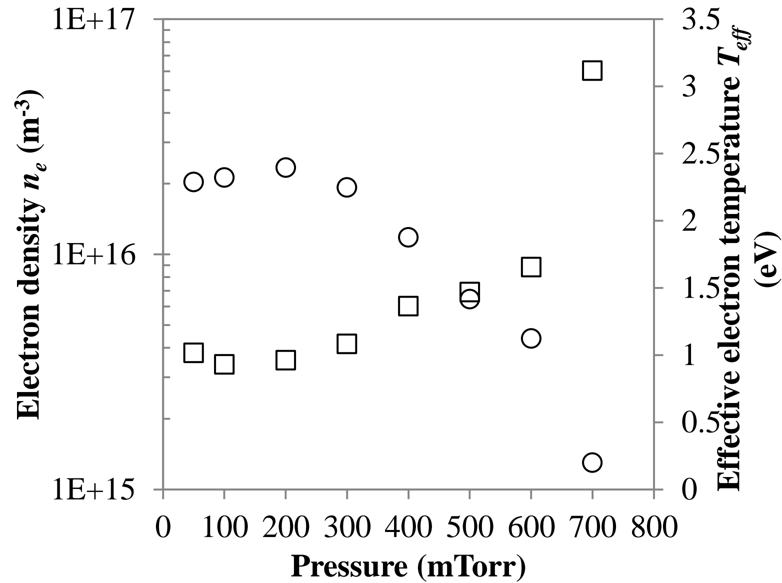

Figure 6.7 Variations of electron density n_e (○) and effective electron temperature T_{eff} (□) measured using Langmuir probe with L2 setup for different gas pressures in O_2 discharge operated at 200 W.

6.3.1 Comparison of O_2 electron kinetics measured between two Langmuir probe arrangements – Effect of Inadequate probe compensation

To more precisely verify the hypothesis, EEPFs measured in O_2 discharge operated at 200 W for different gas pressures with Langmuir probe using two arrangements L1& L2 were compared as in figure 6.8 and the corresponding measured electron parameters comparison were shown in shown in figure 6.9.

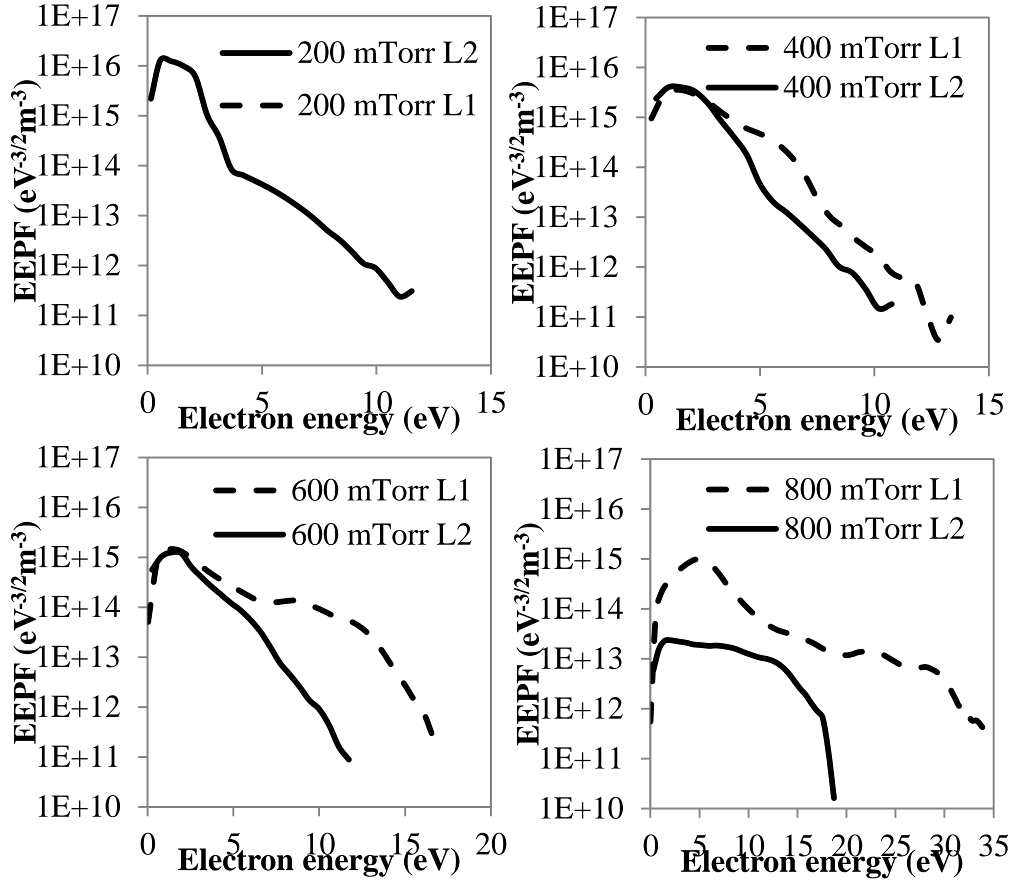

Figure 6.8 Comparison of EEPFs measured using two different Langmuir probe arrangements L1 & L2 in O_2 discharge operated at 200 W rf power for different gas pressures.

Additional peak structures were not found on EEPFs measured using modified Langmuir probe arrangements L2 in O_2 discharge at 200 W. This suggested for pressures > 200 mTorr, IVCs obtained using L1 arrangements were distorted as part of probe assembly, especially reference electrode was out of plasma [1, 22]. Also, ionizing tail in measured EEPF was found to decrease with gas pressure in L2 in contrast to L1 arrangement. To further investigate, ionization rate, k_{iz} was calculated using equation 6.1[23]

$$k_{iz} = \int f_n^p(\varepsilon)\sigma(\varepsilon)v(\varepsilon)d\varepsilon \qquad 6.1$$

where $f_n^p(\varepsilon)$ – normalized EEPF, $\sigma(\varepsilon)$ – ionization cross section of O_2 [24] as a function of electron energy, ε and $v(\varepsilon)$ – electron velocity dependent on mean electron energy.

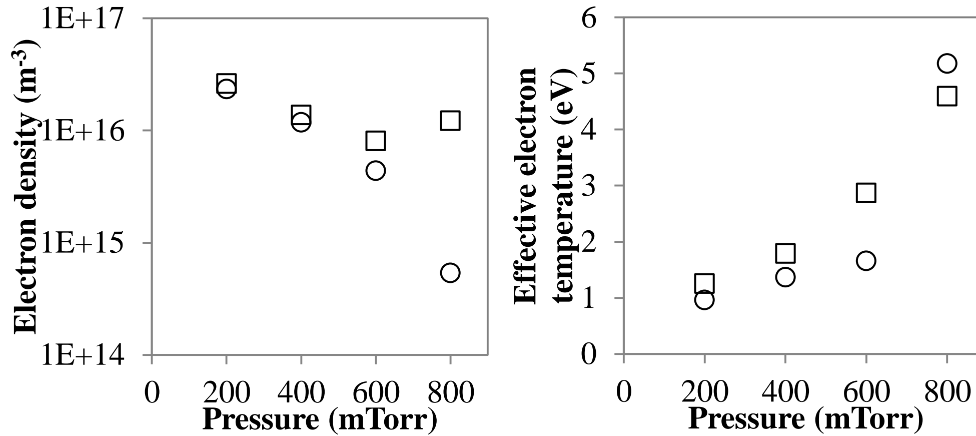

Figure 6.9 Comparison of electron density (left) and effective electron temperature (right) measured using Langmuir probe with L1 (□) and L2 (○) arrangements for different gas pressures in O_2 discharge at 200 W.

Calculated ionization rate with L2 Langmuir probe arrangement was found to decrease with increase in gas pressure as shown in figure 6.10 and was in accordance to particle balance law in [17]. Transition due to electron heating mechanism with increase in gas pressure in O_2 discharge was observed through EEPFs and other electron parameters measured using L2 Langmuir probe arrangement was more obvious than with L1 setup here and elsewhere [16] in this capacitive discharge. These results clearly suggested reference electrode, in L1 setup, failed to account for any changes in local plasma potential as it was moving away from plasma due to confinement of discharge, visually observed, with increase in pressure. However, second derivative of measured IVC using L2 setup found to flatten at 800 mTorr O_2 pressure and produced broader structure on measured EEPF at higher energy. This could be due to poor compensation, because of spatial variations in plasma potential between probe tip and compensation electrode [1, 6, 18, 22]. This behavior of inadequate

probe compensation would be demonstrated in radial and spatial direction with O_2 and Ar discharge respectively in the following section.

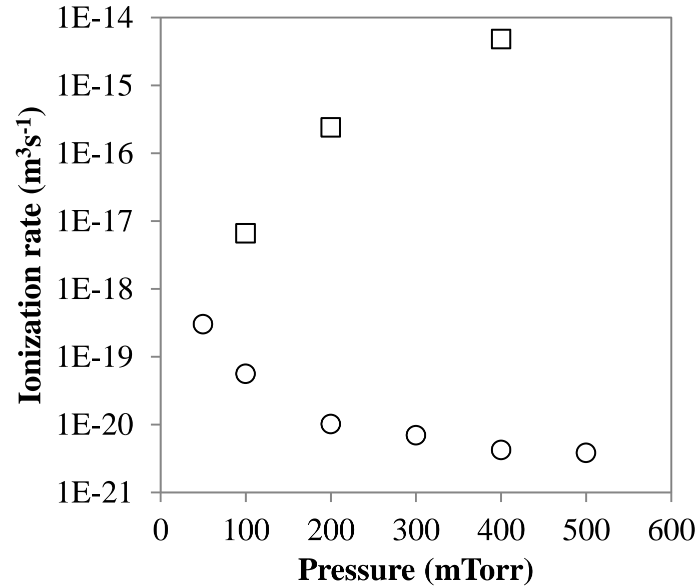

Figure 6.10 Calculated ionization rate using L2 Langmuir probe arrangement (○) was compared to ionization rate in reference [16] (□).

Spatial measurements were carried in 300 mTorr Ar discharge operated at 100 W rf power using Langmuir probe. To exclude the phenomenon of distortion of IVC due to presence of significant negative ions in the discharge, argon was used in this particular case. The main body of the Langmuir probe was positioned in axial centre through top view port of the chamber, as shown in figure 6.11 (a) while the reference electrode position was fixed radially in plasma bulk through one of the side view port of the chamber. The position of main probe was varied axially between powered and grounded electrode of chamber with the help wilson seal as shown in figure 6.11 (b).

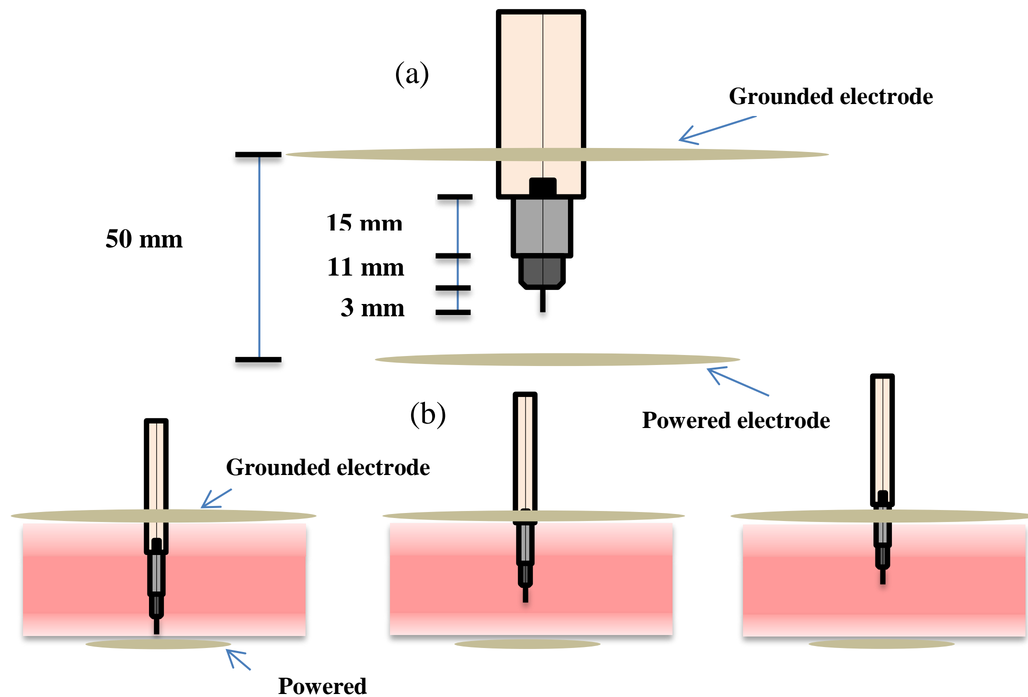

Figure 6.11 (a) Spatial arrangement of Langmuir probe with dimensions of probe assembly. (b) Schematic of different positions of Langmuir probe in spatial direction.

Spatial Langmuir probe measurements were performed in Ar discharge at 300 mTorr gas pressure with 100 W rf power and measured EEPFs as a function of distance from powered electrode (PE) were shown in figure 6.12. Additional peak structure found to be more pronounce, as expected with increase in distance from powered electrode due to inadequate compensation. Note the reference electrode position was fixed at radial centre (plasma bulk) during these measurements. When the probe tip was at ≈ 11 mm from PE, a part of compensation electrode could be in sheath region as additional peak began to appear due to distortion in IVC caused by variation in plasma potential between probe tip, predominantly in plasma bulk and compensation electrode. On other instance where compensation electrode was completely out of plasma (probably in sheath region) for probe tip position at discharge centre axially i.e., ≈ 26 mm from PE and measured EEPF had broader structure at higher energy. Similar broad features on measured EEPFs were observed in hydrogen capacitive

discharge due to inadequate compensation [22]. To further strengthen the argument on probe compensation, investigation was extended in radial direction as O_2 electron kinetics was studied radially. Langmuir probe arrangement was same as L2 setup except the main probe was moved away from discharge centre (DC) to measure EEPF at different radial positions. Measured EEPFs as a function of radial position for different O_2 gas pressures were shown in figure 6.13.

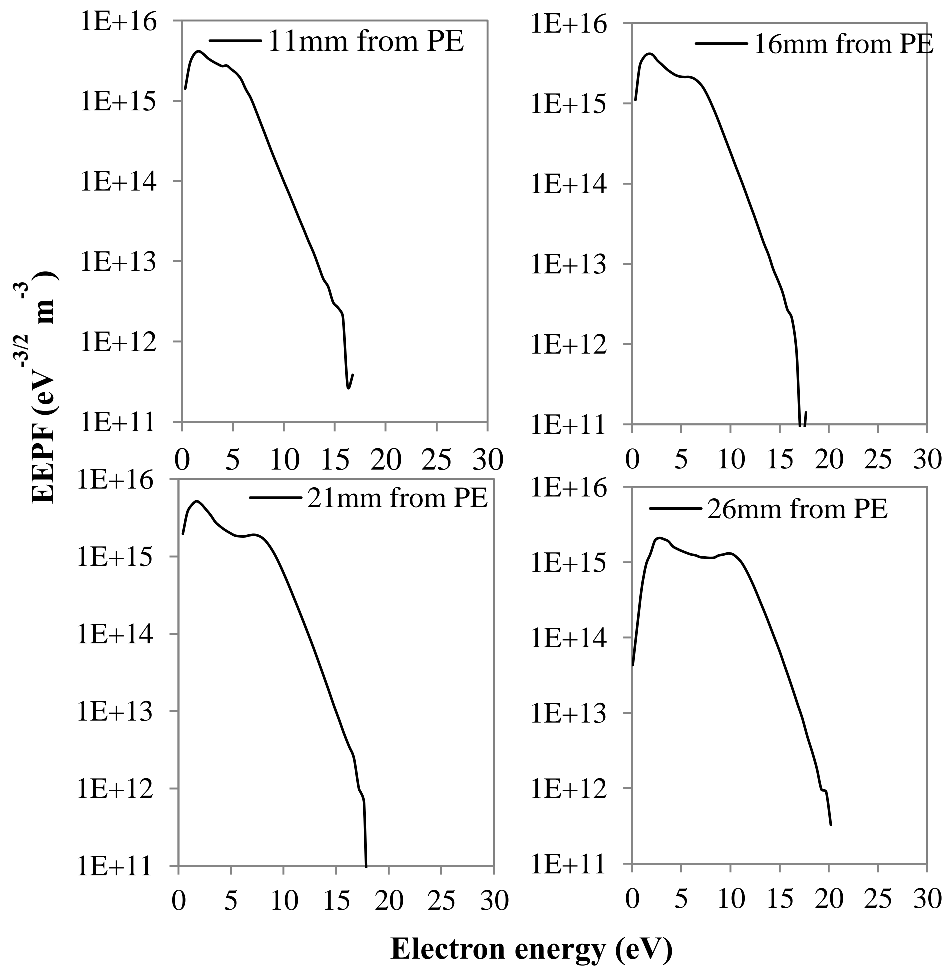

Figure 6.12 Plots of EEPFs measured spatially in 300 mTorr Ar discharge operated at 100 W as function of distance from powered electrode (PE).

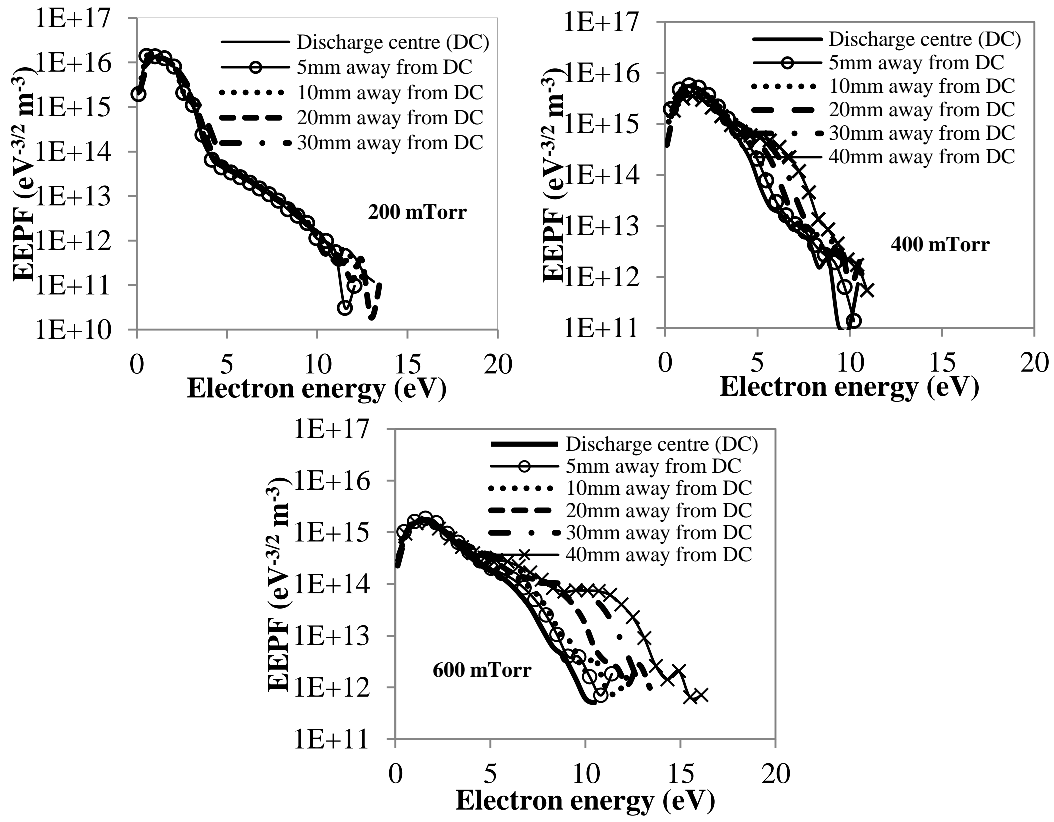

Figure 6.13 Measured EEPFs as a function of distance from discharge centre (DC) in radial direction for different (200, 400 & 600 mTorr) O_2 pressures operated at 200 W.

Structures were observed on measured EEPFs especially at 400 & 600 mTorr pressure for probe to be furthest away from discharge centre (DC). With increase in O_2 gas pressure, discharge confinement was visually evident and mentioned in section 6.2.1. Particularly at 600 mTorr pressure, as the main probe was moved away from plasma bulk, additional peak began to grow as compensation electrode was slowly falling in dark region, presumably sheath. When the probe tip was positioned ≈ 30-40 mm from plasma bulk, most part of compensation electrode was in dark region and caused distortion to measured IVCs. So, these investigations signified additional peak or enhanced EEPF tail on measured EEPF could predominantly due to distortion in IVC rather than

super-elastic collision process or energetic electron beam under conditions explored.

6.4 Measurement of absolute atomic oxygen density using optical emission spectroscopy and Langmuir probe

Previous sections investigated the possible causes for structure observed in measured EEPFs in pressure evolution studies on O_2 electron kinetics in capacitive discharge. With improved Langmuir probe arrangement, probe compensation was restored and undistorted IVCs were obtained. In this section, optical emission spectroscopy and Langmuir probe diagnostic techniques were employed to obtain quantitative measurements of atomic oxygen, [O] in the discharge as function of gas pressure in O_2-Ar (96/4%) discharge operated at 100 W. For conditions explored in this study, EEDFs were measured using Langmuir probe as function of gas pressure, as shown in figure 6.14 to investigate for any discharge transition due to electron heating and corresponding electron density and effective electron temperature were also measured as shown in figure 6.15.

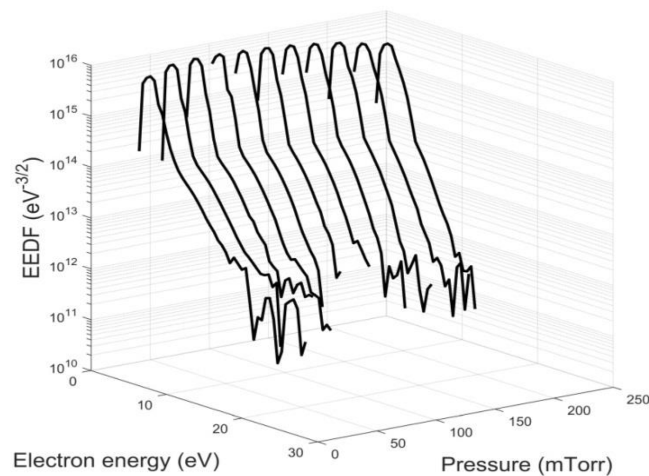

Figure 6.14 Evolution of EEDF as a function of pressure in O_2-Ar discharge operated at 100 W.

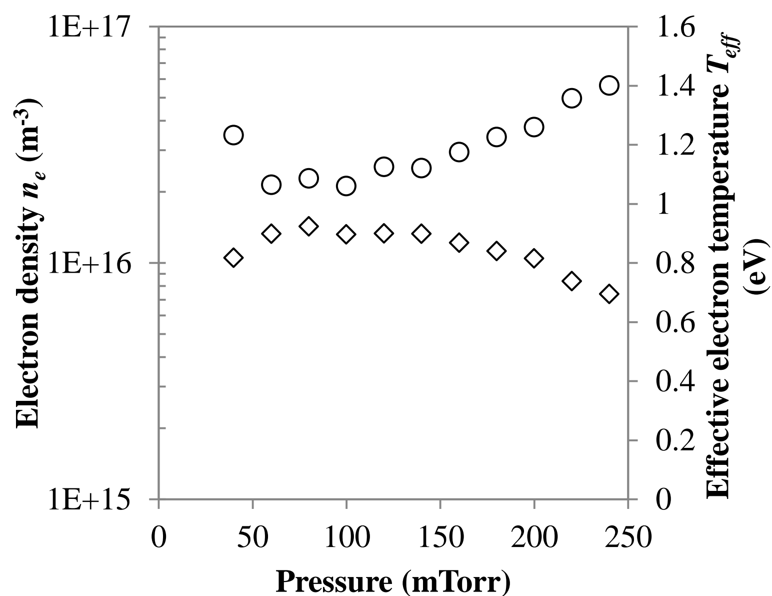

Figure 6.15 Measurements of electron density (◊) and effective electron temperature (○) as a function of gas pressure in O_2-Ar discharge operated at 100 W.

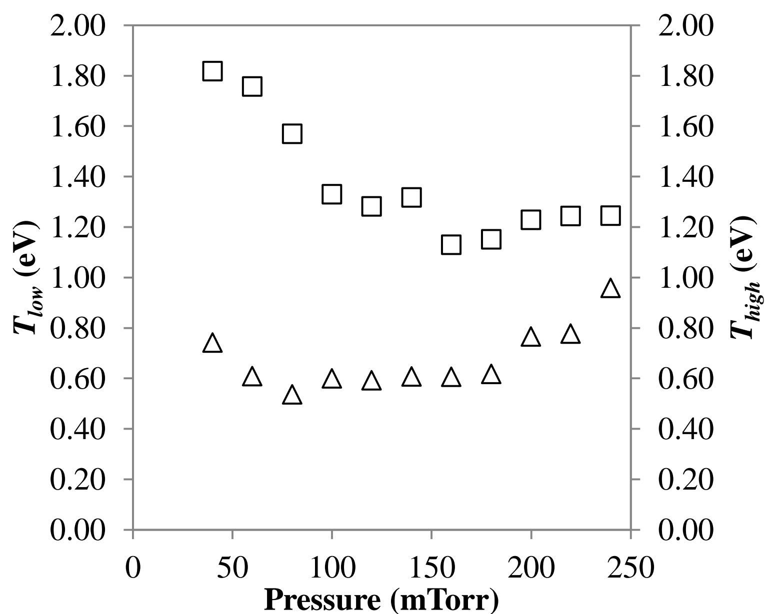

Figure 6.16 Variations of temperatures of low (Δ) and high (□) energy electron groups as a function of gas pressure in O_2-Ar discharge operated at 100 W.

For investigated pressure, shape of EEDFs was bi-Maxwellian and no drastic change was observed in electron parameters like n_e and T_{eff}. From these kinetic behaviors of electrons, one can suggest the discharge was predominantly in collisionless regime (stochastic mode). As electron distribution had two electron groups i.e., low (1.4< ε <5 eV) and high (5< ε <25) eV energy electrons as shown in figure 6.14, temperature of low (T_{low}) and high (T_{high}) energy electron groups were determined using –1/slope from the plot of ln $f_e(\varepsilon)$ *vs* ε. Slopes were obtained using linear fit to the plot of ln $f_e(\varepsilon)$ *vs* ε at their corresponding energy range of electron groups and results were shown in figure 6.16. T_{high} was found to decrease by ≈ 0.67 eV between pressures 40 and 180 mTorr whereas T_{low} decreased only by ≈ 0.12 eV. For pressures 180 mTorr < P < 240 mTorr, T_{low} was found to increase by a factor of ≈ 1.3 but T_{high} remained constant between these pressures. These variations in T_{low} and T_{high} were expected with increase in pressure. At low pressures, low energy electron groups in plasma bulk trapped in ambipolar potential well due to insufficient energy. However with increase in gas pressure, these electrons could gain energy due to with interactions with molecules or atoms in the discharge. Thus for pressure > 180 mTorr, T_{low} increased by factor of ≈ 1.3 and T_{eff} which predominately determines bulk electron temperature, also increased by similar factor. Fast electrons which were responsible for electron-impact processes like ionization, excitation and dissociation exists close tail of EEDF. Since there was not much decrease in tail of EEDF, contribution of electron-impact dissociative excitation along with direct excitation would be significant to determine atomic oxygen density in discharge using actinometry. Thus improved actinometry model with dissociative excitation contribution was adopted [25] to determine [O] as shown in equation 6.2

$$[O] = \frac{I_O}{I_{Ar}}[Ar]\frac{k_e^{Ar}}{k_e^O}\frac{\lambda_{Ar}}{\lambda_O}\frac{h\nu_{Ar}}{h\nu_O}\frac{A_{ij}^{Ar}}{A_{ij}^O}\frac{\left(k_{q_{O_2}}^O[O_2] + k_{q_{Ar}}^O[Ar] + \sum_j A_{ij}^O\right)}{\left(k_{q_{O_2}}^{Ar}[O_2] + k_{q_{Ar}}^{Ar}[Ar] + \sum_j A_{ij}^{Ar}\right)} - \frac{k_e^{diss\,O}}{k_e^O}[O_2] \quad (6.2)$$

where I_O and I_{Ar} were time averaged optical emission intensities of atomic oxygen at 844 nm and argon at 750 nm respectively; k_e^O and k_e^{Ar} were direct electron-impact excitation co-efficients of atomic oxygen and argon respectively; $k_e^{diss\ O}$ was excitation co-efficients due to dissociative mechanism; $[Ar]$ and $[O_2]$ were neutral densities of argon and molecular oxygen calculated using ideal gas law; λ_{Ar} and λ_O were spectral response of the detector which depend on wavelength measured through spectrometer calibration for argon and atomic oxygen emission lines respectively; $h\nu_{Ar}$ and $h\nu_O$ were photon energy of argon and atomic oxygen respectively; A_{ij}^{Ar} and A_{ij}^O were rates of spontaneous emission for transitions to Ar ($1p_0$) and O($3s^3S$) states respectively; $k_{q_{O_2}}^O$ and $k_{q_{Ar}}^O$ were rates of quenching of O by molecular oxygen and argon respectively; $k_{q_{O_2}}^{Ar}$ and $k_{q_{Ar}}^{Ar}$ were rates of quenching of Ar by molecular oxygen and argon respectively; $\sum_j A_{ij}^O$ and $\sum_j A_{ij}^{Ar}$ were total rates of spontaneous emission of the excited state to all lower states in atomic oxygen and argon respectively and which were equivalent to reciprocal of their respective natural life time, τ of the excited level. The experimental values and constants essential for determining [O] in equation 6.2 were shown in table 6.2.

Table 6.2 Experimental values and constants [26] for determining [O]

States	λ (a.u)	$\sum_j A_{ij}$ (s^{-1})	$k_{q_{O_2}}$ (m^3s^{-1})	$k_{q_{Ar}}$ (m^3s^{-1})
O ($3p^3P$)	0.22	2.85×10^{7}	9.40×10^{-16}	0.25×10^{-16}
Ar ($2p_1$)	0.11	4.17×10^{7}	7.60×10^{-16}	0.16×10^{-16}

Excitation rate co-efficients required for determining [O] in equation 6.2 was calculated using following equation 6.3 [25],

$$k_e = \int_0^\infty f_n(\varepsilon)\sigma(\varepsilon)\sqrt{\frac{2\varepsilon}{m_e}}\,d\varepsilon \qquad (6.3)$$

where $f_n(\varepsilon)$ was normalized EEDF; m_e was mass of electron; $\sigma(\varepsilon)$ was energy (ε) dependent excitation cross section for specific excitation mechanism i.e., direct excitation cross section for O and Ar were obtained from [27] and [25] respectively while cross section for dissociative excitation of O was obtained from [28].

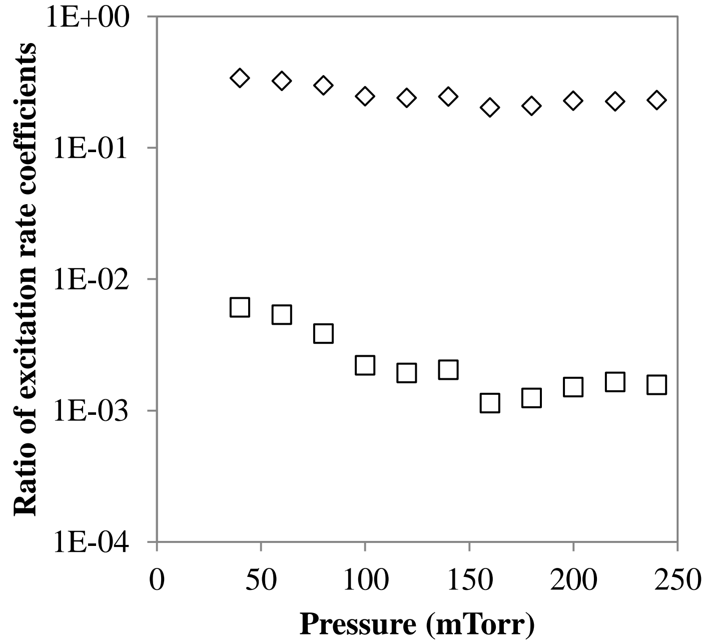

Figure 6.17 Variations of calculated k_e^{Ar}/k_e^{O}(◊) and $k_e^{diss\ O}/k_e^{O}$(□) as a function of pressure in O_2-Ar discharge operated at 100 W.

In order to compute accurate excitation rate co-efficients, distribution function of electrons at energies above 15 eV was vital. Unfortunately, in most cases Langmuir probe measured EEDF at these higher energies were noisy and unreliable as shown in figure 6.14. Therefore, theoretical extrapolation of distribution function for energies up to 25 eV was performed to evaluate reliable excitation rate co-efficients. That is, linear relationship to energies just below 15 eV was evaluated from plot of ln $f_n(\varepsilon)$ vs ε and distribution under Maxwellian assumption was extrapolated using this relation. This Maxwellian fit to measured EEDFs at high energies was reasonable as it caused

insignificant changes to electron parameters and usually no drastic changes to EEDFs were expected at these higher energy regime was found elsewhere [29, 30]. Thus, ratio of calculated excitation rate co-efficients required to determine [O] were shown in figure 6.17.

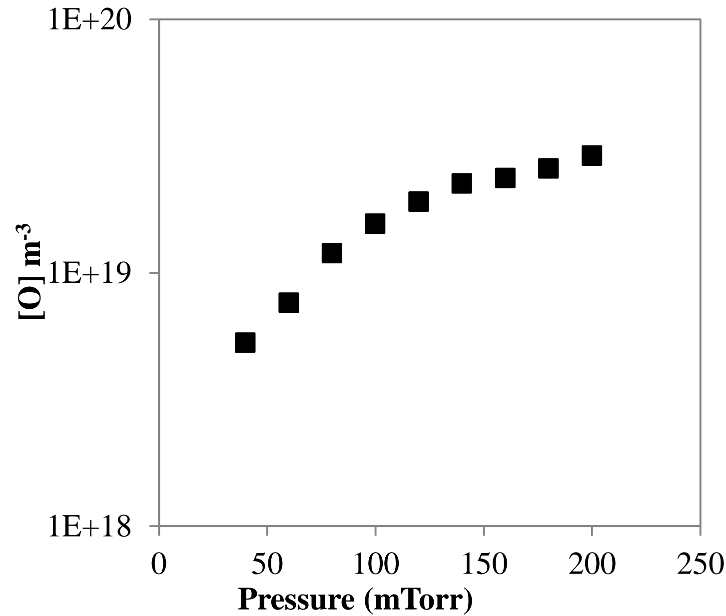

Figure 6.18 Atomic oxygen density determined using actinometric signal and excitation rate co-efficients calculated from EEDF measured using Langmuir probe (□) as a function of gas pressure in O_2-Ar discharge operated at 100 W.

Ratio of both excitation co-efficients k_e^{Ar}/k_e^O and $k_e^{diss\,O}/k_e^O$ found to decrease with pressure. However for decrease in pressure, $k_e^{diss\,O}/k_e^O$ was found to increase by a factor of ≈ 3.9 while k_e^{Ar}/k_e^O increased only by a factor of ≈ 1.5. This could indicate that dissociative excitation can be very much significant for low O_2 pressures in this discharge. By using these values, excitation rate co-efficients along with other constants (in table 6.2) values were substituted in equation 6.2 to determine [O] as a function of pressure and shown in figure 6.18. Relative variation of [O] with pressure was compared to TALIF measurements [31] as shown in figure 6.19. To investigate atomic oxygen

density using TALIF, a two-photon excitation of 225.6 nm and ensuing fluorescence at 884.6 nm was used in an Innolas Splitlight 600 Nd : YAG laser operated at 10 Hz frequency. Two photon excitation of xenon gas at 224.3 nm and the following fluorescence at 834.9 nm were recorded to calibrate the system for absolute atomic oxygen density.

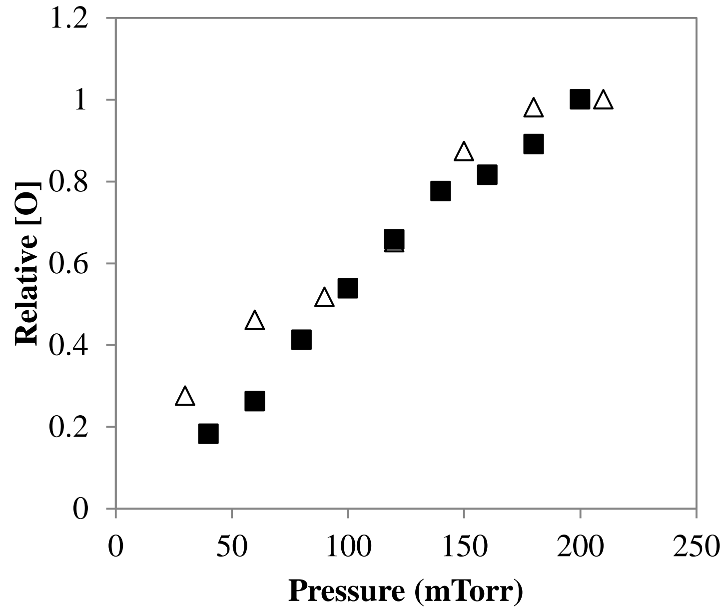

Figure 6.19 Pressure variation of relative atomic oxygen density measured using actinometry (■) was compared with TALIF measurements (Δ) from [31] in O_2-Ar discharge operated at 100 W rf power.

Good quantitative agreement was achieved for atomic oxygen density measured using both diagnostic techniques. And also density of oxygen atoms produced through dissociative excitation, $[O]_{diss}$ found to decrease with increase in pressure and obviously, very much significant at low pressures as shown figure 6.20. In fact, large population of energetic electrons in high energy regime of EEDF tail could be reason for excitation through dissociative channel at low pressures. However, $[O]/[O]_{diss}$ was found to increase marginally for pressures above 160 mTorr and it was mainly due to decrease in oxygen production rate, where oxygen atoms can be lost through recombination at walls [28].

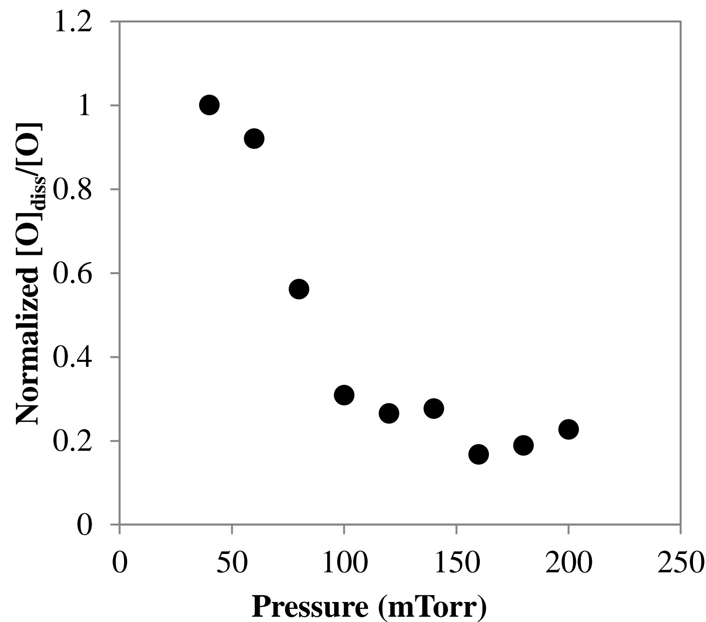

Figure 6.20 Variations of atomic oxygen production rate through dissociative excitation mechanism as a function of pressure in O_2-Ar discharge operated at 100 W rf power.

6.5 Conclusion

This chapter investigated the possible cause for additional structure on measured EEPF at pressures > 200 mTorr in O_2 discharge at 200 W rf power with L1 Langmuir probe arrangement. Structure observed because of IVCs distortion caused due to variation in plasma potential between probe tip and reference electrode, which was not completely in plasma bulk for certain operating conditions. And inadequate rf compensation also caused additional peak on measured EEPF. With improved Langmuir probe arrangement (L2), discharge transition with increase pressure due to change in electron heating mechanism was studied in O_2 CCP discharge. In addition, atomic oxygen density in O_2-Ar discharge was investigated as function of gas pressure using EEDF measured with Langmuir probe and optical emission spectroscopy. And

this measurement on [O] was compared to TALIF measurement for validation. Good agreement was achieved for investigated conditions.

6.6 Reference

[1] Godyak, V., Piejak, R.and Alexandrovich, B., (1992), "Measurement of electron energy distribution in low-pressure RF discharges", *Plasma Sources Sci.Technol.,* Vol.1 (1), pp. 36.

[2] Godyak, V., Piejak, R.and Alexandrovich, B., (1992), "Evolution of the electron-energy-distribution function during rf discharge transition to the high-voltage mode", *Phys.Rev.Lett.,* Vol.68 (1), pp. 40.

[3] Godyak, V., Piejak, R.and Alexandrovich, B., (1993), "Probe diagnostics of non-Maxwellian plasmas", *J.Appl.Phys.,* Vol.73 (8), pp. 3657-3663.

[4] Gahan, D., et al. (2011), "Characterization of an asymmetric parallel plate radio-frequency discharge using a retarding field energy analyzer", *Plasma Sources Sci.Technol.,* Vol.21 (1), pp. 015002.

[5] Abdel-Fattah, E., Bazavan, M.and Sugai, H., (2011), "Langmuir probe diagnostics of electron energy distributions with optical emission spectroscopy in capacitively coupled rf discharge in nitrogen", *J.Appl.Phys.,* Vol.110 (11), pp. 113303.

[6] Scanlan, J.V.and Hopkins, M.B., (1992), "Langmuir probe measurements of the electron energy distribution function in radio-frequency plasmas", *Journal of Vacuum Science & Technology A,* Vol.10 (4), pp. 1207-1211.

[7] Donnelly, V. (2004), "Plasma electron temperatures and electron energy distributions measured by trace rare gases optical emission spectroscopy", *J.Phys.D,* Vol.37 (19), pp. R217.

[8] Crintea, D., et al. (2009), "Plasma diagnostics by optical emission spectroscopy on argon and comparison with Thomson scattering", *J.Phys.D,* Vol.42 (4), pp. 045208.

[9] Gans, T., Schulz-Von Der Gathen, V.and Döbele, H., (2004), "Spectroscopic measurements of phase-resolved electron energy distribution functions in RF-excited discharges", *EPL (Europhysics Letters),* Vol.66 (2), pp. 232.

[10] Abdel-Rahman, M., et al. (2005), "Space and time resolved rotational state populations and gas temperatures in an inductively coupled hydrogen RF discharge", *Plasma Sources Sci.Technol.,* Vol.14 (1), pp. 51.

[11] Schulze, J., et al. (2007), "Space and phase resolved plasma parameters in an industrial dual-frequency capacitively coupled radio-frequency discharge", *J.Phys.D,* Vol.40 (22), pp. 7008.

[12] Schulze, J., et al. (2010), "Phase resolved optical emission spectroscopy: a non-intrusive diagnostic to study electron dynamics in capacitive radio frequency discharges", *J.Phys.D,* Vol.43 (12), pp. 124016.

[13] Conway, J., et al. (2013), "Use of particle-in-cell simulations to improve the actinometry technique for determination of absolute atomic oxygen density", *Plasma Sources Sci.Technol.,* Vol.22 (4), pp. 045004.

[14] Lee, M., Lee, H.and Chung, C., (2010), "Comparison of pressure dependence of electron energy distributions in oxygen capacitively and inductively coupled plasmas", *Physical Review E,* Vol.81 (4), pp. 046402.

[15] Pulpytel, J., Morscheidt, W.and Arefi-Khonsari, F., (2007), "Probe diagnostics of argon-oxygen-tetramethyltin capacitively coupled plasmas for the deposition of tin oxide thin films", *J.Appl.Phys.,* Vol.101 (7), pp. 073308.

[16] Kechkar, S. (2015), "Experimental investigation of a low pressure capacitively-coupled discharge", *PhD Thesis, School of Physical Sciences, Dublin City University,* .

[17] Lieberman, M.A. and Lichtenberg, A.J., (2005)*, Principles of plasma discharges and materials processing,* , John Wiley & Sons,.

[18] Hopkins, M. (1996), "Langmuir probe measurements in the gaseous electronics conference rf reference cell", *J.Res.Natl.Stand.Technol,* Vol.100 pp. 415.

[19] Godyak, V.and Piejak, R., (1990), "Abnormally low electron energy and heating-mode transition in a low-pressure argon rf discharge at 13.56 MHz", *Phys.Rev.Lett.,* Vol.65 (8), pp. 996.

[20] Capitelli, M., et al. (2008), "Electron energy distribution functions and second kind collisions", *Plasma Sources Sci.Technol.,* Vol.18 (1), pp. 014014.

[21] Amorim, J., et al. (1999), "Superelastic collisions of electrons with the c3Πu metastable state in hydrogen dc positive column", *Chem.Phys.,* Vol.246 (1), pp. 275-282.

[22] Mahony, C., et al. (1999), "Structure observed in measured electron energy distribution functions in capacitively coupled radio frequency hydrogen plasmas", *Appl.Phys.Lett.,* Vol.75 (3), pp. 331-333.

[23] Deegan, C.M. (1999), "Characterisation of the heating mechanism in a capacitively coupled argon rf discharge", *PhD Thesis, School of Physical Sciences, Dublin City University,* .

[24] Straub, H., et al. (1996), "Absolute partial cross sections for electron-impact ionization of H 2, N 2, and O 2 from threshold to 1000 eV", *Physical Review A,* Vol.54 (3), pp. 2146.

[25] Katsch, H., et al. (2000), "Detection of atomic oxygen: Improvement of actinometry and comparison with laser spectroscopy", *J.Appl.Phys.,* Vol.88 (11), pp. 6232-6238.

[26] Niemi, K., Schulz-Von Der Gathen, V.and Döbele, H., (2001), "Absolute calibration of atomic density measurements by laser-induced fluorescence spectroscopy with two-photon excitation", *J.Phys.D,* Vol.34 (15), pp. 2330.

[27] Laher, R.R.and Gilmore, F.R., (1990), "Updated excitation and ionization cross sections for electron impact on atomic oxygen", *Journal of Physical and Chemical Reference Data,* Vol.19 (1), pp. 277-305.

[28] Pagnon, D., et al. (1995), "On the use of actinometry to measure the dissociation in O2 DC glow discharges: determination of the wall recombination probability", *J.Phys.D,* Vol.28 (9), pp. 1856.

[29] Singh, H.and Graves, D.B., (2000), "Measurements of the electron energy distribution function in molecular gases in an inductively coupled plasma", *J.Appl.Phys.,* Vol.87 (9), pp. 4098-4106.

[30] Gahan, D., Dolinaj, B.and Hopkins, M., (2008), "Comparison of plasma parameters determined with a Langmuir probe and with a retarding field energy analyzer", *Plasma Sources Sci.Technol.,* Vol.17 (3), pp. 035026.

[31] Kechkar, S. Atomic oxygen characterisation in a (RIE) O_2/Ar discharge using Laser-Induced Fluorescence and Mass Spectrometry. 2011.

Chapter 7- Conclusions

Production of radical species in plasma would play a vital role in plasma etching process for manufacture of nano-sized ICs in modern semiconductor industry. Parameters which would govern plasma etching are etch rate, anisotrophy, aspect ratio, etc., can be controlled with quantitative knowledge on concentration of radical species at various operating conditions. In this regard, density of radical species was investigated in this research work in a reactive ion-etching (RIE) capacitively coupled rf (13.56 MHz) plasma source. Various plasma diagnostics tools such as appearance potential mass spectrometry (APMS), actinometry, Langmuir and hairpin probes were employed in this work to estimate radical concentration and plasma parameters at various discharge conditions. In this work, investigated plasma contained gases such as SF_6, O_2 and Ar which are most commonly used in industry, especially for deep Si etching applications. Depending on investigation, gases were operated at different feedstock mixtures and concentration of reactive species such as [F] and [O], responsible for plasma etching, were measured using diagnostic techniques at different plasma conditions.

7.1 APMS - Variation of absolute fluorine atom density

In this work, absolute atomic fluorine density was investigated in $SF_6/O_2/Ar$ capacitively coupled plasma discharge using APMS technique. Variation of absolute density of atomic fluorine as a function of feedstock mixture and at various operating conditions was summarized in the following section.

7.1.1 Effect of O_2 content

For deep silicon etching applications, atomic oxygen produced through molecular dissociation of O_2, would form passivation layer (SiO_xF_y) with Si substrate to protect side walls from isotropic etching of high density fluorine radicals to obtain high anisotrophy. Moreover, concentration of atomic fluorine can vary significantly with dilution of SF_6 plasma with O_2 due to gas-phase reactions. Absolute fluorine atom density measured using APMS was found to

increase with small addition (≈ 5%) of O_2 to SF_6 plasma. In pure SF_6 discharge, atomic fluorine can be lost to reactor walls through surface recombination process. With dilution of SF_6 discharge with O_2, atomic oxygen radicals would readily chemisorbed onto aluminium reactor walls due to higher sticking coefficients than fluorine atoms and thus, smaller surface coverage for adsorption of fluorine atom to wall surface. This could significantly reduce to F-atom loss rate to walls and increase fluorine radical concentration in the discharge. In addition to this, fluorine atoms can also be produced through gas-phase reactions in SF_6-O_2 discharge and this would enhance atomic fluorine density. Absolute [F] was found to reach a maximum at 20% and 30% O_2 concentrations in $SF_6/O_2/$ Ar discharge operated at pressures 70 and 200 mTorr respectively.

However, absolute [F] was found to decrease with further increase in O_2 concentration and this could be due to decrease in SF_6 partial pressure in discharge. Also, with increase in O_2 concentration, energy of plasma electrons could decrease significantly and this would effectively decrease atomic fluorine production through dissociation of SF_6 molecules. Therefore, to gain precise control over the atomic fluorine density in SF_6/O_2 discharge, oxygen concentration must be carefully chosen and oxygen dilution can be varied between 20-30 % in this $SF_6/O_2/Ar$ capacitive discharge to obtain higher atomic fluorine production.

7.1.2 Effect of gas pressure and rf power

For plasma etching applications using SF_6 plasma, it would be necessary to understand the fluorine production rate with gas pressure. Variation of absolute [F] measured using APMS was investigated as function of gas pressure (30-250 mTorr) in $SF_6/O_2/Ar$ (70/26/4 %) plasma. Absolute [F] was found to rise with increase in gas pressure in $SF_6/O_2/Ar$ (70/26/4 %) discharge operated at 100 W rf power. Increase in SF_6 partial pressure and effective dissociation of SF_6

molecule by high energy plasma electrons could be the cause for increase in atomic fluorine density as measured electron density found to be a weak function of gas pressure under investigated condition. However, dissociation fraction ([F]/[SF_6]) was found to decrease beyond 200 mTorr gas pressure and this could be due to change in electron heating mechanism with increase in pressure, which would be obvious in capacitive discharge. Any change to electron kinetics with increase in gas pressure can cause significant variations to energy of electron population and thereby can affect atomic fluorine production from dissociation of SF_6 molecule by energetic electrons.

Power variation of absolute [F] was investigated using APMS at 40 mTorr, 70 mTorr and 200 mTorr gas pressures with different feedstock mixtures of $SF_6/O_2/Ar$ in this capacitive discharge. For this investigation, the nominal input power was varied between 30 and 600 W. Absolute [F] was found to increase with applied rf power for all the pressures investigated here. As measured electron density was found to increase with increase in applied rf power, therefore absolute [F] was expected to increase with power provided negligible variations to electron temperature or EEDF and F-atom loss rates with rf power. However, marginal drop in absolute [F] and dissociation fraction was observed at 40 mTorr gas pressure in $SF_6/O_2/Ar$ (85/10/5 %) plasma for rf power > 250 W. With increase in rf power, if drop in electron temperature was significant, then dissociation degree of SF_6 would decrease and obviously, this can reduce atomic fluorine production.

7.2 Fluorine actinometry – For industrial applications

Modern semiconductor industry would demand high degree of uniformity in processing plasma for modification of materials using various plasma processes such as etching, deposition and sputtering for manufacture of ICs. Any process drift in processing plasma would cause significant variations to etch profile aspect and this would have undesirable impact on device performance. Any

significant variations in the outcome of processing plasma would largely depend on the density of atomic radicals produced in the plasma. Thus, one could control the process drift in processing plasma by observing any variations in atomic radical density. One of the commonly used non-invasive, compact diagnostic tools for industrial purpose would be optical emission spectroscopy, an industrial sensor and technique used with it, in this work to monitor particle densities of reactive species in processing plasma was actinometry. In this work, fluorine actinometry, within its limitations, was adopted to monitor relative variation in fluorine atom density using actinometric signal, I_F/I_{Ar}. Moreover, for validation of fluorine actinometry, relative atomic fluorine density measured using APMS and actinometry was compared under various discharge conditions.

Both techniques had poor correlation on relative [F] variations at low pressures in $SF_6/O_2/Ar$ discharge with $\leq$ 20% O_2 content. Optical atomic fluorine emission signal measured at 703.7 nm could have additional excitation mechanism apart from direct excitation of ground state atomic fluorine. However, good quantitative agreement was achieved between both techniques on relative [F] variations for pressures $\geq$ 200 mTorr in $SF_6/O_2/Ar$ discharge with > 20% O_2 content. Based on this good correlation between actinometry and APMS measurements, proportionality constant (K) for fluorine actinometry was evaluated in this work for first time in capacitively coupled $SF_6/O_2/Ar$ discharge. Value of K evaluated in this work was found to be lowest in comparison to other published values in various fluorine based discharges and this was due to lower estimate of absolute [F] measured using APMS, employed to evaluate K. To understand the dependence of evaluated K in this work, absolute atomic fluorine density was calculated using K was compared to APMS measurements under various plasma discharge conditions. Measured absolute [F] had satisfactorily good agreement with calculated [F] when actinometric signal had less significant additional excitation contribution apart

from direct excitation and not much variations to EEDF under investigated conditions.

7.3 Electron kinetics in oxygen discharge

Depending on discharge operating conditions, electron heating mechanism can vary in capacitive discharge. For variation in gas pressure from low to high, discharge transition due to change in electron heating process can be apparent i.e., collisionless (stochastic mode) to collisional (ohmic heating) regime. Discharge mode transition can cause significant variation to energy gained by plasma electrons and this would affect temperature of electrons along with ionization rates of species produced in the plasma. Moreover, any variations in energy of electrons would affect plasma etching process because such variations would have significance impact on rate of chemical reaction between reactive species with substrate and energy for ion bombardment. A Langmuir probe was used in this work to investigate electron heating mode transition in O_2 plasma using parameters such as electron energy probability function (EEPF), electron density (n_e), and effective electron temperature (T_{eff}).

The main objective was to investigate the possible cause for structure observed in measured EEPF in oxygen discharge for pressures > 400 mTorr. Moreover, at these conditions, inverse proportionality between ionization rate constant and neutral gas density, in accordance to particle balance equation was violated. Although, addition peak structure can appear in EEPF due to super-elastic collisions of electrons with metastable O_2 molecules but distortion of measured probe current-voltage characteristics (IVCs) can also create structure on measured EEPF. Distortion in IVCs can be mainly due to poor rf compensation by compensation electrode on the probe and any disturbance to probe offered by plasma sheath resistance. With increase in pressure, confinement of plasma was visually observed and the reference electrode could be out of plasma. In such scenario, when probe tip was biased, reference probe would fail to

compensate for any DC shift in the plasma potential due to resistance offered by plasma sheath and obviously cause distorted IVCs. This hypothesis was investigated with modified Langmuir probe setup and IVCs were measured for same pressures (100 – 800 mTorr) in oxygen discharge operated at 200 W rf power.

With modified Langmuir probe arrangement, undistorted IVCs were obtained and for increase in pressure from 50 to 700 mTorr, EEPF changed from a bi-Maxwellian with 1.01 eV T_{eff} to Druyvesteyn-like distribution with 3.11 eV T_{eff}. For pressures > 600 mTorr, discharge was clearly found to be in collisional regime accompanied with abrupt changes to n_e and T_{eff}. However, for pressure > 700 mTorr, IVCs obtained using modified Langmuir probe arrangements was distorted due to inadequate rf compensation of compensation electrode and this verified using spatial and radial probe measurements in argon and oxygen discharge respectively.

In addition to this, absolute atomic oxygen concentration was investigated as function of gas pressure ranging from 30 – 200 mTorr in O_2-Ar (96/4 %) discharge operated at 100 W rf power. Absolute [O] was measured using actinometry and required excitation rate co-efficients were calculated from electron energy distribution function (EEDF) measured using modified Langmuir probe arrangement. Atomic oxygen density was found to increase with pressure and good agreement was achieved with TALIF measured [O] under similar investigated conditions. Moreover, dissociative excitation contribution to oxygen actinometric signal was found to decrease with increase in pressure similar to actinometric signal of fluorine atom.

7.4 Highlights of this work

- For first time in a parallel-plate capacitively coupled RIE discharge, absolute atomic fluorine density was experimentally investigated as

function of various process parameters such as gas pressure, feedstock mixture and rf power in $SF_6/O_2/Ar$ and SF_6/Ar plasmas.

- Fluorine actinometry technique was used to monitor relative fluorine atom density in the same plasma discharge using non-invasive, low cost and compact sensor known as optical emission spectroscopy.
- Sensor measurements used to monitor relative variations in atomic fluorine density was successfully validated using most reliable diagnostic tool (mass spectrometry) and can be used with good confidence in an industrial environment.
- Proportionality constant (K) required for fluorine actinometry to compute absolute [F], was evaluated for the first time in capacitively coupled $SF_6/O_2/Ar$ discharge. Validity of K was successfully verified within the limitation of fluorine actinometry.
- Electron kinetic behaviour was investigated as a function of gas pressure in O_2 plasma using Langmuir probe and discharge transition from collisionless (stochastic) to collisional regime (ohmic heating) was apparent due to change in electron heating mechanism with increase in gas pressure.
- Structure on measured EEPF in pressure evolution studies in this work, was mainly due to distortion of IVCs caused by inadequate rf compensation by compensation electrode on the probe and uncorrected variations in plasma potential when probe tip was biased.
- Variations of [O] measured using actinometry and Langmuir probe techniques had good agreement with TALIT measurements under similar investigated conditions.
- Dissociative excitation contribution to actinometric signal (for both fluorine and oxygen) was very much significant at low pressures (< 80 mTorr) in this capacitive discharge and decreased with increase in gas pressure.

7.5 Scope for future work

This section would briefly discuss the scope of future work based on investigations carried out in this research work

- Investigation of electron kinetics in SF_6 based discharge can provide quantitative knowledge on parameters such as EEPF, n_e and T_e. Information on these parameters under various experimental conditions can provide insight to rates of gas-phase reactions and ionization processes. Moreover, any variations to [F] under investigated conditions can be readily understood with precise knowledge on energy of electron population.
- To monitor variations of [F] more realistically using fluorine actinometry, knowledge on additional excitation mechanism (especially dissociative excitation) would be essential. Dissociative excitation contribution to fluorine actinometric signal can be investigated using high-resolution spectrometer such as scanning Fabry-Perot interferometer. This investigation can reveal the significance of dissociative excitation under various discharge conditions.
- Numerical studies can be performed in SF_6/O_2 discharge to gain information on various aspects which could be difficult to obtain experimentally. With absolute [F] measured in this work as benchmark, numerical investigations can provide knowledge on F-atom production and loss channels, variations of electron and gas temperatures.

Appendix A: REPORT ON MASS SPECTROMETER

A.1 Introduction

Mass spectrometry is a diagnostic technique that can be used to measure neutral, ionic and metastable species. This report focuses on various challenges faced during experiments using a mass spectrometer (MS) from Hiden Analytical (EQP 300). The variation in atomic fluorine density was investigated in both SF_6/Ar and SF_6/O_2/Ar capacitive discharges. However, throughout experiments the performance of EQP was affected by factors like contamination, loss of signal. The possible sources which led to these challenges were investigated and consequences of ignoring them are discussed. In addition, there were issues with data acquisition due to high background signal. High beam to background signal ratio was achieved using the recommended data acquisition technique and this reduced the background signal to a low level.

A.2 Experiment

A schematic of the plasma source and MS used in this work is shown in figure A.1.

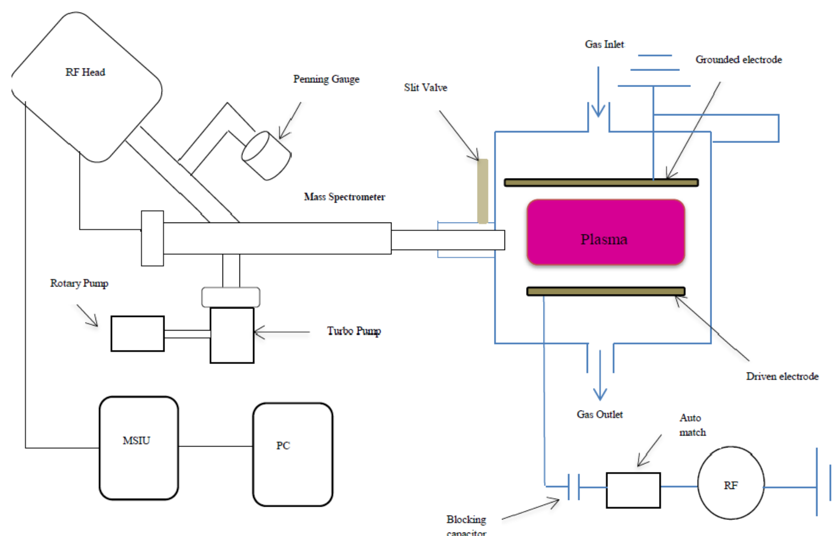

Figure A.1 Experimental setup of Hiden EQP 300 mass spectrometer

The mass spectrometer used in this report was an EQP 300 from Hiden Analytical [1]. The sampling head of the MS can be inserted directly into the plasma region. As the sensitive probe is enclosed within a metal enclosure and this allows the sampling head to be inserted directly into the plasma region. The ionization source is located ≈ 2 – 3 cm behind the orifice; this reduces the background signal to offer good sensitivity [2]. The orifice on the sampling head was 150 µm in diameter. Plasma was generated using 13.56 MHz RF excited capacitively-coupled plasma source. A variable gate valve was used to control the chamber pressure. Neutrals generated in the plasma enter the MS chamber through the orifice and then to the ionization source. Filaments generate an electron beam which ionizes the neutrals. These ions were directed to triple filter quadruple mass analyser using electrostatic lenses where they are filtered with respect to their mass to charge ratio. Secondary electron multiplier (SEM) was used to detect the ions.

A.3 Precautions & Observations

A.3.1 Filaments

The filaments in the ionizer are made from oxide coated iridium. These filaments generate electrons which are accelerated towards a cage. The maximum operating EQP pressure for filaments is 1E-4 Torr. Filament lifetime depends on its operating conditions. The filament may demand excess current when the emission current value was increased for electron energy scans from less than 20 eV [3] and operating the filaments in this region may lead to filament damage.

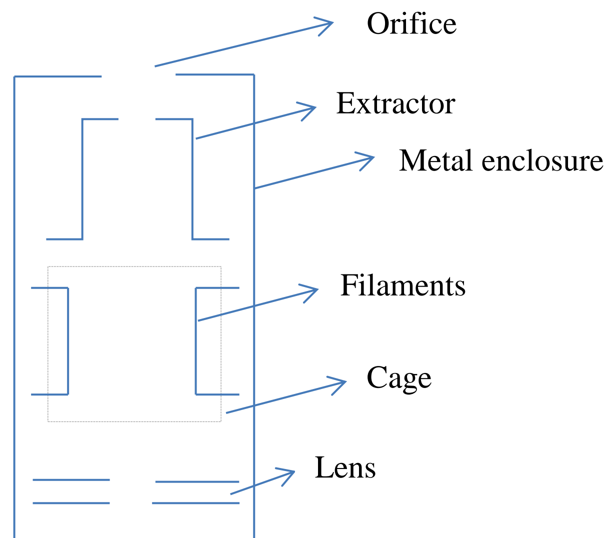

Figure A.2 Schematic of electron impact ionisation source in EQP 300

Figure A.2 shows a schematic representation of electron impact ionization source which incorporates the filaments extractor, cage and lens. These filaments may get etched on prolong exposure to the gases like oxygen and fluorine and this will reduce the life time of filaments. Such reactive gases could also contaminate the ionization source or coat the filaments by its residue. In such scenario, regular degassing of filaments together (with multiplier voltage set to 0 V) can prolong filaments lifetime.

A.3.2 SEM Detector

The detector used is an ion-counting Secondary Electron Multiplier (SEM) for detection of ions. Sensitivity of the device is high with low background noise. In most operating environments, the device provides good life time with correct usage. However, SEM detector should not be operated for EQP pressure higher than the recommended operating pressure of 5×10^{-6} Torr and for SEM counts higher than 1E7 c/s. Violation in either case will deteriorate the performance of SEM detector significantly.

A.3.2.1 Operating Voltage

The detector should be operated at a particular voltage which corresponds to the plateau region of the multiplier scan for longer life time. Multiplier voltage scan is recommended to perform with argon gas by maintaining EQP pressure at 5.2×10^{-7} Torr. An example is shown in figure A.3 to obtain operating voltage from multiplier scan.

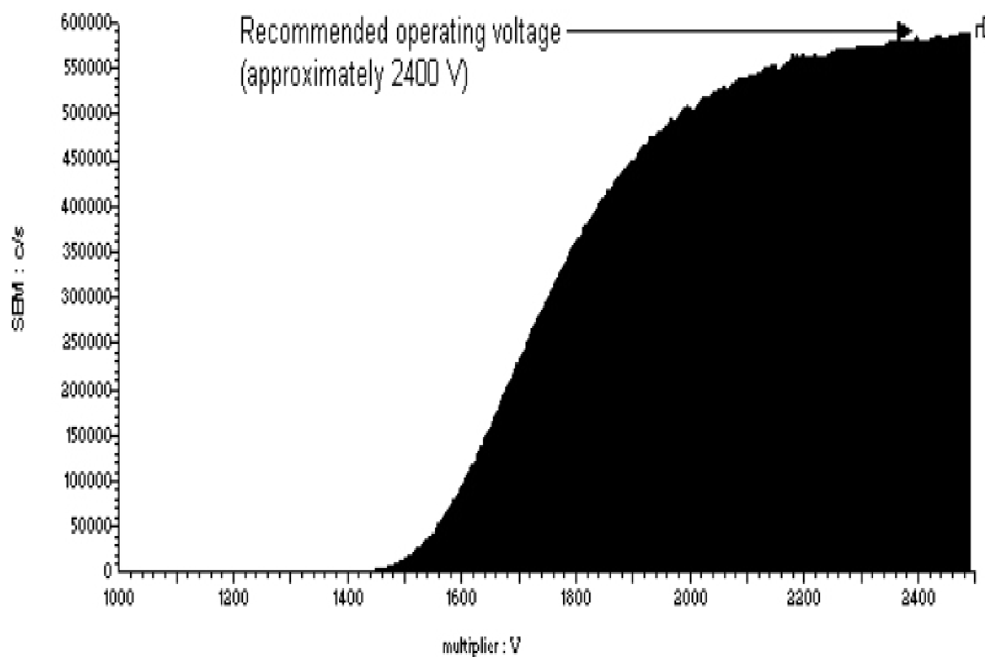

Figure A.3 Detector operating curve [3]

The detector life time can be analysed with the help of this plateau region. When the plateau region extends to higher voltages then the detector is nearing or at the end of its lifetime. Figure A.4 shows different multiplier voltage scans (Detector operating curve) performed on different dates with argon gas by maintaining EQP pressure around 5.2×10^{-7} Torr.

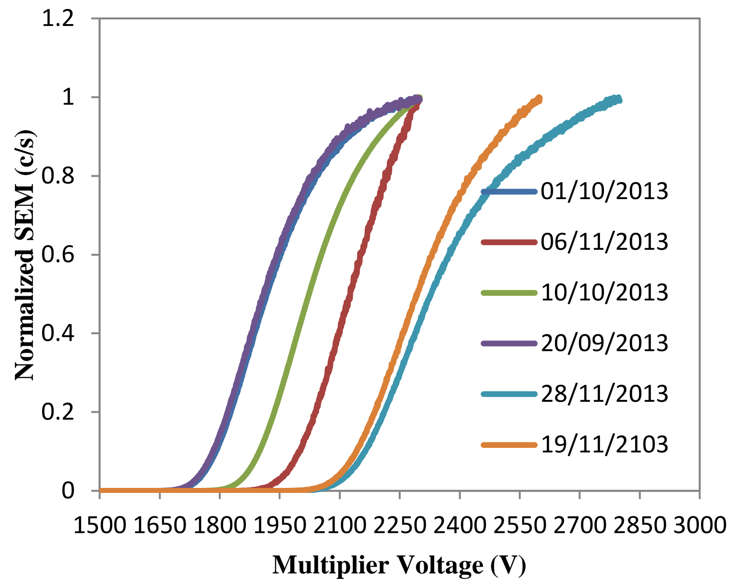

Figure A.4 Detector operating curves on different dates with shift in plateau region

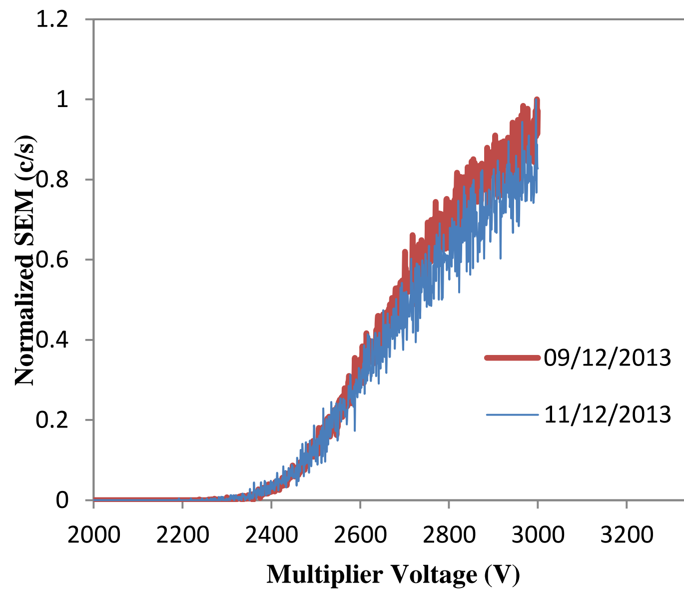

Figure A.5 Detector operating curves on different dates with poor signal-to-noise ratio

It was evident from figure A.4, that there was shift in the plateau region and this indicated deterioration of SEM detector. Initially the plateau region starts

around 2250 V (on 01/10/2013 in figure A.4) and reaches close to 3000 V (on 28/11/2013 in figure A.4). This is clear indication that detector may be nearing its lifetime. Low signal to noise ratio (as shown in figure A.5) and loss signal can also be an additional indication for poor performance of SEM detector. Thus, before any experiments with MS, it is recommended to perform multiplier voltage scans to ensure the performance of SEM detector.

A.3.3 Tuning EQP Analyser

Tuning of the electrodes is very much essential to maximize the performance of EQP. The number of tuning that require is overseen by the particular application. The situation where tuning may be appropriate are listed in Hiden manual Section 4.2 [3].

A.3.3.1 RGA Tune

Residual gas analyser (RGA) tune will optimize tune settings for various components such as: DC Quad, Energy, Flight focus, Focus2, Horizontal, Lens2 and Vertical. RGA scans will generate a tune file (*.tun) with updated tune settings. This updated tune settings will adjust the variables like emission, electron-energy, flight focus, etc., and it is recommended to import the tune file onto Global: RGA box for any of mass, electron-energy, MID or MAP scans to maximize the performance of EQP. Figure A.6 shows a typical RGA tune scans generated with EQP analyser. RGA tune scans were performed with argon gas with EQP pressure at 5.2×10^{-7} Torr.

RGA spectra can also indicate when EQP becomes severely contaminated. The contamination could be at the two regions- Ion source and penning gauge. The contamination may occur when the reactive/aggressive gases like fluorine and oxygen, react with other gases as well as with each other. If energy scans peak at negative voltage then ion source is severely contaminated. This is due to electrons charging-up contaminated parts of the ion source and ions were formed at negative energy voltage. The performance of EQP will be highly

altered with the contaminated probe and at times loss of signal by a few orders of magnitude in RGA mode may indicate possible contamination in the EQP probe. Figure A.7 shows RGA energy scans of contaminated and clean ion source.

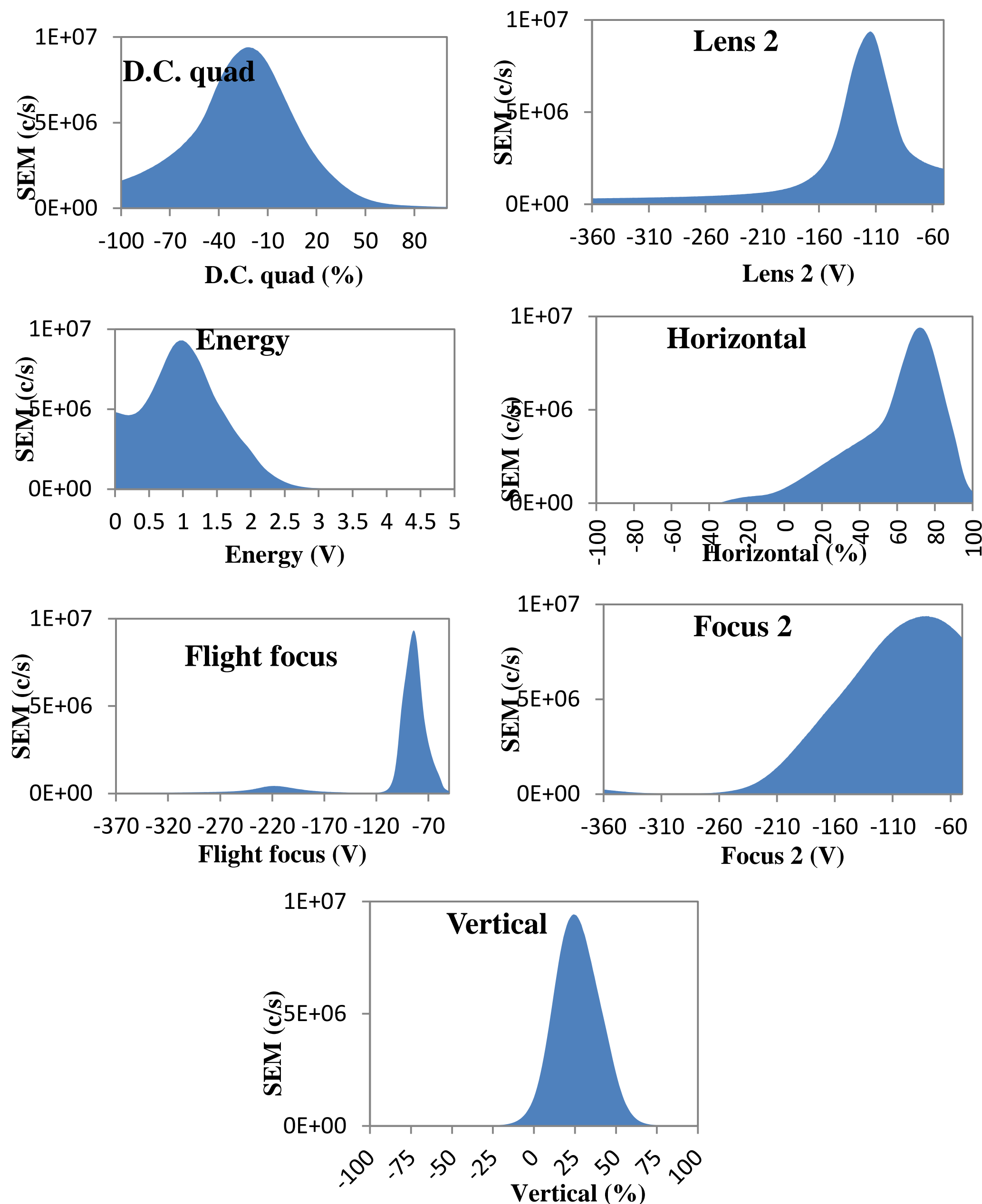

Figure A.6 Typical RGA tune scan at 40 amu (argon) generated at 5.2×10^{-7} Torr EQP pressure.

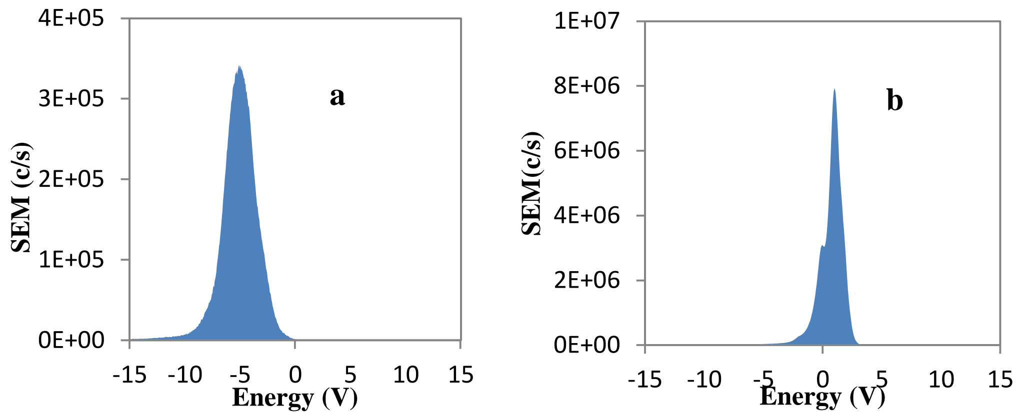

Figure A.7 Typical RGA energy spectra from a probe with a. (on left) maximum signal intensity at a negative energy voltage indicates slight–contaminated source and b. (on right) maximum signal intensity at a positive voltage indicates clean source. Both the scans were performed at 40 amu with 5.2×10^{-7} Torr EQP pressure.

A.3.3.2 MAP Scans

This scan would give broader knowledge of each variable and also helps to tune the electrode for better performance. This scans were usually performed with the updated tune setting from the RGA tune scans. MAP scans would give better understanding of any issues with the EQP like contaminations, SEM detector life. In most cases, any issues with EQP would be reported to Hiden Service Engineers by providing them with MAP scans. This will help them to address and diagnose any issue at the earliest.

A.3.4 Penning Gauge

The Compact Cold Cathode gauge was used for vacuum measurement in a pressure range of $5x10^{-11}$ to $1x10^{-2}$ mbar. It consists of two electrodes- cathode and anode. High voltage is applied between these electrodes via a series resistor. Negatively charged electrons leave the cathode towards the anode. These electrons ionize neutral gas molecules which sparks a gas discharge. The current from this gas discharge is a parameter for pressure.

Prolong usage and exposure of these gauges to reactive gases can also contribute to the contamination. A contamination layer can be formed in the gauge and it may fall onto the EQP probe if the gauge was in direct line of sight to quadrupole. Figure A.8 shows the pictures of contaminated gauge.

Figure A.8 Pictures of the contaminated gauge with the debris in the gauge (left) and debris made to fall on the paper (right) when gauge was tapped.

The sensitivity of the cold cathode gauges were altered by the contamination layer, which is formed due to sputtering process occurring on the cathode of the gauge. Debris (sputtered material) falls onto the cathode and reaches the anode where it forms a contamination layer. This debris will affect the sensitivity of the gauge and alters the electrical potential distribution. This would ultimately lead to malfunction of gauge. This would lead to loss of sensitivity, high background signal at lower mass and mass shift in EQP. Sensitivity of EQP was clearly affected with such contamination on penning gauge as seen from some of parameters from MAP scans shown in figure A.9.

Due to contamination in the EQP probe, an offset was observed in mass spectrum as shown in figure A.10. Argon gas was made to flow through the chamber and mass scans were performed at 70 eV with 100 μA emission current. For Ar^+ the peak will be around m/e = 40 instead we observed peak

around *m/e* = 42. The offset of 2 amu can be due to contamination in the probe which altered the mass scale in the EQP.

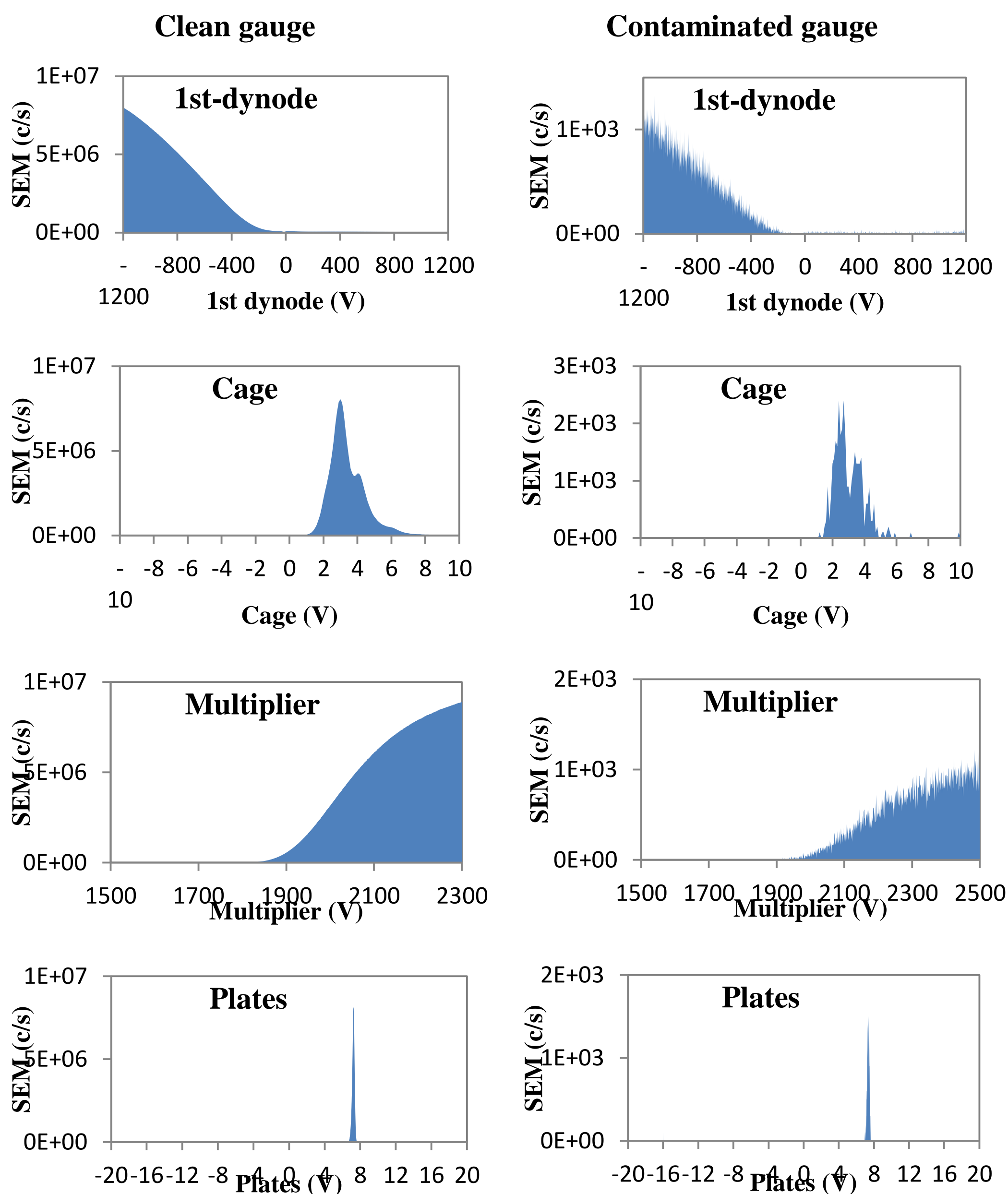

Figure A.9 MAP scans (of few parameters) comparison of clean and contaminated gauge at 40 amu generated at 5.2×10^{-7} Torr EQP pressure

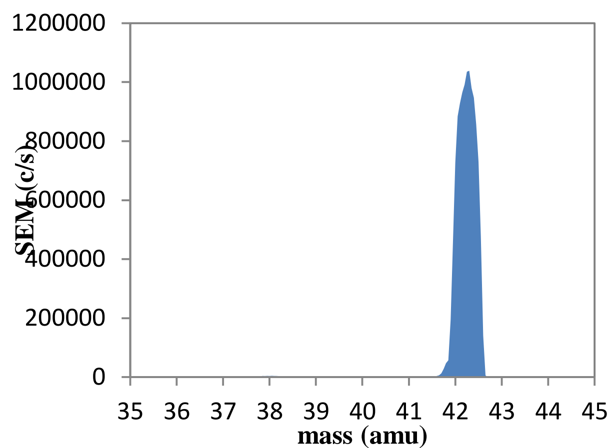

Figure A.10 Mass spectrum with argon gas. Mass offset (m/e = 40 to 42) was observed due to contamination in EQP

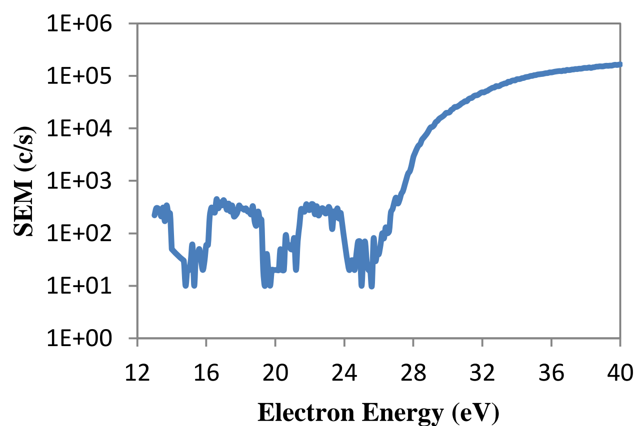

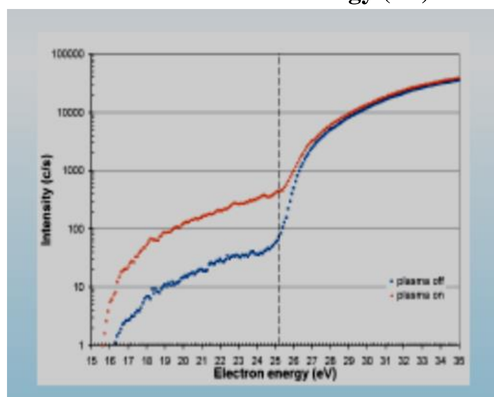

Figure A.11 Electron energy scan of N in N_2 plasma with the contaminated gauge (left) in comparison to appearance potential scans for N (right) with the plasma on and off from Hiden [3]

To further confirm the severity of contamination in the EQP, electron energy scans of N with 100 μA emission current was performed.

Consider the following processes:

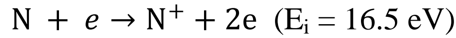
$N + e \rightarrow N^{+} + 2e$ (E_i = 16.5 eV)

and dissociative ionization of N_2;

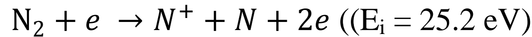
$N_2 + e \rightarrow N^{+} + N + 2e$ ((E_i = 25.2 eV)

where E_i is the threshold ionization.

The behaviour of our electron energy scans of N in N_2 plasma in figure A.11 with contaminated gauge showed abnormal disparity in its direct ionization energy range i.e., between 16 to 25.2 eV. From this comparison, it can be said that poor signal to noise ratio was due to contamination. To be more specific, it was due to contamination from the penning gauge. Thus, it was recommended to perform regular check on the penning gauge to ensure it is always free from any debris.

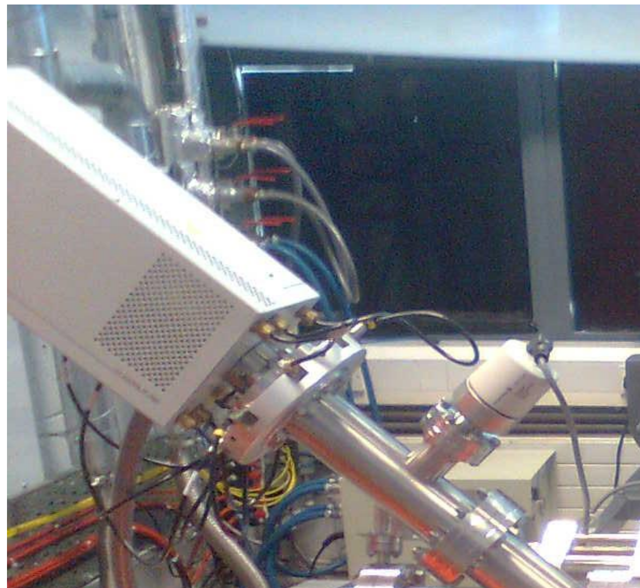

Figure A.12 Penning gauge was in direct line of sight to quadrupole. This set up will contaminate the EQP probe if debris were formed in the gauge.

The position of penning gauge in the EQP is very vital. In the figure A.12, the penning gauge was mounted directly onto the quadrupole. Any debris from the gauge may fall onto the quadrupole and this will affect the performance of EQP by contaminating the probe. Penning gauge was fitted with a right angle elbow joint to avoid such direct line of sight arrangement to the quadrupole rods in the EQP.

A.3.5 Bake-Out

Bake-out are usually performed to remove water vapour and any contaminants present inside the MS. The precautions and procedure to bake-out the system is available in Hiden manual (Section 3.3 & 7.4.3) [3]. Bake-out was usually performed after the following action with EQP:

- Filament renewal/replacement
- Contamination check in MS
- Event of vacuum failure

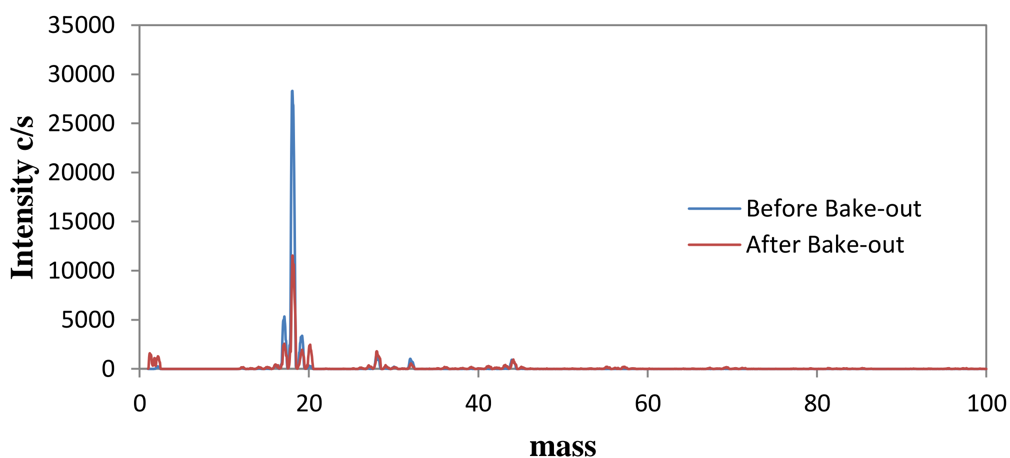

Figure A.13 Mass spectrum before and after bake-out with no gas.

A comparison of mass spectrums- before and after bake-out is shown in figure A.13. The electron energy was set to 70 eV. Before bake, we observed significant peaks at *m/e* = 17, 19 and 18 being the dominant. After two days of bake-out, close to two fold decrease was observed in the peak at *m/e* = 18.

Similarly, notable reduction to other significant peaks was observed. Baking also created few new fragments but those are very much negligible. During bake-out, both filaments can be energized manually and the procedure is mentioned in Hiden manual (Section 7.4.3) [3].

A.3.6 Electron Energy Calibration

Electron energy (EE) calibration was performed to account for any shift in the electron energy scale. Argon (as its ionization potential is well known i.e., 15.75 eV) was used to calibrate the electron energy scale of the EQP. Figure A.14 shows the EE calibration at two different pressures and emission currents. It was clear that for same gas operated at two different pressure and emission current, two different offset in electron energy scale was observed. This observation was misleading and further investigation was essential.

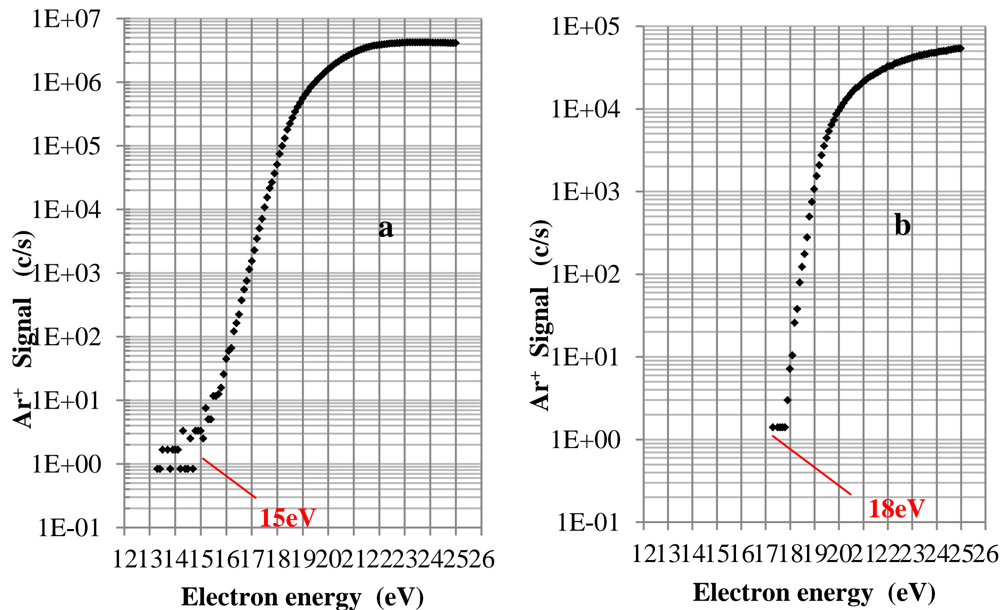

Figure A.14 Argon electron energy scans (a) E_{th} = 15 eV with argon pressure of 60 mTorr and emission current of 500 µA. (b) E_{th} = 18 eV with argon pressure of 5 mTorr and emission current of 100 µA.

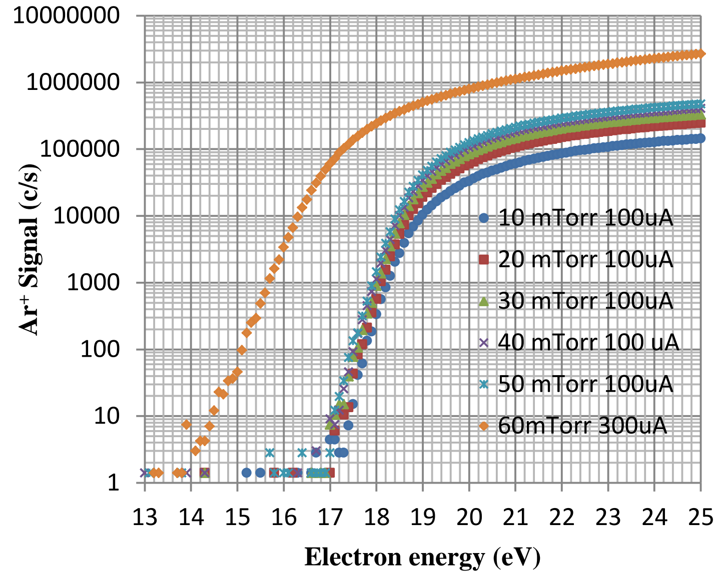

Figure A.15 Variation of ionization threshold for Argon for different pressure at 100 µA and 300 µA emission current.

EE scans of argon for gas pressures ranging from 10 to 50 mTorr with 100 µA emission current had an offset around +1.25 eV. However, EE scans of argon with 60 mTorr gas pressure and 300 µA emission current showed an offset around -1.75 eV. The later one may be correct as the Ar^+ ions densities were increased and electron energy scans were performed at higher emission current for better signal strength. In the following equation, the signal is proportional to emission current i.e., signal increases as emission current is increased.

$$S = \alpha\, I_e\, \sigma(E)\, n_i$$

where S is signal (c/s), I_e is the emission current in the ionizer, $\sigma(E)$ is the electron energy dependent cross section of the relevant ionization process, n_i is the number density of neutral species of interest in the ionizer and $\alpha = \beta\, T\, \theta\, l_{cage}$; β is the extraction efficiency of the ions from the ionizer, T is the species mass-to-charge ratio dependent transmission efficiency of the quadrupole mass filter, θ is the species mass-to-charge ratio dependent sensitivity of the SEM and l_{cage} is the length of the ionizer cage.

A.4 Acquisition technique

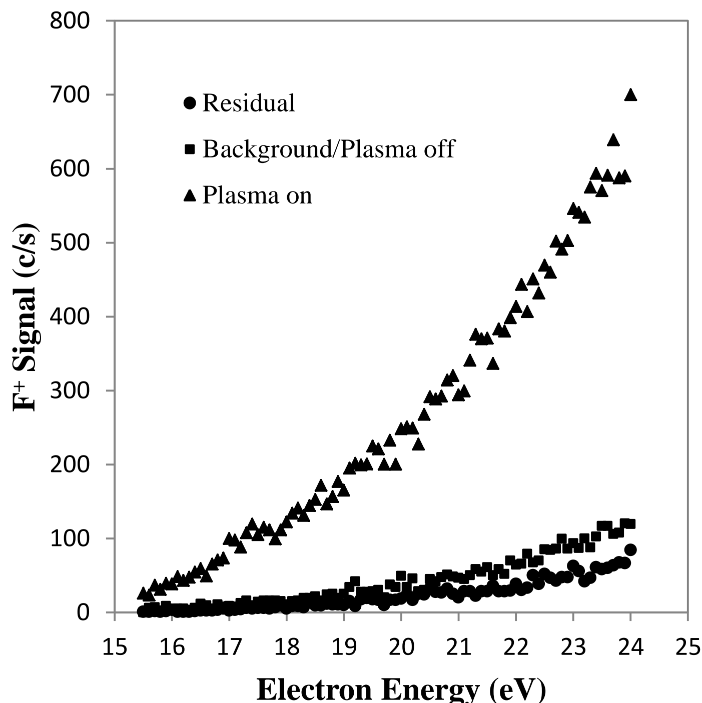

Figure A.16 Electron energy scans of F^+ in $SF_6/O_2/Ar$ plasma with 100 μA emission current and 40 mTorr gas pressure.

An example of EE scans of F^+ was shown and there were three signals- plasma on, plasma off/background and residual signals as shown in figure A.16. Residual signal was mostly due to the contamination in the chamber and is detected with no gas flow into the MS. Plasma off/ Background signal was obtained with flow of gas into the MS and it caused by thermal dissociation of SF_6 molecules. Residual, background signal and also from F atoms originating from the plasma contributes to plasma on signal.

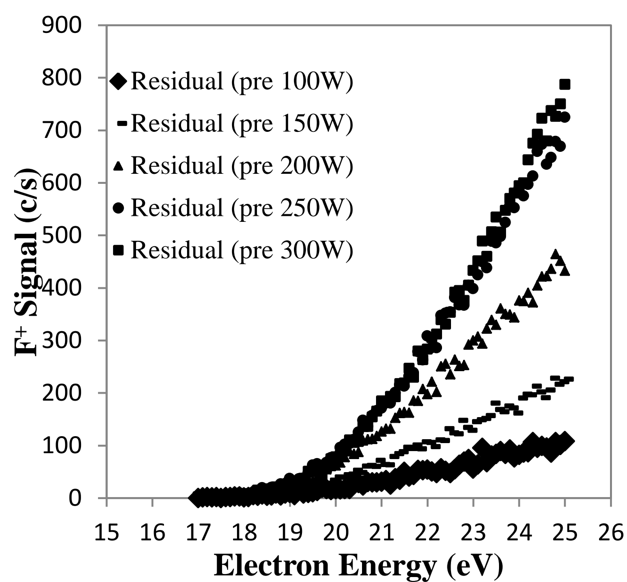

Figure A.17 Residual electron energy scan of F^+ before each plasma strike with no gas flow at 100 μA emission current.

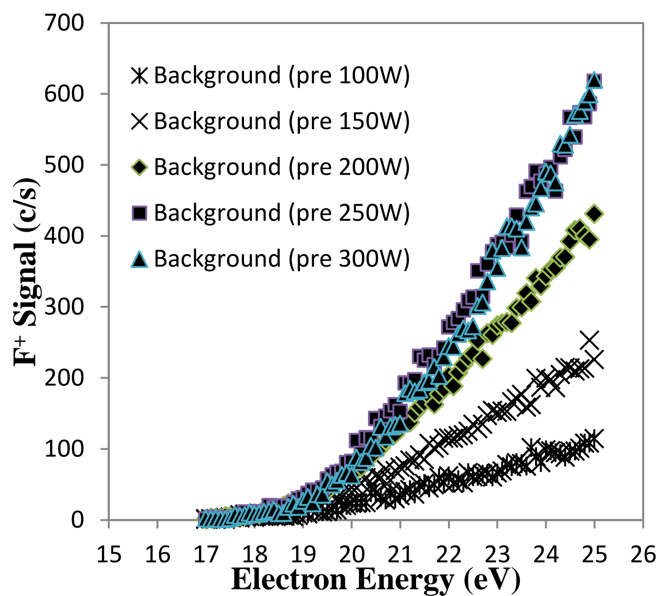

Figure A.18 Background electron energy scan of F^+ before each plasma strike with 85% SF_6, 10% O_2 and 5% Ar at 100 μA emission current and 40 mTorr gas pressure.

During experiments, the residual and background signals were found to vary significantly. To confirm this behaviour, the residual and background signal were measured before each plasma strike and their results were shown in the figure A.17 & A.18 respectively. It was evident that the residual and background signals varied significantly for similar experimental conditions. Residual signal and thermal dissociation of SF_6 were the major contributions to background signal. By suppressing the residual signal, background signal can be kept to minimum. If background signal was large, then it would lead to unreliable measurements. So an acquisition technique was proposed to keep the residual signal at low level (very much negligible). The following acquisition procedure was adopted:

- Background F signal was measured.
- Slit valve closed. Gas flow was stopped and allowed EQP to reach its base pressure. Simultaneously strike plasma (with slit valve closed) to stabilize the walls.
- Energised or Degassed for 40 mins through software with both filaments on.
- Slit valve open. Plasma on signal was measured.
- Energised or Degassed for 40 mins through software with both filaments on.

Energising the filaments would help to remove the coating formed on it and this coating believed to contribute significantly to rise in residual signal. By adopting above acquisition technique, residual signal was kept to low and insignificant as shown in figure A.19.

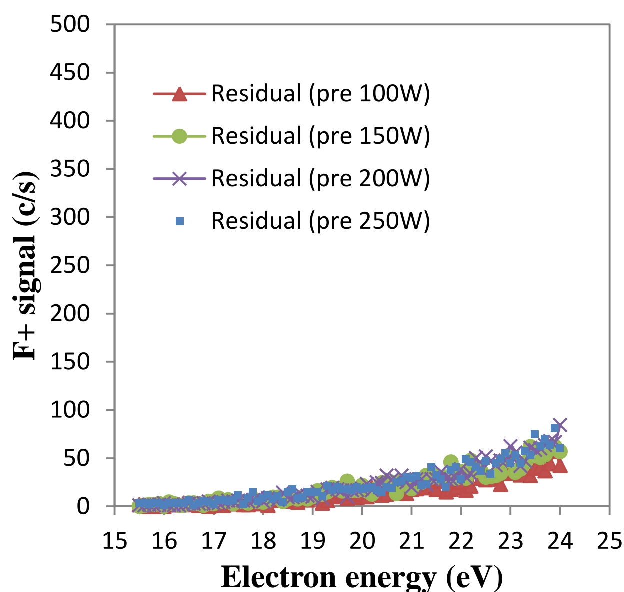

Figure A.19 Residual electron energy scan of F^+ before each plasma strike with no gas flow at 100 µA emission current using new acquisition technique

A.5 Conclusions

Few experimental challenges faced with the MS were discussed in this report and also attempted to recommend possible solutions to overcome those. Most of these experiments were aimed to obtain the absolute density of fluorine radical with feedstock mix of $SF_6/O_2/Ar$ (85/10/5%).

Contamination was the major challenge in the MS and it affected the performance of the EQP. Energy scans revealed the possible contamination in the ion source as it peaked at negative voltage. Degassing of both filaments simultaneously would significantly reduce contamination at ion source and protect the filaments life time. Moreover, the penning gauge should be checked regularly for any debris in it and also ensure the gauge is not in direct line of sight to the quadrupole rods in the EQP.

For a long life of the detector, it should be operated within the recommended operating pressure. The performance of the detector can be analysed using multiplier voltage scans. To maximise the performance of the EQP, tuning of

electrodes is very much essential. The RGA scans will tune the electrodes and MAP scans will aid to understand the performance of the EQP.

The acquisition can be performed once the tuning and MAP scans look good. The proposed acquisition technique increased the beam to background ratio by suppressing the residual signal to negligible level. This acquisition technique suited well SF_6 dominated mixture. It may also work for O_2 dominated mixture.

A.6 References

[1] Hiden. EQP and EQS Analysers. 2009.

[2] Singh, H., Coburn, J.W.and Graves, D.B., (1999), "Mass spectrometric detection of reactive neutral species: Beam-to-background ratio", *Journal of Vacuum Science & Technology A,* Vol.17 (5), pp. 2447-2455.

[3] Hiden. EQP/EQS Analyser Operator's Manual. 2009;HA-085-003(F Revision 1).